The development of methods to valorise rice husk to produce value-added products

Eksuree Saksornchai

PhD

University of York

Chemistry

September 2023

Abstract

In this work, the development of sustainable routes to valorise rice husk waste biomass of Thai origin for production of value-added products (bio-derived mesoporous materials and cellulose fibres) were successfully prepared through microwave-assisted methods in almost all steps with mild conditions. Microwave heating has been found to be an energy-efficient and cost-effective method to fabricate a range of bio-derived materials from rice husk without sacrificing the quality of the materials. Due to rice husk is a silica-rich material that can be extracted for preparation of silicate solution to use as a source of silica to produce mesoporous silica material (SiO_2) and ordered mesoporous silica material (SBA-15). Moreover, bio-oil derived from rice husk can be also used as carbon source for carbon-silica composite material (CSC). All as-prepared materials exhibit type IV isotherms typical for mesoporous structure which is beneficial for methylene blue removal. The removal efficiency demonstrated that SBA-15 can remove nearly 100% of methylene blue (MB) within an hour (98.15%), CSC can remove 78.30% of MB while SiO_2 can remove only 43.22% of MB. The adsorption isotherms of all materials were fitted with the Langmuir isotherm. SBA-15 possesses the highest $q_{e,cal}$ value of 126.58 mg/g, suggesting that mesoporous SBA-15 holds the most promising adsorption property for cationic dye. In addition, rice husk-derived cellulose microfibres/nanofibres were also successfully prepared by the development of greener procedures via organosolv microwave-assisted pretreatment followed by mild chemical processing for using as reinforcing agent to develop biodegradable composite film preparations. Bio-composite films possess good mechanical and optical properties (transparency) and thermal stability which offer an advantage for food packaging, film packaging or sustainable alternative materials.

List of Contents

List of Tables

List of Figures

Acknowledgements

First of all, I would like to express my gratitude to my supervisor, Dr. Duncan MacQuarrie for his suggestions and kind support. Without his kindness and patience, I could not have completed my thesis. I also thankfully acknowledge the support from Prof. Avtar Matharu for his suggestions as IPM.

I would also like to thank Dr. Clare Steele-King for her help with SEM and TEM. Thank you to Adrian Whitwood for training XRD and XRF techniques for analysis. Many thanks to technicians' team and staff.

In addition, I am deeply grateful to the University of Phayao for my PhD scholarship and the opportunity to study and live abroad. I would like to thank the Royal Society of Chemistry (RSC) for the partially granted financial support for attending the 7th Green & Sustainable Chemistry Conference.

I also owe my sincere gratitude to my dear friends for encouragement, and all support.

Finally, words cannot express my gratitude to my family especially my mom (Saisunee) and my dad (Anek) for their love and great support throughout my life.

Declaration

I declare that this thesis is a presentation of original work, and I am the sole author. This work has not previously been presented for a degree or other qualification at this University or elsewhere. All sources are acknowledged as references.

Parts of this research has been presented at the following conferences:

1. '7th Green & Sustainable Chemistry Conference', Dresden, Germany on 22/05/2023.
2. 'PhD Student Poster Presentation', University of York, Department of Chemistry, on 24/03/2022.

Chapter 1

Introduction

1.1 Background and Scope of Thesis

1.1.1 Project 1: Microwave-assisted synthesis of bio-derived mesoporous materials from rice husk for methylene blue removal

Currently, the whole world is facing many environmental concerns. As such, air pollution, waste disposal, agricultural pollution and water pollution are some of the main problems. One of the biggest environmental concerns is about how to manage agricultural wastes in the proper way.[1–3] Each year, millions of tons of agricultural wastes, which include rice straw, wheat straw, rice husk, corn stover and bagasse are generated worldwide, but are not properly utilized.[4–7] Large quantities of them are either discarded or burnt in open fields, which are environmentally hazardous strategies. To address these issues, the use of biomass from agricultural residues to produce biofuels, energy and value-added materials can achieve interesting environmental and economic benefits.[8–11]

Among the agriculture wastes, rice husk has been interesting to many researchers because not only are they abundant and sustainable agricultural wastes but also silica-rich biomass. Due to its high silicon content, rice husk ash can be an economically viable raw material to produce renewable silica materials.[12,13] Furthermore, rice husk could also be used as a carbon source to produce high surface area porous carbon materials and carbon-silica composite materials.[14,15] These naturally derived materials can be used in various applications such as adsorption, synthesis of molecular sieves, catalyst support and energy storage after processing by physical and chemical treatments.[16–19]

Over the last few decades, special attention has been paid to the conversion of biomass and renewable materials into bio-oil.[20–22] Agricultural waste is considered as an alternative feedstock for biofuel production due to its abundance and renewable nature, which mainly contains cellulose hemicellulose, and lignin.[22–26]. Bio-oil, potentially one of the most valuable products, is a complex mixture usually containing many types of oxygenated compounds with various chemical properties, such as aldehydes, ketones, phenols, esters, sugars, furans and multifunctional molecules. [16,27–29] It can be used as a feedstock for the production of valuable chemicals, a bio-oil adhesive for Al-Al bonding

and a carbon source that gives rise to the functionality of carbon-silica composite materials.[16,30–32]

Due to the many benefits of bio-oil, it has been continuously studied – resulting in the development of bio-oil production.[33–35] Various methods have been used for producing bio-oil including pyrolysis and microwave-assisted pyrolysis.[11,17,21,36,37] Pyrolysis has been used for several decades and offers an efficient route to thermally decompose organic matter in the absence of air/oxygen at elevated temperatures (typically between 400 and 800 ^{o}C) and converts organic (waste) biomass to bio-oil, gas, and biochar.[28,38–41] The properties of bio-oil derived from biomass pyrolysis are affected by heating characteristics.[42,43] Recently, microwave-assisted pyrolysis has emerged as a promising alternative technique to conventional pyrolysis mainly because of dielectric heating. Basically, a heating rate of 10-200 ^{o}C/s can be achieved by using microwave absorbers, favoring liquid and gaseous products.[44–46] The advantage of microwave heating offers relatively uniform internal heating of feedstock particles to improve bio-oil quality and stability.[17,47–49]

Previous research reported that rice husk is mainly composed of cellulose, lignin, silica. Rice husk ashes usually have high contents of silica, carbon, and some other minerals.[43,50–52] Therefore, rice husk ash is the best candidates as raw materials for silica source for producing silica materials.[53–55] Additionally, rice husk could be converted to bio-oil and biochar simultaneously via thermochemical processes. Z. Ji-lu *et al.* [38] and S. H. Chang *et al.*[37] produced bio-oil using conventional fast pyrolysis from rice husk at different temperature 420-450 ^{o}C and 550 ^{o}C, respectively using high temperature. Whereas Z. Zhang *et al.*[17] reported the conversion of waste office paper to bio-oil via low temperature (<200 ^{o}C) microwave-assisted pyrolysis using lower temperature and more eco-friendly method. But there have been very few reports studied on conversion of rice husk to bio-oil via microwave-assisted pyrolysis.[36,45,55,56] Due to combination of microwave heating with pyrolysis, this offers a potentially more efficient, faster, and low-environmental-impact procedure for large-scale processing of biomass and is defined as a greener method.[57-59] In this research, the microwave-assisted pyrolysis has been used for

producing bio-oil from rice husk, which has been used as carbon sources for carbon-silica composite materials (see Chapter 3, Section 3.5).

More recently, carbon-silica composite materials have drawn considerable attention by many researchers because of their excellent properties. Silica materials are insulating, hydrophilic, biocompatible materials whereas carbon materials are conductive, hydrophobic and have thermal and chemically stable.[60-63] The carbon-silica composite materials can allow for remarkable properties, including mechanical, thermal and dispersion properties and their ability as reinforcement materials that cannot be achieved by either individual component.[38] These composite materials have several potential applications, including catalysis, targeted drug delivery, semiconductor, supercapacitor and sensor and particularly in adsorption.[47,64-66] The conventional starting materials used for synthesis of carbon-silica composite materials are frequently pure chemicals that provide toxicity via their chemical waste. Hence, the starting materials of these processes that reduce or eliminate the use of hazardous substances is one of the aims of this research. Moreover, in the preparation of mesoporous materials, it is very easy to make mesoporous silicas with very controlled structures, but it is very difficult to make mesoporous carbons with the same control over structural regularity.[60,67,68] Carbon-silica composite materials allow the silica to provide the structure and the carbon to provide the active surface phase.

As mentioned before, rice husk is one of the most silica-rich materials which can be extracted as silicate solutions to use as a source of silica to produce porous silica materials (SiO_2) and mesoporous silica materials (MCM-41, MCM-48 and SBA-15) that can be used as a catalyst support, for drug delivery and also as an adsorbent.[69-74] Moreover, bio-oil from rice husk could be used as carbon source for carbon-silica composite materials. Several studies reported the preparation of carbon-silica composites using biomasses as starting materials.[75] H. Chu *et al.*[76] reported that carbon-silica nanocomposites for energy storage were produced via direct carbonisation of rice husk at different temperatures (400, 600 and 900 ^{o}C), L. Wang *et al.*[77] also reported that rice husk derived porous carbon–silica composites for energy storage were synthesised by direct carbonisation under the

inert atmosphere. Both reports provided microporous carbon-silica composite materials. To the best of our knowledge, the porosity should have a specific impact on the material properties or applications.[78,79]

Mesoporous materials are defined as materials having pores between 2 to 50 nm according to IUPAC. These materials are high-performance solids, their pore sizes and unique structures allow interaction with atoms, ions, and molecules.[67,80,81] The mesoporous silica material was usually used as a support or hard template which provides the mechanical strength and physical properties.[82,83] The surface modification of mesoporous materials can be performed via functionalization with inorganic or organic groups on the surface of materials.[84-86] One of the most interesting techniques for modification of silica surface was reported by T. Jiang *et al.*[16] who reported the preparation of carbon silica composites where the variation of preparation temperatures leads to a continuum of functionalities ranging from polar hydroxyl rich surfaces to carbonaceous surfaces.

Thailand is a nation rich in agricultural resources, which provide potential sources of biomass and many major projects for biomass utilisation in Thailand have been mainly focused on power generation.[1,87] Thus, this research will study the valorisation of Thai biomass in alternative applications particularly in the development of a greener method for synthesis of mesoporous materials derived from rice husk, using the silica alongwith the carbonaceous components to generate high surface area mesoporous materials, including, silica (SiO_2), SBA-15, carbon-silica composite and activated carbon for various applications, for instance, wastewater treatment, specifically the adsorption of methylene blue dye from aqueous solution.[88-90]

Moreover, the key challenges of this research are valorisation of rice husk to value-added products using greener routes to save time and energy, as well as attempting to design the method to maximize incorporation of all materials used in the process into the final product under (close to) zero-waste production. [11,91]

1.1.2 Project 2: Rice husk-derived cellulose microfibres/nanofibres for bio-composite film preparation

Apart from the synthesis of bio-derived porous and carbonaceous materials from rice husk, another way to take advantage of rice husk includes the utilisation of the cellulose part.

Over a decade, the production of more sustainable and environmentally friendly materials has gained the attention of researchers at the international level to develop a sustainable method to extract cellulose fibres from lignocellulosic biomass for various applications such as water purification[92], bioplastic film as green packaging materials[93] , reinforcing agents[94], optically transparent functional materials[95,96] and cellulose-based sensors.[66]

Rice husk is a lignocellulosic material which consists of approximately 35-40% cellulose, 15-20% lignin, and 20-25% hemicellulose. [97-99] To date, various approaches to utilise rice husk by cellulose extraction have been investigated through chemical, mechanical and biological extraction.[99,100] In conventional methods, the most common extraction for producing of fibres was carried out by pretreatment methods which mainly use the alkaline treatment and bleaching process and then acid hydrolysis was performed for production of microfibre cellulose and nanofibre cellulose.[98,101-103]

Microwave-assisted pretreatment is one of the most attractive procedures for micro/nano fibre celluloses production, due to it involves no addition of chemicals and has relative moderate operational conditions.[104-106] This hydrothermal treatment, also known as autohydrolysis of biomass, involves the addition of water and increase of temperature-resulting in a decrease of pH in the system due to the ionization of water and the release of carboxylic acids (mainly acetic acid), in combination with the effect of the high temperature and pressure applied.[107,108] In the solid fraction after hydrothermal pretreatment, the cellulose fibre was obtained from rice husk. This autohydrolysis leads to the disruption of the lignocellulosic biomass structure, improving the accessible surface area, and therefore enhancing the subsequent acid hydrolysis to produce micro/nano cellulose fibres.[34,109,110]

Moreover, cellulose fibre can be extracted from the rice husk using alkali and bleaching treatments.[111-113] In alkaline treatment, this step was carried out to purify the cellulose by removing hemicellulose and lignin from rice husk.[114,115] After alkaline treatment step, the bleaching step was used to further remove lignin from fibres which normally use hypochlorite.[99,116] Due to the negative environmental impact of chloride, a chlorine-free technique has been developed for the bleaching step to produce the white colour of cellulose fibres.[117,118] Finally, the production of nano cellulose fibre was also performed by acid hydrolysis.[89,119,120]

Micro and nano cellulose fibres possess valuable characteristics such as a renewability and biodegradability with satisfactory mechanical properties for additive in a polymer matrix.[116,121-123] Due to rice husk fibres remains a highly abundant and low-cost reinforcement filler, thus can be used for plastic composites fabrication for enhancing the mechanical properties of bio-composite films.[124-126]

In this study, production of micro and nano cellulose fibres from rice husk by using organosolv microwave-assisted pretreatment, alkaline treatment, bleaching method and acid hydrolysis have been studied for bio-composite film preparations that can be used in various application i.e. food packaging, smart material for packaging and so on.[127,128]

1.2 Research aims

1.2.1 Aims of Project 1: Microwave-assisted synthesis of bio-derived mesoporous materials from rice husk for methylene blue removal

1. To produce a range of mesoporous materials derived from rice husk, using silica along with carbonaceous components to generate high surface area mesoporous materials, including silica, SBA-15 and carbon-silica composite.
2. To study the adsorption of methylene blue using silica, SBA-15 and carbon-silica composite materials derived from rice husk.

1.2.2 Aims of Project 2: Rice husk-derived cellulose microfibres/nanofibres for bio-composite film preparation

1. To extract and characterise cellulose fibres from rice husk.

2. To study bio-composite film preparations from cellulose fibres and investigate transparency, thermal property, mechanical properties (tensile strength and elongation at break).

1.3 Green Chemistry and the United Nations (UN) Sustainable Development Goals (SDG)

Green Chemistry is an approach to the synthesis, processing, and use of chemicals that reduce risks to the environment and is less hazardous to human health. Many innovative chemistries have been developed over the last decades that are very efficient, effective, and more environmentally benign.[9,129] These methods include new syntheses and methodologies as well as new tools for instructing aspiring chemists how to do chemistry in a more environmentally benign manner.[9] New approaches to develop new greener routes for chemists are a challenge for the chemistry community to use their creativity and innovation to develop new synthetic methods, reaction conditions, analytical tools, catalysts, and processes under the new paradigm of Green Chemistry.

The concept of sustainability and the prospect of Green Chemistry involves in 12 principles were subsequently introduced by Paul Anastas and John Warner in 1998 that chemists should be taking into account while conducting their research, as scientific progress should not be achieved at the expense of causing environmental and socio-economic problems.[130]

The 12 principles of Green Chemistry are as follows:

1. Prevention

It is better to prevent waste than to treat or clean up waste after it is formed.

2. Atom Economy

Synthetic methods should be designed to maximise the incorporation of all materials used in the process into the final product.

3. Less Hazardous Chemical Synthesis

Wherever practicable, synthetic methods should be designed to use and generate substances that possess little or no toxicity to people or the environment.

4. Designing Safer Chemicals

Chemical products should be designed to effect their desired function while minimising their toxicity.

5. Safer Solvents and Auxiliaries

The use of auxiliary substances (e.g. solvents or separation agents) should be made unnecessary whenever possible and innocuous when used.

6. Design for Energy Efficiency

Energy requirements of chemical processes should be recognised for their environmental and economic impacts and should be minimised. If possible, synthetic methods should be conducted at ambient temperature and pressure.

7. Use of Renewable Feedstocks

A raw material or feedstock should be renewable rather than depleting whenever technically and economically practicable.

8. Reduce Derivatives

Unnecessary derivatisation (use of blocking groups, protection/ de-protection, and temporary modification of physical / chemical processes) should be minimised or avoided if possible, because such steps require additional reagents and can generate waste.

9. Catalysis

Catalytic reagents (as selective as possible) are superior to stoichiometric reagents.

10. Design for Degradation

Chemical products should be designed so that at the end of their function they break down into innocuous degradation products and do not persist in the environment.

11. Real-time Analysis for Pollution Prevention

Analytical methodologies need to be further developed to allow for real-time, in process monitoring and control prior to the formation of hazardous substances.

12. Inherently Safer Chemistry for Accident Prevention

Substances and the form of a substance used in a chemical process should be chosen to minimise the potential for chemical accidents, including releases, explosions, and fires.

These principles were taken into consideration throughout the whole thesis.

Project 1: Microwave-assisted synthesis of bio-derived mesoporous materials from rice husk

The synthesis of bio-derived porous materials from rice husk such as silica, SBA-15 and carbon-silica composite materials, as well as their application for methylene blue adsorption, both comply with several of the criteria set out by Green Chemistry Principles. Both silica and carbon sources used for the preparation of SBA-15 and carbon-silica composite materials reported in this thesis are obtained from rice husk (agricultural waste), which is in good agreement with the principles of prevention of waste (Principle 1) and use of renewable feedstock (Principle 7) because it prevents the disposal of waste by utilising the abundant rice husk waste as feedstock for the production of porous materials.

Moreover, the synthesis processes described avoid hazardous chemicals (Principle 3) or harsh conditions thus enhancing the atom economy (Principle 2) of the production system throughout all stages.

In the productions of SBA-15 and bio-oil, microwave-assisted method was performed, which is much more efficient and has less environmental impact compared to conventional heating (Principle 6). In addition, as the contents of the microwave reactor are hotter than their surroundings (due to the nature of the heating), switching off the microwave causes cooling to happen immediately. With a conventional reactor, the vessel is hotter than the contents, so switching off the heating does not have such a rapid response. This is a big safety point, which is often overlooked. This could be described as a good agreement with the principle of Design for Energy Efficiency.

Project 2: Rice husk-derived cellulose microfibres/nanofibres for bio-composite film preparation

The production of micro and nano cellulose fibres from rice husk and the application for bio-composite films production both comply with several of the criteria set out by Green Chemistry Principles.

Cellulose fibre extracted from rice husk described in this thesis is in good agreement with the principles of prevention of waste (Principle 1) and the use of renewable feedstock from abundant rice husk waste (Principle 7) for bio-composite films production.

In the pretreatment method described hazardous chemicals are avoided and also using less hazardous chemicals or harsh conditions (Principle 3) thus enhancing the atom economy of the production system throughout all stages (Principle 2).

In addition, in pretreatment step for cellulose fibres production by using organosolv microwave-assisted method, this method is much more efficient and has less environmental impact compared to conventional heating (Principle 6). In other words, microwave heating has high energy efficiency as the surrounding heat loss can be reduced as compared to conventional heating, which is in good agreement with the principle of Design for Energy Efficiency.

In 2015, the United Nations created 17 Sustainable Development Goals (SDGs) and aimed at improving the planet and the quality of human life around the world to achieve them by 2030.[131] All United Nations (UN) Member States agreed on these 17 goals as a call-to-action for people worldwide to end poverty, ensure prosperity, and protecting the environment as can be seen in Table 1.

Sustainable development has been defined as development that meets the needs of the present without compromising the ability of future generations to meet their own needs. For the SDGs to be achieved, it is crucial to harmonize three core elements and the development must balance social, economic growth, and environmental sustainability. These elements are interconnected and all are crucial for the well-being of individuals and societies.[131] Nowadays, we all know that climate change is already impacting public health, food and water security. Tackling climate change and fostering sustainable development are two mutually reinforcing sides of the same coin; sustainable development cannot be achieved without climate action. It is very important that action in one area will affect outcomes in others. Thus, we need to achieve SDGs for improving sustainability by the combination with green chemistry principles.

As mentioned above, green chemistry principles were taken into consideration throughout this research. Also, SDGs goals which may be linked to green chemistry principles especially for SDG6 (Clean water and sanitation) which relate to reduce agricultural waste for synthesis of bio-derived mesoporous materials from rice husk for wastewater treatment. The as-obtained ordered bio-derived mesoporous material was used as adsorbent for methylene blue dye removal in aqueous solution which normally used in textile industry that can cause the water pollution. Agriculture and untreated wastewater are major threats to water quality in many parts of the world. So, it needed to improve farming practices and wastewater treatment, especially in regions with high population growth which also linked with waste prevention (principle 1).

Moreover, SDG12 (Responsible consumption and production) which relate to ensuring sustainable consumption and production patterns. This SDG12 could relate to many green chemistry principles, for example, 3 (Avoid hazardous substances), 4 (Designing Safer Chemicals), 5 (Safer Solvents), 6 (Energy Efficiency), 7 (Use of renewable feedstocks) and 10 (Biodegradation). As discussed before, both projects of microwave-assisted synthesis of bio-derived mesoporous materials from rice husk and rice husk-derived cellulose microfibres/nanofibres for bio-composite film preparation using mild conditions and also avoid harsh chemicals. Rice husk was defined as renewable feedstocks that can be processed through sustainable routes under microwave-assisted method which has advantage of using energy more efficiently and cost-effectively to reduce greenhouse gas emissions from conventional heating (such as pyrolysis, combustion, etc.). Moreover, bio-derived films reinforced by rice husk microfibres and nanofibres are biodegradable material which could be defined as smart material for sustainability.

Table 1 The list of 17 Sustainable Development Goals (SDGs)[131]

Goal 1	No poverty: End poverty in all its forms everywhere
Goal 2	Zero hunger: End hunger, achieve food security and improved nutrition and promote sustainable agriculture
Goal 3	Good health and well-being: Ensure healthy lives and promote well-being for all at all ages
Goal 4	Quality education: Ensure inclusive and equitable quality education and promote lifelong learning opportunities
Goal 5	Gender equality: Achieve gender equality and empower all women and girls
Goal 6	**Clean water and sanitation**: Ensure availability and sustainable management of water and sanitation
Goal 7	Affordable and clean energy: Ensure access to affordable, reliable, sustainable and modern energy
Goal 8	Decent work and economic growth: Promote sustained, inclusive and sustainable economic growth, full and productive employment and decent work
Goal 9	Industry, innovation and infrastructure: Build resilient infrastructure, promote inclusive and sustainable industrialization, and foster innovation
Goal 10	Reduced inequalities: Reduce inequality within and among countries
Goal 11	Sustainable cities and communities: Make cities and human settlements inclusive, safe, resilient, and sustainable
Goal 12	**Responsible consumption and production**: Ensure sustainable consumption and production patterns
Goal 13	Climate action: Take urgent action to combat climate change and its impacts

Goal 14	Life below water: Conserve and sustainably use the oceans, seas, and marine resources for sustainable development
Goal 15	Life on land: Protect, restore, and promote sustainable use of terrestrial ecosystems, sustainably manage forests, combat desertification, and halt and reverse land degradation and halt biodiversity loss
Goal 16	Peace, justice and strong institutions: Promote peaceful and inclusive societies for sustainable development, provide access to justice for all and build effective, accountable, and inclusive institutions
Goal 17	Partnerships for the Goals: Strengthen the means of implementation and revitalize the global partnership for sustainable development

1.4 The properties and structure of lignocellulosic biomass

Lignocellulose biomass consists of holocellulose (cellulose and hemicellulose) and lignin. Cellulose and hemicellulose are polymers which are linked to the lignin through covalent and hydrogen bonds which leads to a highly robust structure which is recalcitrant to depolymerization.[121,132-134]

Cellulose is a linear homopolymer of D-glucose that linked together in the chain by β-1,4-glycosidic linkages, which includes around several hundreds to more than 10,000 units of glucose in a cellulose molecule.[93,135-137] The molecular chain structure of cellulose shown in **Fig. 1 (a)**. Also, the cellulose strands bundle together binding to each other by hydrogen bonding of the hydroxyl-groups and thus form microfibrils (**Fig. 1 (b)**). Its water insoluble and resistant to depolymerization due to a crystalline matrix structure of cellulose.

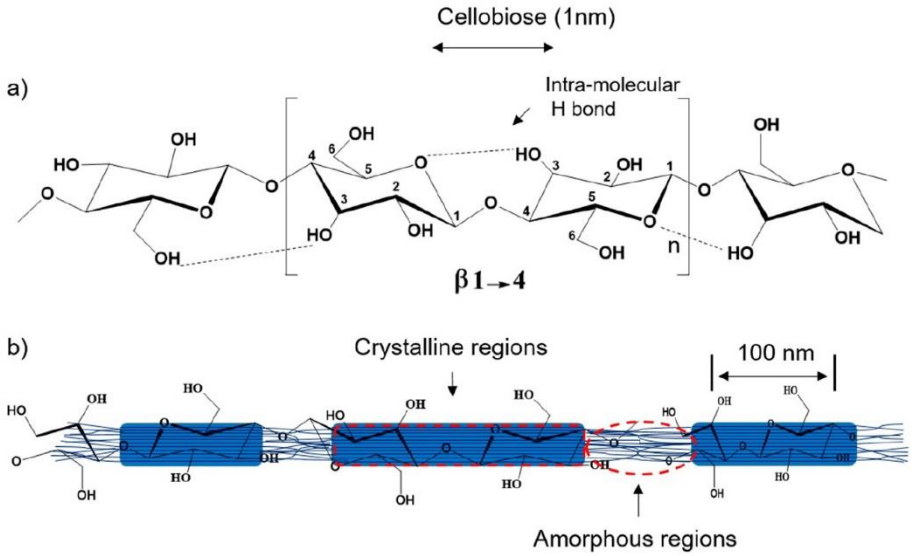

Fig. 1 (a) Schematic of cellulose repeating unit with the β-(1,4)-glycosidic linkage, dotted lines indicate intramolecular hydrogen bond; (b) hypothetical configuration of ordered (crystalline) and disordered (amorphous) regions in cellulose nanofibrils (used as is illustrated from Cellulose Nanomaterials-binding Properties and Applications: A Review by Tayeb *et al.*)[138]

Hemicellulose is a heteropolymer which is composed of several monomers. **Fig. 2** illustrates the molecular chain structure of hemicellulose. The main monomers including hexoses (β-D-glucose, α-D-galactose and β-D-mannose), pentose (β-D-xylose) and α-L-arabinose. Xylans are the major hemicelluloses in agricultural wastes.[139-142]

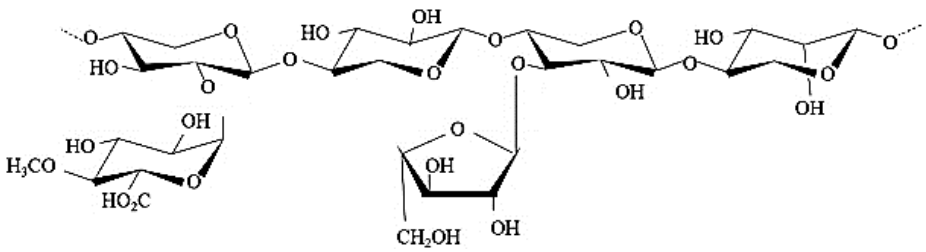

Fig. 2 Structure of hemicellulose

Lignin is a polymer made of mononuclear aromatic units in biomass cell walls which is composed of three phenolic compounds of phenyl propionic alcohol (*p*-coumaryl, coniferyl and sinaphyl alcohol) as can be seen in **Fig. 3**.[143-145]

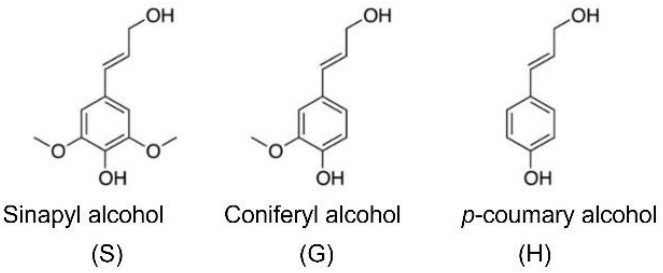

Fig. 3 The three main monomer building blocks of lignin

Generally, lignocellulosic biomass consists of 40-50 wt% cellulose, 20-30 wt% hemicelluloses and 10-25 wt% lignin as can be seen the structure of lignocellulosic biomass in **Fig. 4**.[146-148] The structure of lignin can shield the polysaccharide fraction from external environmental stresses and microbial attacks.[103,149] The highly recalcitrant to degradation and subsequent conversion, which usually leads to high product variation with low selectivity - influenced by the complex and highly ordered structure of cellulose.[93,137]

The structure of lignin can shield the polysaccharide fraction from external environmental stresses and microbial attacks. The high levels of recalcitrance to degradation and subsequent conversion, which usually leads to high product variation with low selectivity is influenced by the complex and highly ordered structure of cellulose.[93,137]

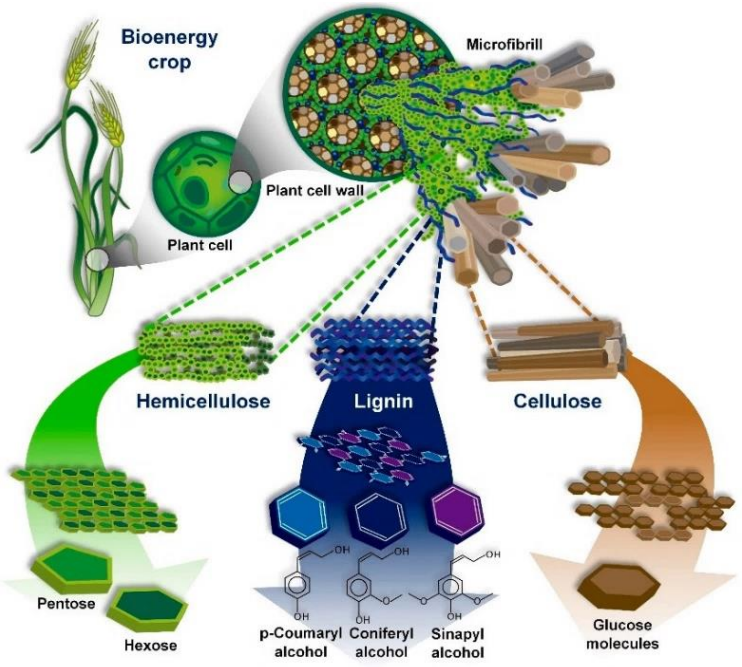

Fig. 4 Structure of lignocellulosic biomass (used as is illustrated from insight into pretreatment methods of lignocellulosic biomass to increase biogas yield: current state, challenges, and opportunities by J. U. Hernández-Beltrán et al.)[150]

Lignocellulosic biomass for valorisation in Thailand from agricultural wastes and weeds such as cassava, rice husk, rice straw, corncob, sugarcane bagasse, oil palm, water hyacinth, napier grass, mission grass and so forth.[1,2,7,151-153] In this study, the experimental will focus on rice husk which is a major by-product of rice production in Thailand.

1.4.1 Rice husk composition and the utilisation of rice husk

Rice (*Oryza sativa*) is one of the most important staple food crops used for human nutrition worldwide and it also the main agricultural product of Thailand. Rice husk (RH), a byproduct from the rice milling process, is an agricultural waste generated around 120 million tons annually (global) [37,108] and approximately 7.5 million tons per year of rice production in Thailand.[154]

The main components of rice husk consist of cellulose (25-35%), hemicellulose (18-21%), lignin (26-31%) and silica (15-17%).[103,155,156] Apart from these structured components,

some other inorganic matters i.e. aluminium, calcium and iron are also included owing to different chemical fertilizers being used and the difference in the soil chemistry in harvest area. [13,98,108,157]

The use of this waste biomass for utilisation has long been a topic of great interest due to its abundance. Many strategies have been explored to fabricate value-added products from rice husk which can be used for various applications.[38,103,158-160] In this work, a wide range of rice husk utilisation has been studied for example, the synthesis of bio-derived porous materials including silica, SBA-15 and carbon-silica composite materials and micro cellulose fibre and nano cellulose fibre extracted from rice husk using as a filler for films preparation to enhance their physical properties.

1.5 Value-added products derived from rice husk

1.5.1 Silica extraction derived from rice husk

Porous silica nanoparticles have been particularly interesting as a potential material for application in drug delivery, catalysis, gas adsorption and enzyme immobilization due to their highly hydrophilic surface, biocompatibility and inert properties.[161] The surface of silica consists of two types of functional groups which including silanol groups (Si-O-H) and siloxane groups (Si-O-Si).[162,163] The silanol groups are on the surface whereas the siloxane groups are non-reactive.[162,164]

Typically, silica derived from rice husk can be obtained by calcination at 500-800 ^{O}C for 5-6 h in muffle furnace.[165] High purity silica can be produced by controlled calcination after acid treatment.[163] Normally, the as-obtained rice husk ash contains about 95% of silica and other inorganic impurities such as MgO, Fe_2O_3, Al_2O_3 and CaO.[63,166] These impurities can be turned into soluble ions through acid pretreatment.[61,63,167] For this reason, rice husk is considered to be the most economically sustainable source of silica which highly porous material.[168]

1.5.2 The synthesis of SBA-15

Santa Barbara Amorphous No. 15 (SBA-15) is a highly stable mesoporous silica molecular sieve developed by researchers at the University of California at Santa Barbara. SBA-15 is

a mesoporous silica that has, due to its textural properties, regular mesoporous structure, high specific surface area, thermal and mechanical stability, distribution, and pore size.[73,74,169] Moreover, its high uniformity is beneficial in the removal of inorganic and organic contaminants in aqueous solutions.[79,84,170,171]

Mesoporous silica SBA-15 can be synthesized by incorporating self-assembly templates into the silica precursor such as tetraethoxysilane (TEOS) to create a mesostructured hybrid form.[54,172] Typically, synthesis of SBA-15 involves two stages including the hydrolysis–condensation stage and the aging stage or hydrothermal step with the overall process requiring a long time period of 40-48 h.[173]

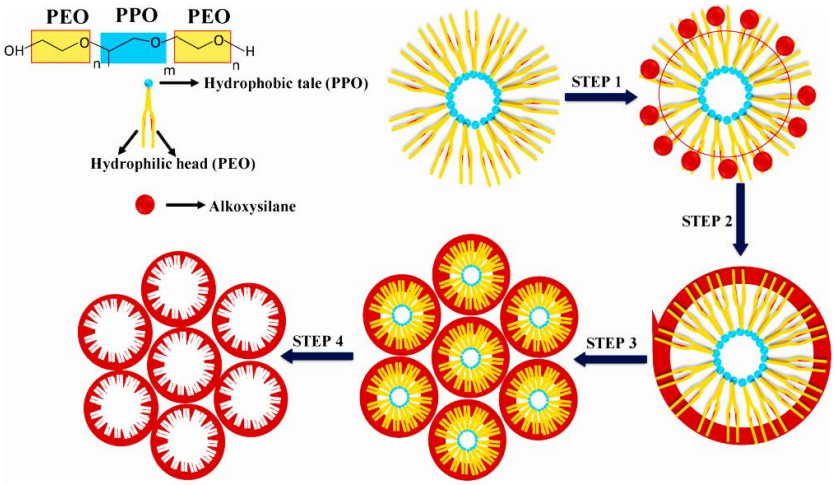

Fig. 5 Schematic of mesoporous SBA-15 silica formation (used as is illustrated from advanced synthesis strategies of mesoporous SBA-15 supported catalysts for catalytic reforming applications: a state-of-the-art review by Singh *et al.*)[174]

In the SBA-15 synthesis procedure, the surfactants (Pluronic P123) are added to an acidic solution (containing conc. HCl and water). The Pluronic P123 forms spherical micelles in the solution. The first steps involve the self-assembly of silica and template species- this occurs under vigorous mechanical or magnetic stirring at a lower temperature (between 25 and 50 °C). When the silica precursor is added it hydrolyses and bonds to the micelle forming a silica network that will become the walls in the particles. At this step the micelles become elongated from spheres to cylinders which together form a hexagonal

structure. The second step (hydrothermal treatment) -involving the mesostructure expansion and consolidation of siliceous pore walls which is usually performed under static conditions at a higher temperature.[76] During the hydrothermal step the temperature is elevated (from 35-40 ^{o}C to 80-120 ^{o}C) which reduces the hydrophilicity of the PEO chains. This leads to the PEO chains going into the core of the micelles and therefore expanding them (increasing the pore diameter) and pushing out the silica walls (reducing the silica wall in SBA-15).[174] The silica then becomes denser and closes the voids from the withdrawn PEO chain, thereby decreasing the microporosity in the wall. Altering the hydrothermal step (time or temperature) are common pore size controllers for SBA-15 material.[78] Many attempts have been investigated to control experimental conditions in both synthesis steps as well as to optimise their temperature and reaction time.[175] The formation of mesoporous SBA-15 can be seen in Fig. 5.

Typically, for the acidic synthesis condition of SBA-15, TEOS has been the most common choice of silica source in the syntheses, however TEOS is high cost. In comparison, silicate solution is cost effective and there are a few reports on the synthesis of SBA-15 by using silicate solution. However, the excess of silicate can lead to a poor structure of SBA-15 which has low specific pore volume. Thus, it is a challenge to utilise rice husk (waste biomass) for producing silicate solution as a silica source for the synthesis of mesoporous SBA-15 with well-ordered structure and high specific pore volume.

1.5.3 Bio-oil production derived from rice husk

Bio-oil is a complex mixture of oxygenated compounds formed by the fragmentation and depolymerization reactions of cellulose, hemicellulose and lignin and also significant amounts of water. It is usually a dark brown, highly viscous mixture which having a distinctive smoky odor and it can be produced from lignocellulosic biomass.[176,177]

Pyrolysis is considered to be a promising method for converting biomass into value-added products and aims to obtain a liquid product (bio-oil), char and gas through thermal decomposition of biomass in the absence of oxygen. Bio-oil yield depending on the composition of biomass feedstock, and pyrolysis parameters such as temperature,

pressure, heating rate and reaction time.[43] However, it cannot be directly used for fuels because of its high viscosity, high water and ash contents, low heating value, instability, and high corrosiveness. Thus, the upgrading of bio-oil properties is a necessary step before using as transportation fuel.[20,176,178]

Herein, the preliminary research on low temperature (<270 °C) microwave-assisted pyrolysis of rice husk to yield bio-oil which can be used as a carbon source for the carbon-silica composite materials production will be discussed in latter section. [30,32,46]

1.5.4 Carbon-silica composite materials (CSCs) derived from rice husk

Carbon-silica composites materials (CSCs) have drawn considerable attention due to a unique functionality of the graphitic carbon coating within the porous structure of silica supports such as SBA-15.[32] The coated polymer layer over the silica materials is subsequently converted to carbonaceous layers through a pyrolysis step or acid treatments to yield the CSCs. In a typical synthesis procedure, a solution obtained by dissolving a source of carbon such as sucrose, glucose and bio-oil to use as carbon source.[32,179,180] Then, silica source such as porous silica, SBA-15 or MCM-41 was added into the solution. A mixed solution was stirred and dried in the oven. Finally, carbonisation under a nitrogen atmosphere was used to produce CSCs. The carbon species in the materials vary significantly based on the carbonisation temperature, resulting in a continuum functionality ranging from polar hydroxyl groups to aromatic surfaces of CSCs. These CSCs can offer great prospect with relation to adsorption due to their combination of great mechanical stability, high adsorption capacities resembling those of activated carbons and porosity that allows them to be used as adsorbents for a range of species.[53,87,179,180]

In this research, the development of fully bio-derived composite materials was produced via the use of microwave-assisted pyrolysis of rice husk to produce bio-oil as carbonaceous matter and bio-derived SBA-15 as a silica source synthesised from silicate solution derived from rice husk, to provide both precursor necessary for the synthesis of carbon-silica composite materials.

1.6 Application of mesoporous materials for methylene blue dye adsorption

Methylene blue (MB) is a cationic dye soluble in water. Structure of MB shown in **Fig. 6**. MB is a heterocyclic aromatic chemical compound with the molecular formular of $C_{16}H_{18}ClN_3S$. It widely used in dyeing cottons, coating and coloring papers but it is toxic, carcinogenic, and non-biodegradable that can cause a severe threat to human health and environmental pollution, due to it being usually released into natural water. So, various treatment procedures have been investigated for MB dyes removal from wastewater such as photodegradation, chemical oxidation, and adsorption. Adsorption is the most commonly applied method of wastewater treatment because of its simplicity of design, insensitivity to toxic substances, efficiency in treatment and cost-effective.[181-183]

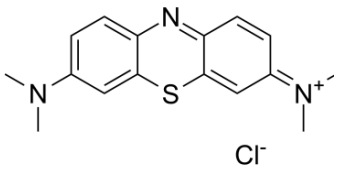

Fig. 6 Structure of methylene blue dye

1.7 Production of cellulose from rice husk

Cellulose is one of the representative bio-materials that is abundantly existed in natural plant such as agricultural waste and invasive plants. Defibrillated cellulose, including micro/nano cellulose fibre and cellulose nanocrystal could be extracted from purified cellulose fibres after a complete dissolution of the non-crystalline fractions by chemical hydrolysis, while the nano cellulose fibre produced by high pressure and/or shearing forces of mechanical fibrillation or acid hydrolysis after pretreatment.[184-186] Typically, nanocellulose is a strong light substance obtained from plant matter, including nanosized cellulose fibrils and crystals which could be obtained after acid hydrolyisis step.[187] As it is eco-friendly, and biodegradable and can be used extensively in biomaterials-based industries such as pharmaceutical, biomedical, and eco-friendly food packaging and

sensor materials. Production of nanocellulose from lignocellulosic biomass and its applications are shown in Fig. 7.

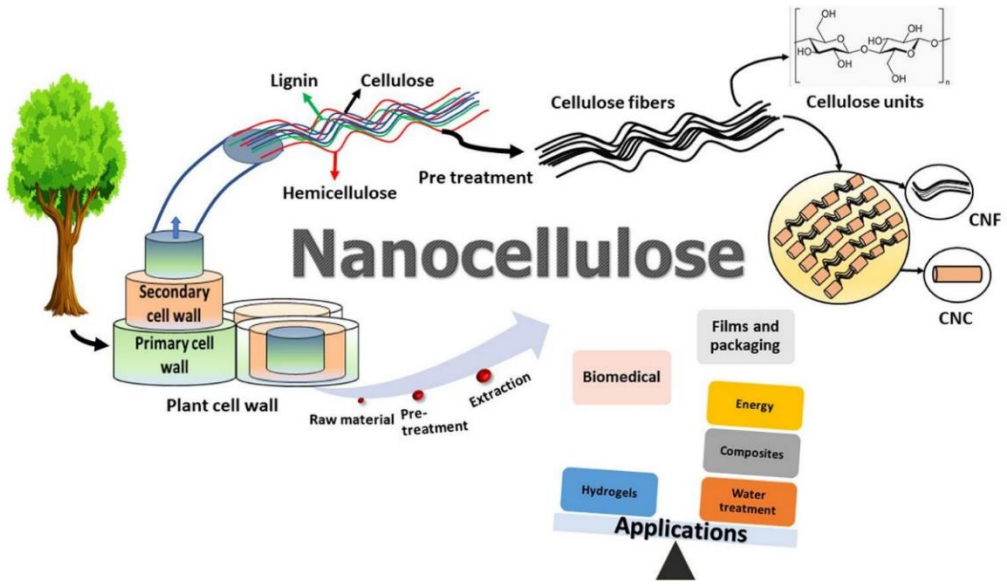

Fig. 7 Schematic of nanocellulose production and its applications (used as is illustrated from nanocellulose based biodegradable polymers by C. Zinge *et al.*)[139]

1.7.1 Cellulose microfibres and cellulose nanofibres

The cellulose strands bundle together binding to each other by hydrogen bonding of the hydroxyl-groups and thus form microfibres (in micron range) which consists of cellulosic domains (crystalline and amorphous domains).[121] Cellulose microfibres (CMF) and cellulose nanofibres have been great interest for used as a bio-based reinforcing agent. Generally, the fabrication of cellulose microfibres does not require acid hydrolysis, which used for converting microfibres to cellulose nanofibres.[136,188,189] Cellulose nanofibres (1–100 nm in width and >10,000 nm in length) has lower crystallinity than cellulose nanocrystal that can be used in various application, for example, packaging industries, cosmetics, energy storage systems, medical applications and etc.

1.7.2 Pretreatment step for extraction of cellulose microfibres and cellulose nanofibres from rice husk

The significant use of agricultural waste to useful products gives farmers a second income stream and avoids the use of fossil-based stuff. As described above section, lignocellulosic biomass is high in cellulose and undesired compounds, such as hemicellulose and lignin. The pretreatment process can be done before the extraction of nanocellulosic materials in order to remove the ashes, waxes, and undesired polymers such as hemicelluloses and lignin and enhance the quality of cellulose, pretreatment process is needed.[113,190,191]

1.7.2.1 Organosolv fractionation for isolation of cellulose, hemicellulose and lignin fraction from rice husk

Typically, organosolv fractionation was used for lignin isolation by using a variety of organic solvents such as ethanol, acetone, methanol, organic acids (i.e., formic acid, acetic acid), inorganic and organic bases, ketones, ethylene glycol, esters and combined solvents with and without catalysts (acid, alkaline, etc.).[192] The lignin from this fractionation process is known as organosolv lignin, which is a promising lignin source for depolymerisation to bio-based valuable chemicals because its structure is highly pure, unaltered, and sulfur-free- resulting in benefit for catalytic applications.[19,193,194] Moreover, hemicellulose extracted by organosolv extraction also possesses good activity, high purity and similar structure to that of native hemicellulose, providing the possibility for further utilisation. Due to ethanol and water being highly effective in microwave energy absorption, the combination of an organosolv process together with microwave heating can offer an interesting new technology for the utilisation of lignocellulosic biomass.[195]

1.7.2.2 Alkaline pretreatment for removal of non-cellulosic materials from rice husk

Recently, biomass pretreatment methods for removing non-cellulosic materials in agriculture wastes. The alkaline treatment is used for removing the amorphous polymer of hemicellulose and the remaining lignin. Generally, aqueous KOH or NaOH solution was used in this step (4–20 wt%), which is stirred with holocellulose for 1–5 h to remove alkali-soluble substances, hemicellulose and other impurities covering the external surface of

the fibres cell wall.[184] Then, the obtained solid products are washed by distilled water until reaching the neutral pH and finally dried to provide the as-obtained fibres products from this treatment.[94]

The important modification done by alkaline treatment is the disruption of OH bonding in the fibres network structure by ionizing the hydroxyl groups in fibres to become alkoxide which leads to the separation of the interfibrillar regions from the cellulose fibres. The possible mechanism shown in the following eq.

$$\text{Fibre-OH} + \text{NaOH} \rightarrow \text{Fibre-O-Na+(alkoxide)} + H_2O$$

The dissolution of noncellulosic constituent in alkali condition would create voids in the fibre structure which are responsible for producing great swelling and fine structure that can change the physical structure, dimensions, morphology and mechanical properties.

1.7.2.3 Bleaching step using chlorine-free method for delignification of rice husk

Bleaching step is an additional necessary step for further removing the residual cementing material- mainly lignin- in the alkali treated fibres, thus this step is also known as delignification. One of the simplest and greenest oxidizing agents available is hydrogen peroxide. Anomera, a company based in Quebec, Canada, has developed a process to produce nano cellulose fibre.[196] The use of hydrogen peroxide (H_2O_2) can act as oxidizing agent to delignify lignocellulosic fibres. Bleaching treatment step, the high exodus of lignin and hemicellulose which hinder its adhesion with polymer matrices could produce relatively pure cellulosic fibrils which provide enhanced interfacial adhesion with the polymer matrix. Generally, the bleaching step is necessarily repeated by increasing numbers of times or stages until the permanent white fabrics are achieved.[117,118]

1.7.2.4 Acid hydrolysis for nanocellulose production from rice husk

Acid hydrolysis is one of the main processes for the extraction of nanocellulose from lignocellulosic biomass. Because of the combination of ordered and disordered regions in cellulose chains, the disordered regions can be easily hydrolysed by acid and the ordered parts are left as the remaining.[136]

Sulfuric acid is the most commonly used reagent for acid hydrolysis since it can not only strongly isolate nanocrystalline cellulose, but also make the nanocellulose dispersed as a stable colloid system due to the esterification of hydroxyl group by sulfate ions.[187] The main controlling factors which affect the properties of obtained nanocellulose are reaction time, temperature, and acid concentration.[187] However, the drawback of acid hydrolysis is the acid wastewater generated from the washing process in order to neutralise the pH value of the nanocellulose suspension. The washing process is usually performed by adding cold water followed by centrifugation until neutral pH is reached.[94,197]

1.8 Application of cellulose for using as reinforcing agent in bio-composite film preparation

Micro and nano cellulose fibres have excellent properties and are biodegradable which is attractive for applications in many fields such as nanocomposite materials, surface modified materials, and transparent paper with special functions.[198-202]

Nanocellulose has been used as the filler in polymer matrix due to its excellent mechanical properties. Nanocomposite materials have special properties such as high mechanical strength with light weight and transparency.[203,204] Moreover, it was found that the mechanical properties of synthetic polymers, including the tensile strength and stiffness of the polymer reinforced by nanocellulose extracted from lignocellulosic biomass are significantly increased when compared with the pure base polymers.[205,206]

Besides, its low toxicity, renewable, good biocompatibility, and excellent physical properties, nanocellulose is also widely applied in medical field. Besides the above applications, nanocellulose can be also applied in other fields. For instances, it can be used as the thickener in cosmetics, the texturing agent in food, filler of special textiles, biodegradable package, CO_2 adsorbent, and oil recovery.[207]

Biodegradable films are thin layers which formed as plastic films. It generally produced through the casting technique or extrusion and are used to wrap foods. The

biodegradable films produced from biopolymers have a vital role to reduce the environmental impact caused by the disposal of nonbiodegradable plastic residues.[208,209] Polyvinyl alcohol (PVA) is a well-known synthetic polymer of great industrial value with unique characteristics. Among polymers such as polyethylene, polypropylene, etc. PVA is one of the biodegradable polymers which could be replace other polymers to produce biodegradable composite materials.[125,210] It has many advantages for a variety of applications including, film preparation, packaging materials, paper coatings and filtration materials due to its properties, for example, biodegradability, chemical resistance, water-solubility, biocompatibility, good optical and physical properties and good thermo-stability. However, PVA materials have relatively low mechanical strength that might need modification for preparation by using reinforcing agents.[211] Although the properties of pure PVA films are extensively customisable through alterations of these parameters, PVA alone is still generally too brittle and inflexible for many uses.[212]

1.8.1 Bio-composite films from biodegradable polymer and cellulose fibres from rice husk

Pure PVA film is transparent to UV light but has low tensile strength and low resistance to heat and moisture as well as does not have antibacterial activity. Therefore, polymer composites have gained a great deal of attention for being a simple method to enhance or modify physiochemical or biological properties of developed bio-composite films.[201,213] Many efforts have been carried out in order to improve the functional properties of these films to minimise the weaknesses of PVA, including mixing with other or other materials such as micro/nano cellulose fibres to enhance their properties.[125,213,214] Cellulose is a highly crystalline polymer which is the main structural compound of the plant cell wall, being one of the most abundant polymer on earth. It also has distinct properties such as biocompatibility, biodegradability, and chemical stability, make it a potential material as nanofillers for films preparation.[209,215,216]

1.9 Technologies for biomass conversion to value-added products in Thailand

Thailand has been successful agricultural society due to the country's well-endowed natural resources, from diverse crops to farming. Over the last decades, the growth in

bioenergy in Thailand has been significant. This can be considered as being due to biomass conversion, mostly from agricultural wastes and weeds due to their being widely abundant, low-cost, and non-edible materials.[1,151] A vast amount of them are generated each year but are not properly utilised. To address this issue, the use of these residues for conversion to value-added products such as biofuels, chemicals and alternative or sustainable materials, can achieve immense benefits to both the environment and economy.[1,6,217]

Interestingly, the major economy of Thailand is based on agricultural products. From the total crops that were harvested in Thailand in 2019 i.e. rice (18,716 Kilotonne), sugarcane (131,717 Kilotonne), cassava (29,368 Kilotonne), corn (470 Kilotonne), palm oil (15,535 Kilotonne)[158]. These residues are recognised as lignocellulosic biomass which, to the best of our knowledge, the Thai government, academic and industrial communities have been strongly focused on in an attempt to valorise them.[1,2,217]

Bioethanol and biofuel in Thailand are mainly produced by fermentation process (biochemical technology) that have been reported.[1,218] At the same time, the development of technologies for various applications has been continuously studied for conversion of various biomass feedstocks into a range of valuable products in the preceding decade, for example bioderived adsorbent, supercapacitor, carbon-based support and catalyst- support, ion exchanger, cellulose nano fibre and so on.[19,65,91,219,220]

Besides, water pollution has seen a dramatic increase in concern in Thailand due to industrial and agricultural processing, which generates a large quantity of toxic waste in the form of heavy metals, organic dyes and other toxic chemicals.[1,6,218] Historically, this has meant that waste effluents have been discharged to the natural resources. Now, manufacturing is facing escalating costs for correct disposal of hazardous waste.[221] Therefore, many researchers have been developing bioderived or carbon-based adsorbents derived from biomass residues with the aim to deal with waste management and water purification as well.[222,223]

Presently, it is still a significant challenge to develop processes with the aim of maximising conversion efficiency with high specificity of products as well as to minimise waste generated (close-to-zero-waste).[7,224]

1.9.1 Pretreatment/fractionation procedures for biomass treatments

In Thailand, several pretreatment and fractionation procedures have been applied for biomass treatment, for instance, alkaline pretreatment, hot compressed water (HCW) and organosolv pretreatment.[194,225,226] In this following part of various pretreatment and fractionation steps both advantages and disadvantages have been discussed in this section.

1.9.1.1 Alkaline pretreatment for removal of non-cellulosic materials from biomass

A pretreatment step is necessary to facilitate enzymatic attack of lignocellulosic structure, and alkaline pretreatment has been widely used for this stage.[111,112] Alkaline pretreatment is used for removal of lignin and decrease in the crystallinity of cellulose as well as to improve enzymatic digestibility of the pretreated biomass.[114] A synergistic enzyme system for the hydrolysis of alkali-pretreated rice straw has been optimised.[227] The investigation of two-stage pretreatment in dilute sodium hydroxide (2 %) followed by dilute sulfuric acid 1% combined with microwave radiation in order to enhance enzymatic hydrolysis of corncobs.[228] Microwave-assisted alkaline (NaOH) pretreatment that can effectively remove approximately 85% lignin content in mission grass by using 3% (w/v) NaOH and 15:1 liquid-to-solid ratio at 120 ^{O}C temperatures for 10 min.[229] The optimal conditions of the pretreatment step of tiger grass have been reported.[230] It was found that tiger grass treated with microwave-assisted alkaline (NaOH) pretreatment using 15:1 liquid-to-solid ratio (LSR) 1% (w/v) NaOH at 140 ^{O}C for 15 min, followed by microwave-assisted H_2SO_4 pretreatment using 15:1 LSR, 0.5% (w/v) H_2SO_4 at 200 ^{O}C for 5 min were the optimal condition for producing of the maximum monomeric sugar released (30.2 g/100g of NaOH-pretreated solids).

1.9.1.2 Hot compressed water (HCW) for delignification of biomass

Hot compressed water (HCW) is a hydrothermal method which is one of the promising approaches for fractionation.[107,108] A new green pretreatment method for removal of lignin in biomass residues has been developed by using hot compressed water with no catalyst required and selective hemicellulose elimination without cellulose destruction. Pressure is applied to maintain water in the liquid state at elevated temperatures in the range of 160–240 ^{O}C.[107,231] Under these conditions the superheated liquid water auto-ionises into hydronium ions which act as a promoter for cleavage of ester bonds of acetyl side chains of hemicelluloses - resulting in formation of acetic acid, which then autocatalyses hydrolysis of the hemicellulose and alteration of lignin structure. This leads to increase enzyme accessibility to the cellulose fibres.[231,232] The effect of lignin on the hydrolysis and/or dehydration of biomass under HCW condition has been reported.[109] In the presence of acid (H_3PO_4) in the system has influence on the hydrolysis/dehydration of biomass model compounds. The high amount of H_3PO_4 improved product yields of glucose, xylose, cellulose and xylan. To remove lignin the condition of 50 ^{O}C for 30 min with admixed 5% H_2O_2 were used. The percentages of cellulose, hemicellulose, and lignin after pretreatment are 64.0%, 15.0%, and 7.0%, respectively. The lignin content in the pretreated corncob was about 7%, and the lignin removal was achieved at 62% so the delignified corncob provided significant improvement of product yields. The HCW pretreatment for agricultural residues including sugarcane bagasse (BG), rice straw (RS), corn stover (CS), and empty palm fruit bunch (EPFB) was investigated.[107]

This step has been developed for improving digestibility of recalcitrant agricultural feedstocks prior to enzymatic hydrolysis into composite sugars which found that LHW pretreatment at 200 ^{O}C for 5–20 min resulted in high levels of hemicellulose solubilisation into the liquid phase and improvement on enzymatic digestibility of the solid cellulose-enriched residues.[233,234]

1.9.1.3 Organosolv pretreatment for fractionation of biomass components

Organosolv pretreatment is one of the more favorable procedures which has been applied for pretreatment of agricultural residues. Several advantages of this method include reduction of viscosity in the reaction mixture, high efficiency for removal of lignin and reducing lignin recondensation on the biomass surface.[235,236] Alcohols (i.e. ethanol and methanol) have been used as the primary solvents for organosolv fractionation of different lignocellulosic materials, however, organosolv pretreatment by low boiling point solvents is limited by the highly volatile and flammable nature of the solvents under high pressure conditions.[115,149,225] Energy loss from evaporation occurs when applying low boiling point solvents, leading to the process being impractical for small and medium scale.[236] Therefore, high boiling point solvents as alternatives in the organosolv process has been employed which include organic bases, ketones, and esters but it still has several drawbacks on equipment corrosion and releasing of toxicity from organic solvents and from organic acids (e.g. oxalic acid, acetic acid, formic acid, lactic acid, citric acid, maleic acid, and malonic acid) which can be used as catalyst in this process.[237-239] Additionally, a new novel organosolv technology, namely clean fractionation, has been studied, in which the lignocellulosic material is separated with a ternary mixture of ketone, ethanol, and water in the presence of an acid promoter (i.e. H_2SO_4), which selectively dissolves lignin and hemicellulose, leaving cellulose as an undissolved solid.[19,193] The resultant single phase liquor is treated with water obtaining an organic phase containing lignin and an aqueous phase containing hemicellulose which could offer high selectivity for separation of the primary biomass components.[226]

1.9.2 Thermochemical technology for biomass conversion

Most of thermochemical technology for biomass conversion in Thailand, conventional heating and pyrolysis, has been employed for the production of biochar, bio-oil and gaseous products for many decades.[41,177] Previously, coals such as lignite have been widely used as fossil resource of Thailand.[177,240] However, the careless utilisation of lignite has a negative effect on the environment from air pollution which increases the rate of

global warming. This concern has resulted in growing interests in alternative and sustainable energy resources including non-edible biomass resources, for example, agricultural residues, weeds, woods as well as industrial waste in terms of potential resources which are easily available sources with low-cost.[7,217]

1.9.2.1 Conventional pyrolysis for bio-oil and bio-char production from biomass

Generally, many reviews of pyrolysis process in Thailand have been focused on the investigation of the optimal condition of conventional pyrolysis conditions which are suitable for individual types of biomass, and cover topics such as types of reactor, heating rate, reaction time and pyrolysis temperature for biomass conversion,[241-246] which found that the optimum temperature for bio-char and bio-oil yield were usually obtained of about 500 ^{O}C and 550 ^{O}C, respectively.[41,177] Besides, slow pyrolysis conditions at low temperature (200- 300 ^{O}C), called torrefaction, is an alternative used in order to increase fixed carbon content and reduces volatiles content.[18]

1.9.2.2 Conventional hydrothermal process for production of bio-oil and value-added chemicals from biomass

Meanwhile, the condition of conventional hydrothermal process including hydrothermal gasification, hydrothermal liquefaction and hydrothermal carbonisation have been studied. Hydrothermal gasification for H_2 and CO production has been investigated to optimise conditions for different residues.[247,248] Hydrothermal liquefaction and solvothermolysis liquefaction to produce the bio-oil from sugarcane bagasse[249] and from corncob [250] have been reported. It was found that the oil from liquefaction with catalytic addition also had higher heating value than original raw biomass.

In case of pyrolysis, to obtain value-added chemicals, improve the quality of products or even upgrade bio-oil from selective pyrolysis of biomass, the control of reaction pathways has been attractive in recent years, with researchers using catalysts such as zeolites, aluminas, silica-aluminas and metal oxides.[251] Both torrefaction and pyrolysis are the most frequently used for pretreatment steps before further conversion into liquid products or energy. Fast pyrolysis is a potential conversion technique to transform biomass into liquid

bio-oil via the thermochemical process which can maximise the oil yield, a highly oxygenated acidic and viscous liquid.[252] It is expected to largely contribute in the short-term to bio-oil production because of its potential versatility and environmental acceptability.[176]

1.9.3 Microwave processing for production of bio-oil, bio-char and value-added chemicals from biomass

Notwithstanding that the microwave processing has been continuously adopted, it has not been widely used for biomass conversion in Thailand. There are just a few researches which report on microwave pyrolysis to produce char and bio-oil.[32]

Microwave carbonisation of biomass is one of the novel thermochemical technologies in which biomass is irradiated with microwaves, offering several advantages over conventional heating.[45,253] The pilot scale of continuous biomass carbonisation of coconut shell using microwave heating for producing charcoal and wood vinegar yields has been developed for reducing the production time of charcoal. However, this approach has some important limitations. A single standing wave would give a highly inhomogeneous temperature distribution in the heated sample, while a multi-mode cavity can be designed to provide more uniform heating.[254] So, the design of scaled-up reactor for microwave induced pyrolysis of oil palm shell had been studied to produce liquid bio-oil and gas.[253]

In this research, agricultural waste like rice husk which is abundant in Thailand, offer a suitable feed stock for biorefinery. Green and sustainable integrated processes play a vital role for utilisation of this residue to convert into a range of value-added products, for example, sustainable chemicals and bio-derived materials, bio-composite materials and so on. Conventional methods used toxic chemicals and some organic solvents as well as conventional heating for processing. The challenges for this research to achieve the goal of sustainable biorefineries are development of methods for valorisation of rice husk to produce value-added products i.e. SiO_2, SBA-15, bio-oil, CSCs and bio-composite films through microwave-assisted approaches such as microwave-assisted pretreatment,

microwave-assisted hydrothermal and microwave-assisted pyrolysis (to reduce significant reaction time and energy) as greener routes compared to conventional heating, as well as the attempt to design the methods to maximise incorporation of all materials throughout all stages to convert into final products by reducing the use of toxic chemicals and avoid harsh conditions which can be denoted as close-to-zero waste. Schematic overview of value-added products from rice husk shown in Fig. 8.

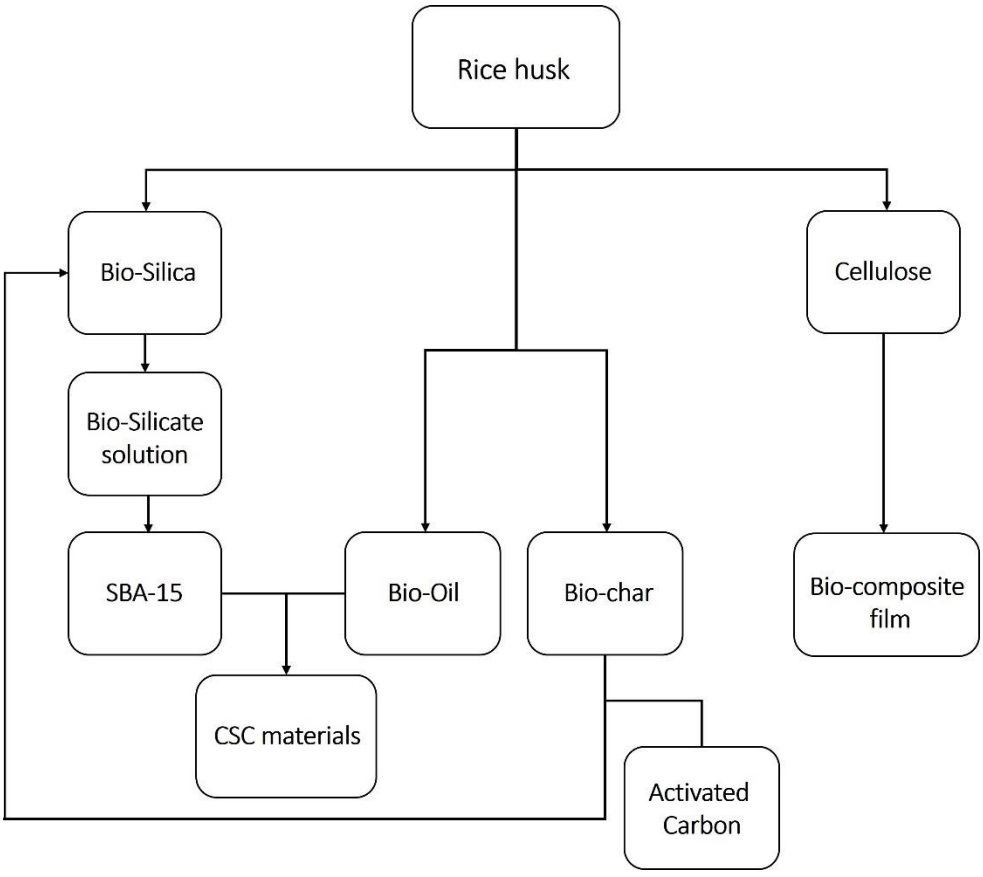

Fig. 8 Schematic overview of value-added products from rice husk

Chapter 2

Experimental

2.1 Material

Rice husk was collected from a local farm (Chiang Mai, Thailand), then washed with deionised water and dried at 110 ^{O}C overnight. Ground rice husks were separated using sieve machine particles (size <100 µm) before storing in sealed container prior to use for experimental.

2.2 Chemicals

PEG-PPG-PEG (Pluronic® P-123, $EO_{20}PO_{70}EO_{20}$), Tetraethyl orthosilicate (TEOS, 98%,), Sodium silicate solution, Hydrochloric acid (HCl: 36%), Sodium hydroxide (NaOH: ≥ 99.7%, glycerol (99%), Formic acid (CHOOH: 99%) and Hydrogen peroxide solution (H_2O_2 30%) were purchased from Sigma-Aldrich. Ethanol (≥ 99%) and Acetone (≥ 99%) and Acetic acid (≥ 99%) were purchased from Fisher Chemical. Methylene blue ($C_{16}H_{18}ClN_3S$) was purchased from Merck. Polyvinyl alcohol (PVA) (Approx. Mw 13,000 g mol-1, 98% hydrolysed) was purchased from Thermo Scientific. DI water was applied for all processes. All chemicals and reagents were used as received without further purification.

2.3 Instrumentation and analysis techniques

2.3.1 X-Ray Powder Diffraction (XRD)

XRD is a nondestructive technique that provides detailed information about the crystallographic structure, physical properties of materials and chemical composition or amounts of minerals species in sample. XRD can be used for the analysis of semi-crystalline fiber system as well. XRD patterns of the materials were investigated using X-ray diffractometers (XRD; Aeris Malvern Panalytical) and were recorded as a function of diffraction angle (2θ) from 5 to 40° with a step size of 0.01° and step time of 0.5 s, operating at 40 kV and 40 mA.

2.3.2 Crystallinity Index (CrI)

The crystallinity index (crystallinity percentage), which governs the mechanical and physical properties of nanocellulose is calculated employing an X-ray diffractometer

(XRD) with Cu Kα radiation at 0.154 nm operating at 40 kV and 40 mA. Crystallinity index (CrI) of the samples was calculated according to the following equation:

$$\mathrm{CrI}\ (\%) = \frac{(\mathrm{I_{200}} - \mathrm{I_{am}})}{\mathrm{I_{200}}} \times 100$$

Where I_{200} is the maximum intensity of 200 planes in crystalline region, whereas I_{am} is the intensity presenting amorphous region.

2.3.3 Small-angle X-ray Scattering (SAXS)

Small-angle X-ray scattering (SAXS) measurements were made using a Xenocs Xeuss 2.0 equipped with a micro-focus Cu Kα source collimated with Scatterless slits. The scattering was measured using a Pilatus 300k detector with a pixel size of 0.172 mm x 0.172 mm. Wide angled x-ray scattering (WAXS) was measured using a Pilatus 100k detector mounted at a 36° angle with a sample to detector distance of 0.164(1) m. This gave an angular range of 19 to 47° 2θ.

Samples were mounted between Kapton tape and measured for 20 minutes. An azimuthal integration of the 2D scattering profile was performed and the resulting data corrected for the absorption and Kapton background.

2.3.4 X-Ray Fluorescence spectroscopy (XRF)

The XRF is non-destructive analytical technique that uses the interaction of X-rays with material to determine its elemental composition. This technique is suitable for solids, liquids and powders. Semi-quantitative elemental analysis of samples was performed on a Horiba XGT 7000 X-ray analytical microscope. Powder samples (~1 g) were compressed into a holder and analysed using a standardless independent parameters method. Each measurement was repeated five times and the average was carried out. XRF can analyse the different elements occurring in a sample material, but will not indicate what phases are present in the sample and how they are combined. On the other hand, XRD will show details about the crystallography of materials.

2.3.5 X-ray Photoelectron Spectroscopy (XPS)

XPS is a quantitative technique for measuring the binding states of elements. A Kratos Axis Ultra DLD system was used to collect XPS spectra using monochromatic Al Kα X-ray source operating at 120 W (10 mA x 12 kV). Data was collected with pass energies of 160 eV for survey spectra, and 40 eV for the high-resolution scans with step sizes of 1 eV and 0.1 eV respectively. Data was analysed using CasaXPS (v2.3.24) after subtraction of a Shirley background and using modified Wagner sensitivity factors as supplied by the manufacturer. XPS is a surface-sensitive technique used to analyze the chemical state of elements and used for surface analysis. While, XRF is used for elemental analysis.

2.3.6 Ultraviolet–Visible Spectroscopy (UV-Vis)

UV-Vis spectroscopy is an analytical technique which can measure the amount of discrete wavelengths of UV or visible light that are absorbed by or transmitted through a sample in comparison to a blank or reference sample. The optical property was studied by a UV-visible spectrometer (Lambda 25, PerkinElmer) Scanning double-beam spectrometer for the UV/Vis range (between 200 nm and 800 nm); operation by PC. Ambient operating temperature between 15 ^{O}C and 35 ^{O}C, using a UV lamp with a resolution of 1 nm.

2.3.7 Attenuated Total Reflection Infrared Spectroscopy (ATR-IR)

Attenuated Total Reflection Infrared Spectroscopy was carried out using a Perkin Elmer FTIR/FTNIR Spectrum 400 Spectrophotometer. The measurement was achieved between 650 cm^{-1} and 4000 cm^{-1} with a resolution of 4 cm^{-1}, and a total of 16 scans were collected.

2.3.8 Brunauer-Emmett-Teller (BET) Surface Area Analysis

The porosity parameters of the all as-synthesised materials were determined by volumetric N_2 adsorption/desorption tests using a micromeritics TriStar II plus (at liquid nitrogen temperature (77K)). The samples were degassed at 180^{o}C for 4 h before measurement. The textural characterisation of samples was carried out by the physical adsorption-desorption isotherms of gas (N_2) and applying the mathematical models to quantify the specific surface area, pore-volume, average pore width, and pore size distribution. Generally, the most reported texture parameter is the specific surface area

(S_{BET}), determined by the model proposed by Brunauer-Emmett-Teller. Thus, S_{BET} was calculated by applying the BET equation to the first part of the adsorption isotherms ($0.05 < P/P_o < 0.3$). V_{total} is the pore volume at a relative pressure of 0.99. and D_{BJH} is the average pore diameter calculated using BJH method.

2.3.9 Thermogravimetric Analysis (TGA)

Netzsch STA 409 was used for TGA, each sample (~ 10 mg) was analysed under a nitrogen atmosphere at a flow rate of 100 mL/min to prevent any thermoxidative degradation with a temperature range from 25°C to 800°C at a heating rate of 10°C/min. The data was collected as a txt. file and processed using Origin 2018TM software.

2.3.10 Simultaneous Thermal Analyser (STA 625)

PL Thermal Sciences STA 625 was also used for TGA analysis. A small amount (~ 7 mg) of sample was accurately weighed into an aluminum TGA pan and heated under nitrogen flow to avoid oxidation of the sample. The programmed temperature started at room temperature, and then increased up to 625 ^{o}C at the rate of 10 ^{o}C /min. To monitor the thermal behavior of the samples STA625 instrument with a heating range of 25 to 625 ^{O}C under the nitrogen atmosphere is used. The derivative of thermograms (DTG) was plotted by the primary thermograms.

2.3.11 Scanning Electron Microscopy (SEM)

Samples were diluted to form 0.01 wt% in absolute ethanol before being dropped onto 200 mesh grids with a carbon support film for 2 h, to allow for evaporation of solvent. Morphology of materials were investigated using a JEOL JSM- 6490LV scanning electron microscope at an accelerated voltage of 15−20 kV after gold or platinum coating by a JEOL JFC−1100 E sputtering device for 85 seconds prior to SEM observation.

2.3.12 Transmission Electron Microscopy (TEM)

Prior to TEM characterisation, powder samples were suspended in absolute ethanol in microcentrifuge tubes and were deposited onto 200 mesh grids with a carbon support film for 2 h, to allow for evaporation of solvent. Then, the dried grid samples were loaded

onto an entry sample holder. Materials were investigated under the various magnifications on transmission electron microscopy at 120 kV (TEM Tecnai 12 BioTWIN instrument with a SIS Megaview 3 camera at a 76-acceleration voltage). TEM was carried out at the Department of Biology, University of York. SEM and TEM were used to determine size and morphology of samples. The measure of particle size of samples was carried out using ImageJ.

2.3.13 ^{1}H Nuclear Magnetic Resonance (^{1}H NMR)

^{1}H NMR were carried out using a JEOL JNM-ECS400 NMR operating at 400 MHz. A single pulse acquisition method was used with a relaxation delay of 4s.1024 scans were taken for each sample. The chemical shifts were recorded at 25 °C in $CDCl_3$.

2.3.14 ^{13}C Nuclear Magnetic Resonance (^{13}C NMR)

^{13}C NMR were carried out using a JEOL JNM-ECS400 NMR operating at 400 MHz. A single pulse acquisition method was used with a relaxation delay of 4s. 2048 scans were taken for each sample. The chemical shifts were recorded at 25 °C in $CDCl_3$.

2.3.15 Solid state ^{13}C cross polarisation magic angle spinning (CPMAS) Nuclear Magnetic Resonance (NMR)

Solid State ^{13}C cross polarisation magic angle spinning (CPMAS) spectroscopy was performed on a 400 MHz Bruker Avance III HD spectrometer using a Bruker 4 mm H(F)/X/Y triple-resonance probe and 9.4T Ascend superconducting magnet. Solid State NMR experiments were run with a spin rate of 10,000 +/- 2 Hz, recycle delays of 1 s, a total number of 512 scans and a linearly ramped contacted pulse of 1 ms. The resulting spectra were processed and analysed using MestReNova software.

2.3.16 Gas Chromatography-Mass Spectrometry (GC-MS)

Gas chromatographic measurements were made with an Agilent Technologies HP 6890 gas chromatograph (or Agilent Technologies 7890B gas chromatograph), with a flame ionisation detector (GC-FID), fitted with a Rxi-5HT capillary column (30 m, 250 mm x 0.25 mm nominal, max temperature 400°C). Helium was used as the carrier gas at a flow rate

of 10 mL/min with a split ratio of 5:1 and a 1 µl injection. The initial oven temperature was 50°C and was increased instantly at a rate of 30°C/min to 300°C and held at this temperature for 5 min, with a total run time of 13.3 min. Injection temperature was 250°C and the detector temperature was 250°C. Electron Ionisation took place on a Clarus 560 MS. Scans were run over 40 m/z to 500 m/z, with a solvent delay of 2 min. The total run time was 13.33 minutes. The MS data was analysed using NIST library version 2.2.

2.3.17 Mechanical testing

The tensile properties of the-as prepared films were investigated by using an Instron® 3367 Universal Testing machine. Prior to tensile testing the as-prepared samples were cut into film strips following the Standard Test Method for Tensile Properties of Thin Plastic Sheeting (ASTM D882) at 25 ^{O}C. Five samples of each film were tested and the standard deviation values were reported which include tensile strength (MPa) and elongation at break (%).

2.4 Methodology

Project 1: Microwave-assisted synthesis of bio-derived mesoporous materials from rice husk for methylene blue removal

In order to extract high purity of silica from rice husk, the process to remove organic components and metallic impurities was investigated. Silica was extracted from rice husk through a simple acid pretreatment (chemical pretreatment) by conventional method and microwave-assisted method adopted from literatures. [64,168]

2.4.1 Preparation of silica derived from rice husk

Yield of silica derived from rice husk

The yield (%) of silica were calculated by Equation,

$$\%\ \text{Yield} = \frac{W_C}{W_0} \times 100\%$$

Where, W_C is the white silica powder weight (g)

W_0 is the weight of dried rice husk (g)

2.4.1.1 Preparation of silica derived from rice husk via conventional method

10 g of dried rice husk was treated by conventional heating via reflux method using 100 ml of 1 M HCl at 100^{o}C for 3 h. Then the mixture was filtrated and washed with DI water several times and dried at 110^{o}C overnight. After that, the resulting white silica powder (1.3430 g) was obtained by calcining at 700 ^{o}C for 3 h.

2.4.1.2 Preparation of silica derived from rice husk via microwave-assisted acid treatment

In this work, silica extracted from rice husk was also explored by using microwave-assisted acid treatment prior to calcination. The air-dried milled rice husk (2.5-5.0 g) was mixed with 37.5-50.0 ml of 1 M HCl at three different solid-to-liquid ratios (1:10, 1:15 and 1:20). Then the mixture was irradiated using CEM MAR 6 (One Touch^{TM} microwave, using EasyPrep^{TM} Plus Easy Prep Teflon 100 ml closed vessels) with a ramp time of 15 min followed by three different holding times (30 min, 45 min and 50 min) at 100 ^{o}C. The resulting mixtures were filtered and then washed with DI water several times until pH ~ 7. The resulting solid was dried at 110 ^{O}C overnight prior to calcination in the muffle furnace at 700^{o}C. After calcination, white powder of silica (0.3-0.6 g of SiO_2/2.5-5.0 g of raw rice husk) was obtained (RH-SiO_2).

The purity of both silicas prepared from conventional method and microwave-assisted method were analysed by X-ray Fluorescence (XRF) spectrometer.

2.4.2 Preparation of bio-derived sodium silicate solution from rice husk

In this part, sodium silicate solution (RH-SS) was prepared from silica extracted from the previous section (see **Section 2.4.1.2**). 1.0 g of the white powder of silica was dissolved in 1M NaOH (10 ml) and subjected to microwave irradiation at 80 ^{o}C with a holding time of 30 min.

The absorbance (%) of commercial sodium silicate solution (Com-SS) at the concentration between 10%-80% were measured by FTIR technique. The calibration curve of absorbance (%) at wavenumber 1000 cm^{-1} versus concentration (%) were used to calculate the accurate concentration of RH-SS for synthesis of SBA-15 in the next part.

2.4.3 Synthesis of SBA-15 via conventional method using different silica sources

In this part, synthesis of SBA-15 involves dissolving of template (2 g of Pluronic P123) in acidic solution followed by addition of silica source (shown in **Table 2**). Then a mixed solution is continuously stirred and heated (hydrolysis step) at 40 ^{o}C for 24 h. Then the mixture kept at 85 ^{o}C (hydrothermal step) for 24 h.[255] Commercial silicate solution denoted as Com-SS and silicate solution derived from rice husk denoted as RH-SS

Table 2 Summary of various conditions for SBA-15 synthesis via conventional method

Sample	Synthesis conditions		
	Silica source	Hydrolysis step	Hydrothermal step
SBA-15-T-C	TEOS	40^{o}C for 24 h	85^{o}C for 24 h
SBA-15-S-C1	100% Com-SS		
SBA-15-S-C2	50% Com-SS		
SBA-15-S-C3	17.5% Com-SS		
SBA-15-RH-C	17.5% RH-SS		

2.4.3.1 Synthesis of SBA-15 via conventional method using tetraethyl orthosilicate (TEOS) as a silica precursor

In the synthesis of SBA-15 through the conventional method using tetraethyl orthosilicate (TEOS) as silica source. The mixed solution is heated (hydrolysis step) at 40 ^{o}C for 24 h and then aged (hydrothermal step) at 85 ^{o}C for 24 h.

In a typical synthesis of SBA-15, 2 g of Pluronic P123 (as a template) was dissolved in 75 g of aqueous HCl solution (1.2 M) and then 4.25 ml of TEOS was added into the solution.[256] The mixture was stirred vigorously at 40 ^{O}C for 24 h. Then, the mixture was heated at 85 ^{O}C for 24 h (without stirring). Finally, the as-synthesised material was filtered, washed by DI water several times, and freely dried at room temperature. The precipitates were calcined at 550 ^{O}C for 6 h to remove template. Finally, the as-synthesised SBA-15 was obtained (1.5578 g) and denoted as **SBA-15-T-C**.

2.4.3.2 Synthesis of SBA-15 via conventional method using commercial sodium silicate solution as a silica precursor

SBA-15 was synthesised by using Pluronic P123 as template and commercial sodium silicate solution (Com-SS) as a silica precursor. 2 g of Pluronic P123 was dissolved in a solution of 18 g DI water and 2.32 g of conc. HCl. 19 g of commercial sodium silicate solution at three different concentrations (100% Com-SS, 50% Com-SS and 17.5% Com-SS) were added dropwise into the mixture solution, stirred vigorously at 40 ^{O}C for 24 h and kept without stirring at 85 ^{O}C for 24 h. The precipitates were washed with DI water several times, dried at room temperature, and calcined at 550 ^{O}C for 6 h. Finally, the SBA-15 materials were obtained (1.5757g, 1.4095 g and 1.2527 g) and denoted as **SBA-15-S C1**, **SBA-15-S C2** and **SBA-15-S C3**, respectively.

2.4.3.3 Synthesis of SBA-15 using sodium silicate solution derived from rice husk as a silica precursor via conventional method

SBA-15 materials are prepared by using Pluronic P123 as a template in acidic media and using sodium silicate solution (RH-SS) derived from rice husk (**Section 2.4.2**) as silica precursor. 2 g of Pluronic P123 was dissolved in a solution of 18 g DI water and 2.32 g of conc. HCl. Then, 19 g RH-SS was added dropwise into the mixture solution, stirred vigorously at 40 ^{O}C for 24. After aging the mixture solution without stirring at 85 ^{O}C for 24 h. The precipitates were washed with DI water several times, freely dried at room temperature. Then subjected to muffle furnace at 550 ^{O}C for 6 h. Finally, the as-synthesised SBA-15 was obtained (1.2789 g) and denoted as **SBA-15-RH-C**.

2.4.3.4 Synthesis of SBA-15 using sodium silicate solution derived from rice husk as a silica precursor via microwave-assisted method

In this part, the synthesis of SBA-15 via microwave-assisted method was carried out in CEM MAR 6. Pluronic P123 (2 g) was dissolved in a solution of 18 g DI water and 2.32 g of Conc. HCl. Then, 19 g of silicate solution derived from rice husk (RH-SS) was added dropwise into the mixture solution, stirred vigorously at 40 ^{O}C for 24 h. Then, the solution was transferred to a sealed vessel and subjected to microwave irradiation at 170 ^{o}C

(power 800 W) with a holding time of 50 min. After cooling and removal from the microwave, the precipitates were washed with DI water several times, dried at room temperature. Finally, the as-synthesised SBA-15 was obtained after calcination at 500 ^{O}C for 3 h.

Then, the effect of temperature in hydrothermal step via microwave-assisted method and the effect of both reaction time of hydrolysis and hydrothermal steps were also studied in the following part.

2.4.3.5 Effect of temperature in hydrothermal step via microwave-assisted method

The synthesis of SBA-15 was carried out via a microwave-assisted method using sodium silicate solution derived from rice husk as a silica precursor as described in the previous part (see **2.4.3.4**). The textural and morphological properties of silica materials are extremely important for applications. To explore the effect of irradiation temperature of hydrothermal step on the structural and physical properties of SBA-15, the range of temperature from 85 ^{O}C to 170 ^{O}C was used for SBA-15 preparation in this work.[72,175]

The effect of reaction temperature in hydrothermal step was studied using microwave-assisted method. After hydrolysis step at 40 ^{o}C for 6 h, followed by the hydrothermal step under microwave irradiation at various temperatures (**Table 3**). Then, the solutions were transferred to sealed vessel and subjected to microwave irradiation (power of 800) at three different temperatures (85 ^{o}C, 100 ^{o}C and 170 ^{o}C) with a holding time of 50 min. After cooling and removal from the microwave, the precipitates were washed with DI water several times, dried at room temperature, and calcined at 500 ^{O}C for 3 h. Finally, the as-synthesised SBA-15 of **MHT-85**, **MHT-100**, **MHT-170** were obtained and characterised.

Table 3 The summary of various conditions for synthesis of SBA-15 via microwave-assisted method at different hydrothermal temperatures

Sample	Synthesis conditions	
	Hydrolysis step	Hydrothermal step
MHT-85		85 ^{O}C for 50 min
MHT-100	40 ^{o}C for 6 h	100 ^{O}C for 50 min
MHT-170		170 ^{O}C for 50 min

2.4.3.6 Effect of reaction time of hydrolysis and hydrothermal steps

In this part, the effect of both hydrolysis time and hydrothermal time for synthesis of SBA-15 derived from rice husk using different time for hydrolysis (4 h, 6 h, 20 h and 24 h) and microwave-assisted hydrothermal at 170 ^{o}C for 30 min and 50 min were investigated as the same as previous procedures (described in section 2.4.3.5).[175]

2.4.4 Production of bio-oil derived from rice husk using microwave-assisted pyrolysis

As mentioned in Chapter 1, one of the objectives of the present work is to study an alternative way to utilise the bio-oil derived from rice husk without upgrading process as the carbonaceous phase in carbon-silica composite materials (CSCs).

The influences of different pretreatment methods on the characteristics of pretreated rice husk and the subsequent fast pyrolysis in terms of product yields, composition, and chemical properties of the as-produced bio-oil were studied.

The microwave-assisted pyrolysis was carried out in CEM Discover SP microwave reactor with round bottom flask (25 ml) which contained 10 g of sample and combined with condenser. The experiments were done in a dynamic power mode with the established MW power limit of 200W. The target temperature was 270 °C, which was maintained for 20 mins. The pressure limit was set to 300 PSI. The vessels were cooled with compressed air and the pyrolysis residues (mixture of bio-oil and bio-char) were washed with acetone

and then evaporated in vacuo to afford bio-oil. The acetone washed residues were dried at 60 ^{o}C for 24 h to yield biochar.

Characterisation of three bio-oil samples include raw rice husk (BO1), DI water pretreated rice husk (BO2) and HCl pretreated rice husk (BO3) were carried out using gas chromatography-mass spectrometry (GC-MS), Fourier transform infrared radiation (FTIR), ^{1}H and ^{13}C nuclear magnetic resonance spectroscopy (NMR).

2.4.4.1 Pretreatment of rice husk with deionised water

The air-dried milled rice husk (solid-to-liquid ratio 1:10) underwent microwave-assisted pretreatment using DI water at 160 ^{o}C for 50 min. After cooling and removal from the microwave, the resulting rice husk was filtered and dried at 80 ^{o}C for 24 h to obtain the pretreated rice husk to produce bio-oil in the next step.

2.4.4.2 Pretreatment of rice husk with hydrochloric acid

The air-dried milled rice husk (solid-to-liquid ratio 1:10) underwent microwave-assisted pretreatment using 1M HCl at 120 ^{o}C for 50 min. After cooling and removal from the microwave, the precipitate was filtered. Then the sample was washed with DI water several times and dried at 80 ^{o}C for 24 h to obtain the pretreated rice husk to produce bio-oil in the following step.

2.4.5 Carbon-silica composite (CSC) materials derived from rice husk

The carbon-silica composite materials fully (100%) derived from rice husk were synthesised using wet impregnation, followed by carbonisation at different temperatures in the range of 300-800 ^{O}C. The as-obtained SBA-15 derived from rice husk (as prepared in previous section) was used for CSC materials preparation as a silica support. Also, the bio-oil derived from rice husk (BO3) was used as a carbon precursor for the CSCs.

2.4.5.1 Optimisation of the SBA-15 and bio-oil ratio for carbon-silica composite preparation

It is well demonstrated that the ratio of silica and bio-oil amount is a significant factor in controlling the pore width of the resultant composite and the thickness of the

carbonaceous layer. To optimise the appropriate ratio of silica/bio-oil for carbon-silica composite preparation, mixing solution was prepared by dissolving different amounts of bio-oil into the desired amount of acetone, followed by the addition of SBA-15. After shaking at room temperature overnight, the mixture was then evaporated to remove acetone and the resultant solid was carbonised under a nitrogen atmosphere at 500 ^{o}C. Finally, the CSC samples were obtained and denoted as **CSC 1:1** (silica-to-oil ratio 1:1), **CSC 1:2** (silica-to-oil ratio 1:2), and **CSC 1:4** (silica-to-oil ratio 1:4).

For example, 0.5 g of SBA-15 was added to a solution of 0.5 g of bio-oil dissolved in 2 ml of acetone, shaken at room temperature overnight. After acetone was removed on a rotary evaporator then subsequently carbonised at 500^{o}C under nitrogen atmosphere and finally the carbon-silica composites (CSC1:1) were obtained.

2.4.5.2 Effect of temperature for carbon-silica composite preparation

Briefly, the SBA-15 materials are impregnated with bio-oil (silica-to-oil ratio 1:4) diluted with specific amount of acetone. After shaking at room temperature overnight, the mixture solution was then evaporated to remove solvent and subsequently carbonised at different temperatures (from 300^{o}C to 800 ^{o}C) under nitrogen atmosphere and finally the carbon-silica composites were obtained and denoted as **CSC4-300**, **CSC4-400**, **CSC4-500**, **CSC4-600**, and **CSC4-800**.

2.4.6 Study of methylene blue adsorption by as-synthesised mesoporous materials derived from rice husk

2.4.6.1 UV-Vis quantification of methylene blue

The quantitative analysis of methylene blue (MB) was performed on Jasco V-550 UV-Vis spectrometer at 664 nm. A series of concentrations (2-10 ppm) of methylene blue were prepared in DI water. In adsorption analysis, the aqueous mixtures were centrifuged, and the clear supernatant solution subjected to UV-Vis analysis. A calibration curve of MB was used for the determination of MB adsorption onto as-prepared materials.

2.4.6.2 Kinetics of methylene blue adsorption

Batch adsorption experiments were carried out with 30 ml of 100 ppm methylene blue and 15 mg of each SiO_2, SBA-15 and CSC4-600. An adsorbate solution was mixed with an adsorbent and shaken at 150 rpm. A small amount of sample (approximately 1 ml) was withdrawn at different time intervals, centrifuged, and subjected to UV-Vis analysis. The measurements were taken until the adsorption equilibrium was reached (360 min). The adsorption capacity at each time point was calculated and plotted against time.[256]

The adsorption capacity at each time q_t (mg/g) was calculated as follows:

$$q_t = \frac{C_0 - C_e}{W} \times V$$

Where, C_0 (mg/g) is the initial concentration of methylene blue

C_e (mg/g) is the equilibrium concentration of methylene blue

W (g) is the mass of mesoporous silica

V (l) is the volume of the aqueous solution

The removal rate of MB was calculated by the following equation:

$$\%\ \text{Removal} = \frac{C_0 - C_e}{C_0} \times 100\%$$

To further explore the sorption rate of the adsorption process, the dynamics data were tested with pseudo-first order and pseudo-second order kinetic models.

The pseudo-first-order kinetic equation is given as:

$$\log(q_e - q_t) = \log q_e - \frac{k_1}{2.303} k_1 t$$

where, k_1 (1/min) is the adsorption rate constant of the model

The pseudo-second order kinetic equation is given as:

$$\frac{t}{q_t} = \frac{1}{k_2 q_e^2} + \frac{1}{q_e}\, t$$

where, k_2 (1/min) is the adsorption rate constant of the model.

2.4.6.3 Adsorption isotherms

Batch experiments were done to study the adsorption capacities of methylene blue onto SiO_2, SBA-15 and CSC4-600. All sorption operations were carried out by shaking the solution containing dose of adsorbent 0.5 g/l in the desired concentration of methylene blue (10-120 ppm for RH-SiO_2 and 20-200 ppm for SBA-15 and CSC4-600) and shaking at 150 rpm until concentration equilibrium was reached (60 min for SBA-15 and CSC4-600 and 180 min for SiO_2).[19,256]

Each mixture was centrifuged and determined with the UV method (at 664 nm). The equilibrium adsorption capacity of adsorbent q_e (mg/g), is calculated with the formula described below:

$$q_e = \frac{C_0 - C_e}{W} \times V$$

The isotherms data are analysed by adsorption models (Langmuir and Freundlich) to establish the most appropriate adsorption mechanism.

Langmuir model assumes that uniform reversible adsorption takes place on the surface of adsorbent, no interaction occurs among the adsorbed molecules. It forms a monolayer molecular sorption. The formula can be presented in the expression:

$$\frac{C_e}{q_e} = \frac{1}{(q_{max})b} + \frac{C_e}{q_{max}}$$

where, C_e is the equilibrium concentration of dye (mg/l)

q_e is the amount of adsorbate adsorbed per unit of mass of adsorbent (mg/g) at equilibrium

q_{max} is the monolayer adsorption capacity (mg/g)

b is the Langmuir constant

The separation factor (R_L) is an important Langmuir a-dimensional constant which expresses the feasibility of adsorption and can be expressed by the following equation:

$$R_L = \frac{1}{bC_0 + 1}$$

where, C_0 is the initial adsorbate concentration (mg/L)

R_L is the value that indicates the shape of isotherm to be unfavorable ($R_L > 1$), linear ($R_L = 1$), favorable ($0 < R_L < 1$), and irreversible ($R_L = 0$), respectively

Freundlich isotherm predicts that the sorption occurs on the surface of adsorbent through heterogeneous energy, the adsorbed molecules are interactive and the amount of solute adsorbed increases infinitely at higher concentration. It can be expressed in the below equation:

$$\log q_e = \log K_f + \frac{1}{n} \log C_e$$

where, K_f is the Freundlich parameter which is related to adsorption capacity (mg/g)

n is the heterogeneity factor, indicating the adsorption intensity

The factor (1/n) indicates the type of isotherm which are irreversible (1/n = 0) favorable ($0 < 1/n < 1$) and unfavorable ($1/n > 1$), respectively.

2.4.6.4 Thermodynamic adsorption study

To determine the effect of temperature on MB adsorption. Thermodynamic constants including enthalpy change (ΔH°), Gibbs free energy change (ΔG°), entropy change (ΔS°) were calculated to understand the nature and feasibility of the adsorption process of MB. This was performed by calculating the thermodynamic parameters using the following equations:

$$\ln k_c = \frac{\Delta S^\circ}{R} - \frac{\Delta H^\circ}{RT}$$

$$\Delta G^\circ = \Delta H^\circ - T\Delta S^\circ$$

In the case that q_{max} is increased with the increase of temperature, this indicates that high temperature is beneficial to the MB adsorption. If the slope of $\ln(Q_e/C_e)$ versus temperature fitting curve is below zero, then this indicates the endothermic nature of the adsorption process. The temperature dependent adsorption was evaluated by Van't Hoff equation:

$$\ln\left(\frac{Q_e}{C_e}\right) = \frac{\Delta H}{\Delta R} - \frac{\Delta S}{R}$$

where, R is the universal gas constant (8.314×10^{-3} kJ/mol K)

T is the adsorption medium absolute temperature (K).

k_c is a dimensionless thermodynamic equilibrium constant based on equation above.

Plotting $\ln(Q_e/C_e)$ against 1/T gives a straight line with slope and intercept equal to $-\Delta H/R$ and $\Delta S/R$, respectively. Some methods were proposed for the determination of a dimensionless thermodynamic equilibrium constant.

$$\Delta G° = -RT \ln k_c$$

These parameters indicate the trend for the thermodynamic nature of the adsorption process deduced for the estimated thermodynamic constants (i.e. $\Delta H°$, $\Delta G°$, and $\Delta S°$).

2.5 Methodology

Project 2: Rice husk-derived cellulose microfibres/nanofibres for bio-composite film preparation

2.5.1 Organosolv fractionation of rice husk using microwave-assisted method

In this work, organosolv fractionation of rice husk was investigated by using ethanol and DI water in the presence of formic acid for fractionation of cellulose-rich solid fraction, a hemicellulose-rich water-soluble fraction, and a lignin-rich solid fraction. This method was also slightly modified from the publication as reported by Li *et al*.[195]

Typically, ground rice husk (2.00 g) was fractionated using ratio of ethanol/DI water = 50/50 (total volume of 40 ml) and formic acid (5%v/v) was loaded into the vessel. Then, the mixture was irradiated using CEM MAR 6 (One Touch^{TM} microwave, using EasyPrep^{TM} Plus Easy Prep Teflon 100 ml closed vessels) with ramp rate of 15 ^{o}C/min followed by holding time of 15 min at 190 ^{o}C (total time of 30 min). After reaction, the vessel cooled down to room temperature by CEM-Mars default program. Then, the vessel was opened and its contents, consisting of a mixture of liquid and solid, were then transferred to a centrifuge tube. After that, the vessel was carefully rinsed with 10 mL of an ethanol/water (50 vol.%) solution several times and transferred to the centrifuge tube to recover all the materials. Centrifugation was used to separate the solid from the liquid. Then, the solid residue obtained after centrifugation (cellulose-rich fraction) was rinsed with the 50 vol.% ethanol/water solution until the solution remained clear, and dried overnight at 105 °C.
The liquid phase was made up of a mixture of ethanol in DI water along with the hemicellulose and lignin fractions solubilised from rice husk during the microwave experiments. Then, ethanol was removed from the liquid phase by a rotary evaporator, resulting in lignin precipitation so allowing the separation of hemicellulose-rich fraction (water fraction) and lignin-rich fraction (solid fraction) by centrifugation and filtration.[195] After this separation, part of the lignin-rich solid was re-solubilised in ethanol (ethanol fraction) for further analysis. The freeze dryer was then used to obtain lignin-rich solid fraction which will be analysed in future work.

2.5.1.1 Effect of ethanol concentration for organosolv fractionation of rice husk on cellulose-rich fraction

In this part, the effect of ethanol concentration for organosolv fractionation was investigated by using the procedure described earlier (see Section 2.5.1). Briefly, each material (2.00 g) was fractionated using ratio of ethanol/DI water (total volume of 40 ml) in the presence of formic acid (5%v/v). The experiments were carried out in a CEM-Mars microwave system with various conditions were studied and shown in Table 4 to

investigate the optimum ratio of ethanol/DI water. Finally, the-obtained fibre (C1-C4) will be further analysed.

Table 4 Various ratio of ethanol/DI water for orgasolv fractionation of rice husk using microwave-assisted method

Method			Cellulose-rich solid fraction
Condition	Ethanol	DI water	
OS1	45	55	C1
OS2	55	45	C2
OS3	30	70	C3
OS4	70	30	C4

Yield of cellulose-rich solid fraction

The yield (%) of cellulose-rich fraction were calculated by Equation,

$$\%\ \text{Yield} = \frac{W_C}{W_0} \times 100\%$$

Where, W_C is the dried weight of cellulose-rich fraction (g)

W_0 is the weight of ground rice husk before organosolv fractionation (g)

2.5.1.2 Effect of temperature for organosolv fractionation of rice husk on cellulose-rich solid

In this part, the effect of temperature was also studied by using the previous procedure (see Section 2.5.1). Organosolv process of rice husk was performed using CEM Mars microwave system (a 100-ml of EasyPrep Plus® vessels) installed with a thermocouple for internal temperature measurement with a mixing system with the ratio of ethanol/DI water = 55/45 under the microwaved irradiation at different temperature (170 ^{O}C, 190 ^{O}C and 210 ^{O}C) for 15 min with ramp rate of 15 ^{o}C/min. After following the procedure, C170, C190 and C210 were obtained.

2.5.2 Chemical treatment

In this work, the alkaline and bleaching treatment also acid hydrolysis were performed to produce high-purity cellulose in micro and nano scale of cellulose fibres derived from rice husk after organosolv treatment. All treatment methods were modified from the literature as reported elsewhere[94,118,257-259]

2.5.2.1 Alkaline treatment

The alkali treatment was carried out to purify the cellulose by removing lignin and hemicellulose from rice husk fibres. The cellulose rich solid fraction from organosolv fractionation (OS) was treated with an alkali solution (5% w/v NaOH solution) with the solid: liquor ratio = 1:10 w/v. The mixture was transferred into a round bottom flask and treatment was performed at 80 ^{o}C for 3 h. The solid was then filtered and washed several times using DI water. Finally, the as-obtained fibres were dried at room temperature overnight to provide OS-alkaline fibres.

2.5.2.2 Bleaching step using chlorine-free method

After alkaline treatment, OS-alkaline fibres were bleached with chlorine-free method by using a mild condition of 6.0% H_2O_2 acidified by acetic acid (until pH ~ 2) under vigorous stirring at 80 ^{o}C for 4 h. Then, the as-obtained white fibres were filtered by vacuum filtration and washed with DI water until pH ~ 7. Finally, the OS-alkaline-Bleached fibres were obtained.

2.5.2.3 Acid hydrolysis

The resulting rice husk fibres from bleaching step (OS-alkaline-B) were mixed with 50% wt sulfuric acid (solid: liquor ratio = 1:10 w/v) under the vigorously stirred at 45 ^{o}C for 30 min. The hydrolysis was quenched by adding 5-fold excess water (100 ml) to the reaction mixture. The resulting mixture was cooled to room temperature and centrifuged. The fractions were continuously washed by the addition of distilled water and centrifuged. A colloidal suspension (OS-alkaline-Bleached-AH) was obtained. This generated suspension was stored in refrigerator at 4 ^{O}C for further use.

2.5.3 Mechanical treatment

The mechanical treatment by homogenisation was used for cellulose fibres modification by defibrillation to provide microcellulose and nanocellulose fibres in the water suspension.[260] This part described the mechanical treatment by homogenisation of OS fibres and OS-Alkaline-Bleached fibres. Cellulose fibres derived from rice husk by organosolv fractionation at 190 ^{O}C (OS fibre) followed by homogenisation for 1 h prior to prepare bio-composite film series A. The suspension of OS fibres in deionised water subjected to homogenisationed with probe which was immersed in the middle of the suspesion vial to provide defibrillated cellulose.[126] In order to prepare the homogenous form of cellulose fibres derived from chemical treatments (OS-Alkaline-Bleached), the homogenisation process was applied for 15 min prior to prepare the bio-composite films series B which described in the latter part.

2.5.4 Bio-composite film preparation

The bio-composite films from poly (vinyl alcohol) blended with glycerol and the addition of reinforcing agent like micro/nano cellulose fibres from rice husk were prepared using different types of celluloses by the following procedures described in this part. Their properties, including optical properties, thermal properties and mechanical properties of the bio-composite films were also investigated.

2.5.4.1 Bio-composite film preparation: Series A

In this part, the bio-composite film preparation was prepared by following step. Firstly, the mixture of 5% (w/v) PVA solution was prepared by dissolving PVA in deionised water at 85 ^{O}C followed by vigorous stirring until a clear solution was obtained (~ 30 min).

Desired amount of cellulose fibre suspension from organosolv fractionation followed by homogenisation for 1 h at various concentration of 0%-5% was dispersed in the mixture at room temperature. Then, the mixed solution was blended with 2% (v/v) of glycerol as plasticiser under stirring vigorously for 30 min until a homogeneous solution was obtained. Each mixture was cast into Petri dish. Finally, the films were dried in oven at 25 ^{O}C for 24 h. After that, the dried film was peeled from a Petri dish for further analysis. The

resulting films prepared by 0%, 1%, 2%, 3%, 4% and 5% of cellulose fibres addition in film preparation were denoted as A0, A1, A2, A3, A4 and A5, respectively.

2.5.4.2 Bio-composite film preparation: Series B

The bio-composite film preparation in this part (Series B) was performed based on the procedure described earlier (see Section 2.5.4.1) but using different types of cellulose. In this series the OS-Alkaline-Bleached-H was used at various concentrations of 0%, 1%, 2%, 3%, 4% and 5% to obtain the bio-composite films of B0, B1, B2, B3, B4 and B5, respectively. Then, the optical property, thermal stability, and mechanical property of bio-composite films were investigated.

2.5.4.3 Bio-composite film preparation: Series C

In this series, bio-composite film was prepared as the same procedure described earlier (see Section 2.5.4.1). The addition of OS-Alkaline-Bleached-AH (0%, 1%, 2%, 3%, 4% and 5%) was used in series C film preparation. Then, the as-prepared bio-composite films of C0, C1, C2, C3, C4 and C5 were observed their properties include optical property, thermal stability, and mechanical property.

Chapter 3

Microwave-assisted synthesis of bio-derived mesoporous materials from rice husk for methylene blue removal

3.1 Preparation of silica derived from rice husk via conventional method and microwave-assisted acid treatment

As mentioned before in **Chapter 1**, rice husk-derived silica is beneficial in both maximising economic and mitigating environmental issues. Rice husk can be used as an abundant and cost-effective source of silica precursor to produce sustainable high value-added products for further applications. Compared to other synthetic procedures using sodium silicate solution derived from rice husk as the silica source, utilisation of rice husk can provide additional advantages in terms of minimising waste and eco-friendly recycling of waste biomass.[105,261]

In this work, silica extracted from rice husk was explored by using microwave-assisted acid treatment prior to calcination. The aims of this part are to investigate the optimum conditions for obtaining (1) high purity silica for a silica source of SBA-15 production and (2) high surface area and pore volume silica for methylene blue (MB) adsorption. The properties studied include purity of SiO_2 content by X-ray Fluorescence (XRF), functional groups determination by FTIR spectrometry and porosity properties using Brunauer-Emmett-Teller (BET) surface area. The schematic overview of the procedure for preparation of silica derived from rice husk via microwave-assisted method is represented in **Fig. 9**.

Fig. 9 Schematic of the procedure to produce silica derived from rice husk using microwave-assisted method

To extract high quality of silica from rice husk, the process involves removal of metallic impurities and organic components in the rice husk such as calcium, iron, potassium. Typically, the acid pretreatment method using conventional heating via reflux to remove

the impurities from rice husk was performed at 80-100 ^{O}C for 2-24 h prior to calcination in the muffle furnace at 600^{o}C-1000^{o}C.[61,168] This study reported the effective method for extraction of silica derived from rice husk by the microwave-assisted acid treatment to reduce time (from 2-24 h to 30-50 min).

The conditions of pretreatment method for rice husk were represented in **Table 5**. To compare conventional method with microwave-assisted method. The as-obtained silica derived from rice husk after pretreatment method for 30 min, denoted as RH-SiO_2-30, the as-obtained silica derived from rice husk after pretreatment method for 45 min, denoted as RH-SiO_2-45 min also for 50 min, denoted as RH-SiO_2-50 min.

Table 5 The conditions for silica extraction from rice husk

Method	Conditions
Conventional method	100 ^{O}C for 3 h
Microwave-assisted method	100 ^{O}C for 30-50 min

In addition, the various ratio of solid-to-liquid (rice husk to 1M HCl), including 1:20, 1:15 and 1:10 were investigated. The yield of silica extracted from rice husk is shown in **Fig. 10**. It was found that rice husk (solid-to-liquid ratio = 1:10) treated with microwave-assisted pretreatment using 1M HCl at 100^{o}C for 30 min provided the highest yield of 13.28% (1.3280 g of SiO_2/10 g of raw rice husk). It should be noted that this condition used less solvent and reaction time for pretreatment than other conditions.

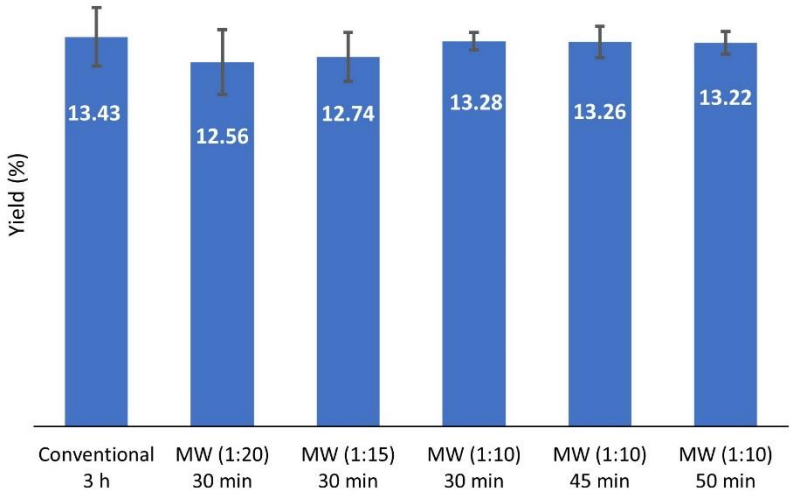

Fig. 10 The yield of silica extracted from rice husk by conventional and microwave-assisted acid treatment at various ratio of solid-to-liquid

3.1.1 X-ray Fluorescence (XRF) analysis of rice husk and silica derived from rice husk

To determine the purity of silica derived from rice husk using conventional method and microwave-assisted method in pretreatment step. The XRF analysis was used to determine the inorganic composition of all samples. XRF spectroscopy is an effective method for qualitative and quantitative analysis of material composition.[256]

The inorganic compositions of raw rice husk and silica derived from rice husk by XRF analysis are presented in Table 6. This result reveals that raw rice husk mainly contains silica (72.24 wt%) and several elements which could be removed by pretreatment, subsequently by calcination to produce high purity of silica. After pretreatment step, followed by calcination the high purity of silicas was obtained (>99.70 wt%) for all conditions. Pretreated rice husk contain silica around 85-86% along with CaO were obtained before calcination thus the calcination was used to remove further impurities from the pretreated rice husk. This indicates that the high-purity silica was successfully obtained by using microwave-assisted acid pretreatment (within 30-50 min) followed by calcination.

Therefore, RH-SiO_2-30 can be easily and rapidly prepared and can produce high-purity silica derived from rice husk, using 1M HCl for 30 min under microwave-assisted pretreatment, followed by calcination at 700°C for 3 h. Moreover, this condition used a lower concentration of HCl and less time than those pretreatment by 2M HCl for 2 h to produce silica (98.67 wt%) reported by Azat *et al.*[261] or pretreatment using 72% H_2SO_4 for 2 h to obtain high purity of silica reported by Chun *et al.*[256] Then, the RH-SiO_2-30 was selected for preparation of sodium silicate solution in the next part due to it has relatively high purity of silica (99.71 wt%) compared to those RH-SiO_2-45 (99.75 wt%) and RH-SiO_2-50 (99.76 wt%) and it can be easily dissolved in NaOH solution.

Table 6 Inorganic chemical compositions of raw rice husk, pretreated rice husk and RH-SiO_2 from different conditions

Element oxide	Raw rice husk	Pretreated rice husk (solid-to-liquid ratio 1:10) (wt%)			RH-SiO_2			
					Conventional method	Microwave-assisted method		
		30 min	45 min	50 min	3 h	30 min	45 min	50 min
SiO_2	72.24	85.29	86.91	85.26	98.90	99.71	99.75	99.76
CaO	25.08	14.71	13.09	14.74	1.10	0.29	0.25	0.24
K_2O	1.700	-	-	-	-	-	-	-
Fe_2O_3	0.98	-	-	-	-	-	-	-

3.1.2 Brunauer-Emmett-Teller (BET) analysis of silica derived from rice husk

Nitrogen porosimetry was used to study the surface area and pore volume of silica derived from rice husk at different conditions. The N_2 adsorption-desorption isotherms of as-obtained silicas including, RH-SiO_2-30, RH-SiO_2-45 and RH-SiO_2-50, exhibit type IV isotherms typical for mesoporous materials, as classified by IUPAC (Fig. 11) Compared to silica (246 m^2/g) obtained using conventional method (3 h for pretreatment and 4 h for calcination) by Kongmanklang *et al.,*[166] in this work the as-obtained bio-derived silicas extracted via microwave-assisted method (30-50 min for pretreatment and 3 h for

calcination) possess higher surface area (276-322 m^2/g) as can be seen in **Table 7**. Moreover, RH-SiO_2-50 possesses the highest BET surface area of 322 m^2/g which could be a good candidate for using as adsorbent for MB removal in the latter part of this work.

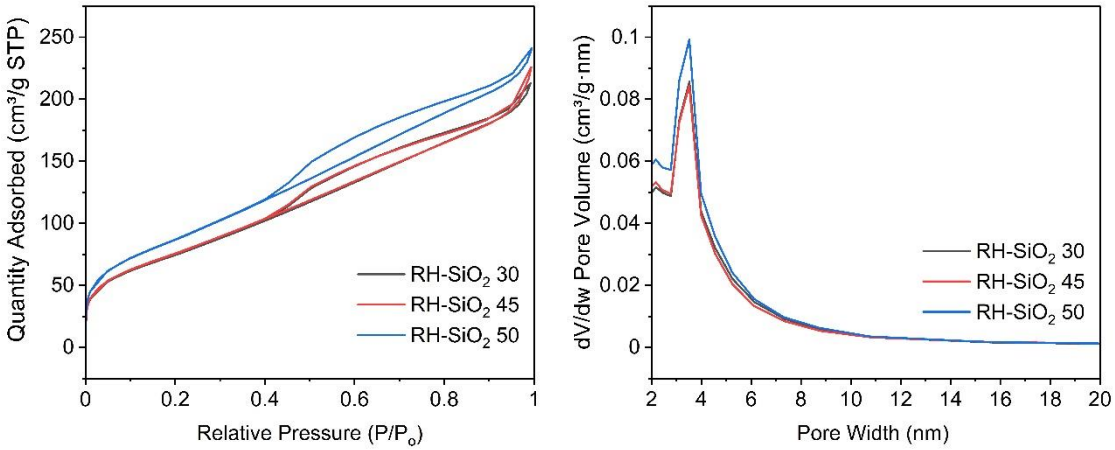

Fig. 11 The N_2 adsorption-desorption isotherms and pore width distributions of RH-SiO_2-30, RH-SiO_2-45, and RH-SiO_2-50

Table 7 Porosity properties of RH-SiO_2 from microwave-assisted pretreatment from rice husk via microwave-assisted acid treatment at 100 ^{O}C for 30-50 min

Microwave-assisted pretreatment	BET Surface area (m^2/g)	Pore volume (cm^3/g)	Average pore width (nm)
30 min	276	0.28	4.12
45 min	281	0.28	4.04
50 min	322	0.33	4.05

Note: All values of porosity properties were measured and calculated by a single measurement using the Micromeritics® TriStar II plus

3.1.3 Fourier-transform infrared (FTIR) analysis of silica derived from rice husk

To investigate the functional groups of RH-SiO_2 obtained from rice husk, FTIR spectrometry was carried out in the range of 4,000–650 cm^{-1}. **Fig. 12** shows FTIR spectra of RH-SiO_2-30, RH-SiO_2-45, RH-SiO_2-50 and RH-SiO_2 conventional method. The strong band at 1,100 cm^{-1} was attributed to the asymmetric vibration of the siloxane bond (Si–O–Si). The presence of band at 800 cm^{-1} was assigned to the symmetric stretching vibration of Si–O–Si bond. This confirms that all samples (RH-SiO_2-30, RH-SiO_2-45, and RH-SiO_2-50 and RH-SiO_2 Conventional method) were defined as silica material.[155,162,163,261,262]

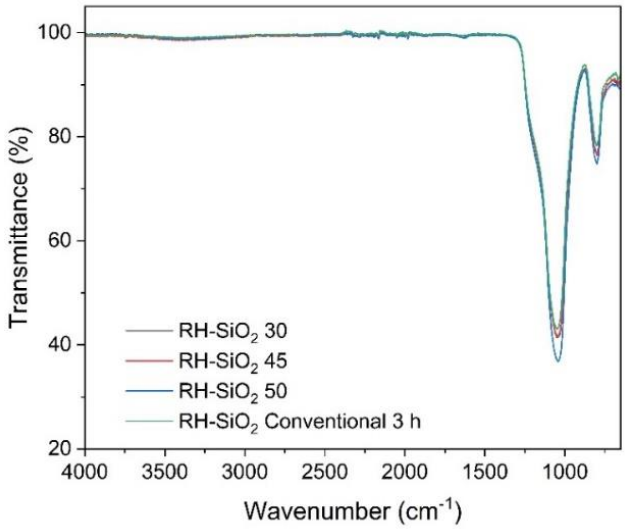

Fig. 12 Infrared spectra of silica derived from rice husk from different methods

3.1.4 SEM and TEM characterisation

Scanning Electron Microscopy (SEM) and Transmission Electron Microscopy (TEM) images of RH-SiO_2-50 are represented in **Fig. 13**. TEM image shows nanostructures of as-prepared silica derived from rice husk even there are some irregular shapes shown in SEM.[100] However, it has the highest surface area compared to others (that was mentioned the previous part) with beneficial for adsorption. So, RH-SiO_2-50 was selected to study MB adsorption in the application part.[170]

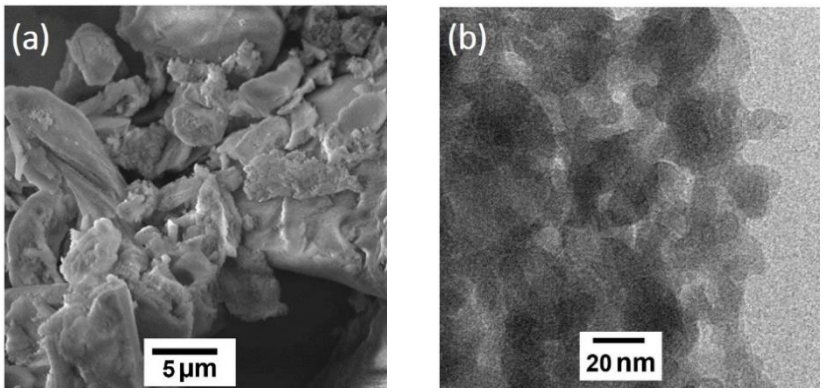

Fig. 13 SEM and TEM images of RH-SiO_2-50

Bio-derived sodium silicate solution from rice husk can be used as silica source for synthesis of ordered mesoporous material such as SBA-15 and CSC materials. This silica source has advantage for the sustainable synthesis because its more cost-effective than TEOS which normally used for preparation of SBA-15 mesoporous material.

3.2 Preparation of bio-derived sodium silicate solution from rice husk

In this part, sodium silicate solution was prepared from silica derived from rice husk from the previous part. As the high purity of RH-SiO_2-30 was found to be 99.7%, so this can be used for preparation of sodium silicate solution. It was also found that RH-SiO_2-30 can be more easily dissolved in NaOH solution than RH SiO_2-45 min and RH SiO_2-50 min.

In typical way, sodium hydroxide used for silica dissolution under vigorous stirring at 80-100 ^{O}C for 1-2 h.[261,263]

The process of silica dissolution represented as follows,

$$2NaOH + xSiO_2 \rightarrow Na_2SiO_3 + H_2O$$

This part described the effective way to prepare sodium silicate solution derived from rice husk via microwave-assisted method. The process to prepare sodium silicate solution shown in Fig. 14. Sodium silicate solution can be easily prepared from bio-derived silicas by mixing with 1M NaOH solution under the microwave irradiation at 80 ^{O}C for 30 min.

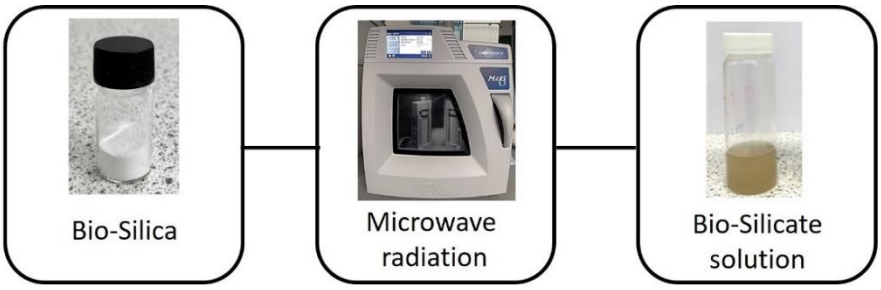

Fig. 14 The preparation of sodium silicate solution derived from rice husk by microwave-assisted method (denoted as RH-SS)

To investigate the effective approach for synthesis of SBA-15 by using RH-SS as a silica source under the acidic condition. It is necessary to obtain accurate concentration of sodium silicate solution to calculate the optimum concentration for SBA-15 synthesis. The method involves using FTIR with a calibration curve (**Fig. 15**) obtained from a series of dilutions of commercial sodium silicate solution (Sigma-Aldrich), denoted as Com-SS. The absorbance (%) of Com-SS at the concentration between 10%-80% were measured by FTIR spectrometer. The calibration curve of absorbance at wavenumber of 1000 cm^{-1} versus concentration were used for calculation the accurate concentration and preparation of RH-SS for the next step.

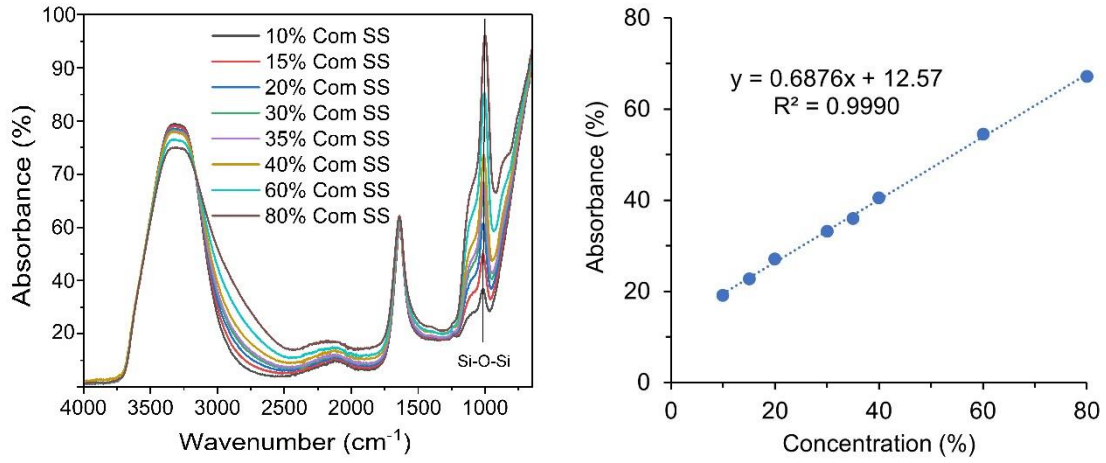

Fig. 15 Calibration curve of commercial silicate solution

It was found that the resulting concentration of sodium silicate solution prepared from RH-SiO_2-30 (denoted as RH-SS-30) compared to Com-SS, calculated from calibration curve was found to be 35% concentration of Com-SS (denoted as 35% Com-SS).

It is necessary to prepare RH-SS at the same concentration as Com-SS and the optimum concentration for using as silica source for preparation of SBA-15 (as described in detail of SBA-15 synthesis, See Section 3.3). Then, optimum concentration of RH-SS was prepared and kept at room temperature for using of all SBA-15 preparations.

Both high concentrations of Com-SS (100% and 50%) were used as silica precursors for SBA-15 synthesis, but it was found that the mixed phases of silica gel and disordered SBA-15 were obtained from those concentrations. The optimum concentration of sodium silicate solution for preparation of SBA-15 was found to be 17.5%. So, this part described the procedures to prepare the optimum concentration of RH-SS (from rice husk) for SBA-15 synthesis in the next section. As previous mentioned, the concentration of resulting RH-SS-30 derived from rice husk calculated to be 35%. This suggested that 50% dilution of the RH-SS-30 can be prepared optimum concentration (17.5%) of RH-SS for using as silica source for SBA-15 preparation. This resulting RH-SS-30 after 50% dilution denoted as 50% RH-SS-30 as can be seen in Fig. 16.

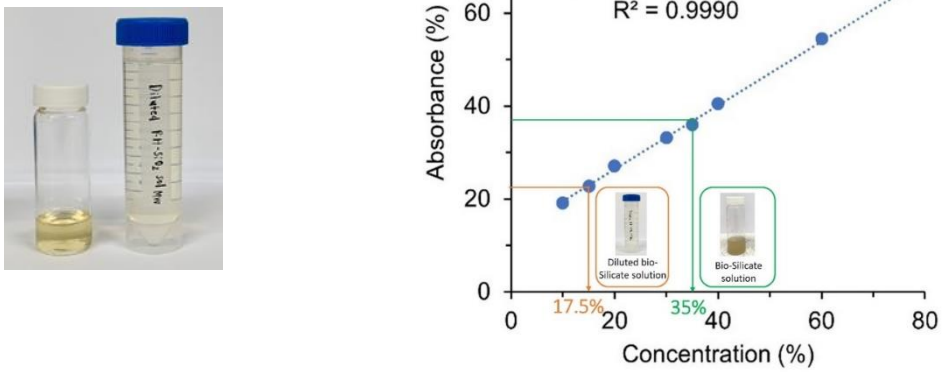

Fig. 16 Sodium silicate solution derived from rice husk at 35% and 17.5% of Com-SS

3.2.1 FTIR analysis bio-derived sodium silicate solution from rice husk and commercial silicate solution

To analysis the functional group of RH-silicate solution compared to commercial silicate solution, FTIR spectrometry was performed. A small drop of silicate solution was placed covering the crystal surface. Spectra were taken from 4000 cm^{-1} to 650 cm^{-1} (64 scans) with a spectral resolution of 4 cm^{-1}. RH-SS-30 reveals the same pattern of Com-SS at the concentration of 35%. As can be seen in **Fig. 17**, RH-SS-30 appears to closely resemble 35% Com SS.

In the synthesis procedure, the FTIR spectra of 50% RH-SS-30 which is the optimum concentration (17.5%) for using as silica source for SBA-15 preparation which also reveals the same pattern of those spectra of 35% Com-SS and RH-SS-30. The two bands at 1000 cm^{-1} and 884 cm^{-1} were attributed to the stretching vibrations of Si-O and Si-O-Si, respectively.[264] These indicate the presence of Si-O-Si linking structure thus confirmed the formation of sodium silicate solution. The peak at 1640 cm^{-1} corresponding to the OH bending mode vibrations of water.[100] Broad band appeared at 3000–3600 cm^{-1} corresponding to the OH stretching vibrations of water.[162,263] This suggests that 50% RH-SS-30 can be used as silica source for the synthesis of SBA-15 in the next part.

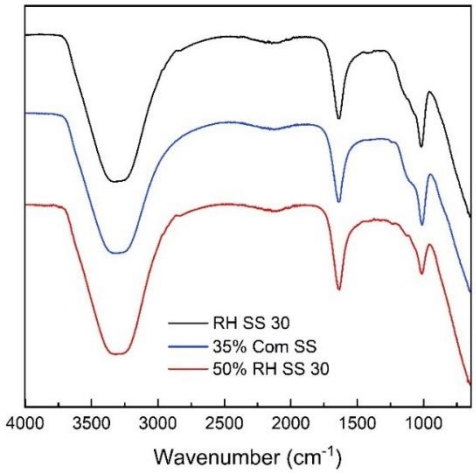

Fig. 17 Infrared spectra of RH-SS-30, 35% Cm-SS and 50% RH-SS-30

3.3 Synthesis of SBA-15 using different silica sources via conventional method

The synthesis of SBA-15 was investigated in this part due to its high surface areas and large volumes of ordered mesoporous structure. Typically, tetraethyl orthosilicate (TEOS) has been the most common choice of silica used as silica source for synthesis of SBA-15 which is more toxic and relatively higher price than sodium silicate solution. So, RH-SS derived from rice husk which can be prepared from the previous session for using as a silica precursor for SBA-15 preparation in this part.

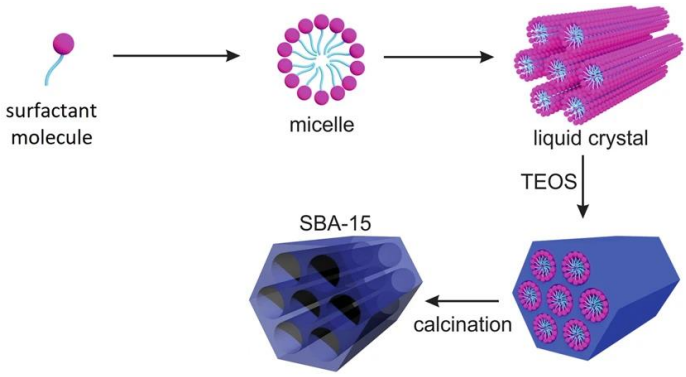

Fig. 18 The proposed procedure for preparation of SBA-15 (adapted from illustration of SBA-15 preparation reported by Zeleňáková et al.)[265]

3.3.1 Optimisation condition for synthesis of SBA-15

Synthesis of SBA-15 involves dissolving the template in acidic solution followed by addition of silica source. The mixed solution is heated (hydrolysis step) at 30–40 ^{o}C for 20–24 h and then aged (hydrothermal step) for 24–48 h at 80–120 ^{o}C. A white solid is obtained after aging. Finally, the material was calcined in a furnace at 500 °C for 3 h for removal of template. The proposed procedure for preparation of SBA-15 is presented in **Fig. 18**.

The attempt relates to the development of a method for the synthesis of SBA-15 with aims of reduction in reaction time for synthesis with low-cost production as well as providing high quality as-prepared materials.[73] This section described the efficient way to control the textural properties including the pore diameter of the as-prepared materials. Hydrothermal steps were modified by using microwave irradiation because its rapid and

homogeneous heating of the entire system which facilitate in the formation of uniform nucleation centres.[73] The as-prepared good-quality SBA-15 samples can be obtained from short time period of preparation (hydrolysis step of 4-24 h and hydrothermal step for 30-50 min), which represents a significant time reduction in comparison to the conventional synthesis (usually used hydrolysis time for 24-48 h and hydrothermal step for 24-48 h).[72,255]

This section reports the comparison of as-obtained SBA-15 synthesised by using different silica sources including TEOS, commercial sodium silicate solution (Com-SS) and sodium silicate solution derived from rice husk (RH-SS) via conventional method. The optimum concentration of sodium silicate solution to prepare SBA-15 was investigated in this part and used for the synthesis of SBA-15 by using RH-SS derived from rice husk (which can be prepared from the previous **section 3.2**).

The various conditions for preparation of SBA-15 via conventional method using TEOS, Com-SS and RH-SS are 94ummarized in **Table 8**. The as-obtained ordered mesoporous SBA-15 prepared by TEOS as a silica precursor by conventional method (denoted as **SBA-15-T-C**) and the as-obtained products prepared by Com-SS via conventional method at various concentration including, 100% Com-SS (denoted as **SBA-15-S-C1**), 50% Com-SS (denoted as **SBA-15-S-C2**), 17.5% Com-SS (denoted as **SBA-15-S-C3**) and the as-obtained products prepared by 17.5% RH SS (denoted as **SBA-15-RH-C)** were studied. Schematic overview of the procedures to produce SBA-15 materials via conventional method is represented in **Fig. 19**.

Table 8 The conditions for preparation of SBA-15 via conventional method

Sample	Synthesis conditions		
	Silica source	Hydrolysis step	Hydrothermal step
SBA-15-T-C	TEOS	40°C for 24 h	85°C for 24 h
SBA-15-S-C1	100% Com-SS		
SBA-15-S-C2	50% Com-SS		
SBA-15-S-C3	17.5% Com-SS		
SBA-15-RH-C	17.5% RH-SS		

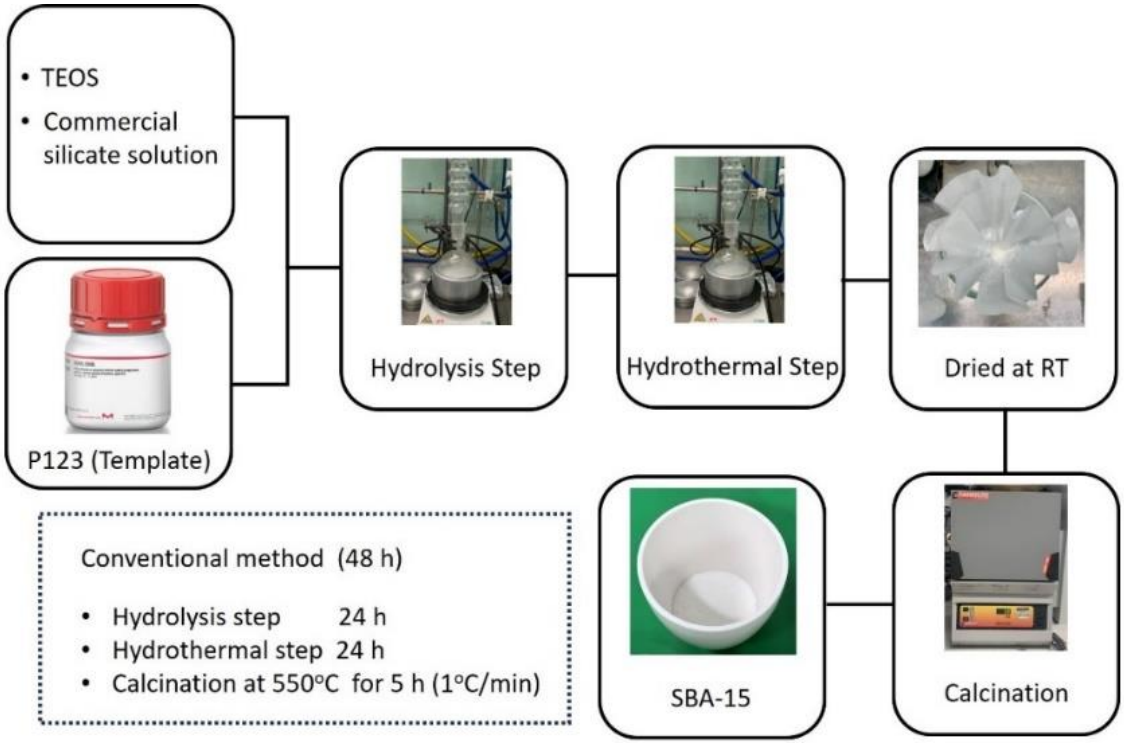

Fig. 19 Schematic overview of the procedures to produce SBA-15 materials via conventional method

3.3.1.1 Brunauer-Emmett-Teller (BET) analysis of SBA-15 prepared with different conditions

The ordered mesoporous SBA-15 materials with high BET surface area and high total pore volume can be successfully prepared by different silica sources. The N_2 adsorption-desorption isotherms and pore width distributions of various prepared samples are revealed in Fig 20 and porosity properties are 96ummarized in Table 9. Type IV isotherms are observed for as-prepared SBA-15-T-C, SBA-15-S-C3 and SBA-15-RH-C materials, with parallel curves typical of H1 hysteresis that indicate the uniform distribution of mesopores (cylindrical-like pore).[265] H1 hysteresis loop exhibits a steep adsorption step, indicating capillary condensation in the pores of mesoporous silica, where the isotherm showed a sharp inflection at a relative pressure P/P_0 of 0.05–0.30. The ordered mesoporous SBA-15 with high BET surface area of 677 $m^2 g^{-1}$ and high total pore volume (0.89 cm^3/g) can be produced by using TEOS (SBA-15-T-C). Whereas the as-prepared SBA-15 were investigated with using various concentrations (100%, 50% and 17.5%) of Com-SS. These results show that only SBA-15-S-C3 produced by using Com-SS (17.5%), exhibits the ordered mesoporous SBA-15 with high BET surface area of 529 m^2/g and possess total pore volume of 0.64 cm^3/g. On the other hand, both SBA-15-S-C1 and SBA-15-S-C2 produced by using relatively higher concentration of Com-SS of 100% and 50%-resulting in the as-synthesised silica materials could not possess a uniform of ordered SBA-15 mesoporous materials as can be seen in Fig. 20.

As can be confirmed by N_2 adsorption-desorption isotherms and pore width distributions of SBA-15 which exhibited a type-IV hysteresis loop with type H1, corresponding to the characteristic of a mesoporous structure.[266] This N_2 adsorption-desorption isotherms of SBA-15-S-C3 is close to the characteristic of a mesoporous structure of the as-prepared SBA-15-T-C. It should be noted that the well-ordered mesoporous SBA-15 was successfully synthesised by the optimum concentration of 17.5% Com-SS via conventional method.

The next stage was to attempt to synthesise SBA-15 material derived from rice husk with the same condition of SBA-15-S-C3 preparation. RH-SS at the optimum concentration of 17.5% used for preparation of SBA-15. Compared to SBA-15-S-C3, the results show that

the as-obtained SBA-15-RH-C displays similar trend of N_2 adsorption-desorption isotherm and pore width distribution. N_2 adsorption-desorption isotherm exhibits type IV with the characteristic of H1 hysteresis loop for SBA-15 structure. SBA-15-RH-C also has high surface area of 553 m^2/g and possess total pore volume of 0.67 cm^3/g, which is close to the value of BET surface area (529 m^2/g) and total pore volume (0.64 cm^3/g) of SBA-15-S-C3. This suggests that sodium silicate solution derived from rice husk can be used as a sustainable silica source for SBA-15 preparation which will be studied for further conditions in the next part.

Table 9 The porosity properties of SBA-15 materials prepared with different conditions

Sample	Surface area (m^2/g)			Pore volume (cm^3/g)			D_{BJH} (nm)
	S_{BET}	S_{micro}	S_{meso}	V_{total}	V_{micro}	V_{meso}	
SBA-15-T-C	677	179	498	0.89	0.09	0.80	5.2
SBA-15-S-C1	311	131	180	0.27	0.06	0.21	3.5
SBA-15-S-C2	324	22	302	0.34	0.02	0.32	4.2
SBA-15-S-C3	529	91	438	0.64	0.04	0.60	4.6
SBA-15-RH-C	553	137	416	0.67	0.07	0.60	4.8

S_{BET} is the BET surface area deduced from the isotherm analysis in the relative pressure range of 0.05-0.3.
S_{micro} is Calculated by the t-plot method.
S_{meso} is Calculated by relation S_{BET} -S_{micro}.
V_{total} is the pore volume at a relative pressure of 0.99.
V_{micro} is Calculated by the t-plot method.
V_{meso} is Calculated by relation V_{BET} -V_{micro}.
D_{BJH} is the average pore diameter calculated using BJH method.
Note: All values of porosity properties were measured and calculated by a single measurement using the Micromeritics® TriStar II plus

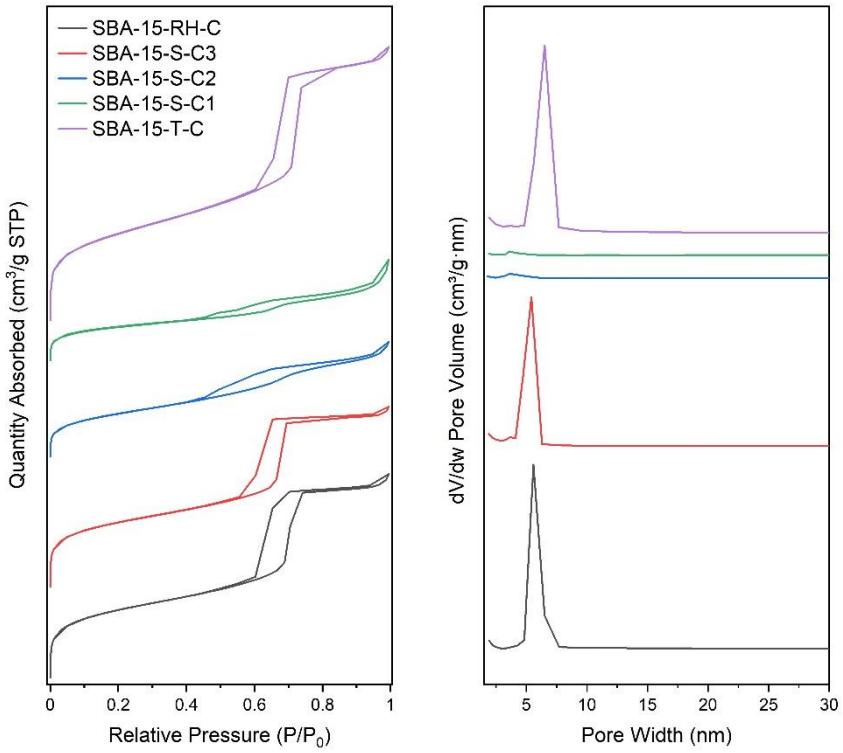

Fig. 20 N_2 adsorption-desorption isotherms and pore size distributions of SBA-15 materials using different conditions for synthesis

3.3.1.2 Small-Angle X-ray Diffraction Scattering (SAXS) of SBA-15 synthesised via conventional method and microwave-assisted method

Small-Angle X-ray Diffraction Scattering (SAXS) patterns of as-prepared SBA-15 materials at 2θ between 0.5-3.0 degree shown in **Fig. 21**. All samples reveal the same SAXS pattern with three characteristic peaks appeared at the (100), (110) and (200) planes, indicating the formation of highly ordered two-dimensional hexagonal *p6mm* mesostructured of SBA-15, which are consistent with TEM images.[267,268]

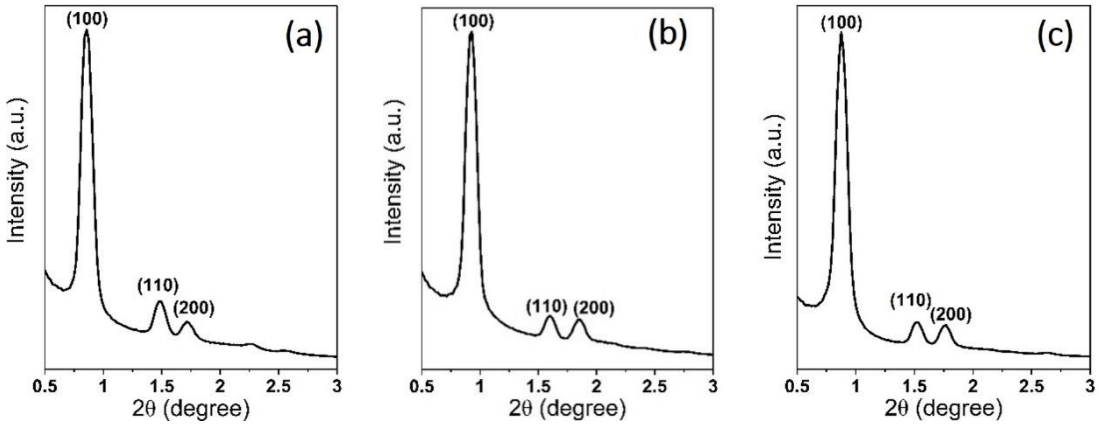

Fig. 21 SAXS patterns of (a) SBA-15-T-C, (b) SBA-15-S-C3 and (c) SBA-15-RH-C

3.3.1.3 SEM and TEM characterisation of SBA-15 synthesised via conventional method and microwave-assisted method

The morphologies of the ordered mesoporous materials were observed by SEM and TEM. The SEM image (Fig 22 (a)) of SBA-15-T-C was produced from conventional method using TEOS as a silica source. This morphology reveals that the aggregation of short-rods like domain with an average diameter size of 0.5 ± 0.1 µm (100 rods measured) - in accordance with the as-obtained SBA-15 reported by Xu *et al*. [267] TEM image (Fig 22 (d)) can also confirm that the as-synthesised SBA-15-T-C consists of the parallel pore channels and highly ordered mesoporous structures of SBA-15.[266] SEM image of SBA-15-S-C3 Fig. 22 (b) displays the agglomerates of long rod-like structure of SBA-15-S-C3 with an average diameter size of 1.0 ± 0.1 µm (100 rods measured), consistent with SBA-15 synthesised by Liou *et al.*[266] SEM image of SBA-15-RH-C also represent uniform long rod-like structures with an average diameter size of 1.0 ± 0.2 µm (100 rods measured) in diameter of individual rod-in accordance with the morphology of SBA-15-S-C3 at the same concentration of (17.5%) Com-SS. TEM images of both SBA-15-S-C3 and SBA-15-RH-C illustrated in Fig 22 (e and f), which show the hexagonal channels of mesoporous materials. The channels are directed across the particle perpendicular to the plane of the base. Regular hexagonal arrangement of parallel cylindrical channels is clearly evident from the TEM images.[267] These can be confirmed that ordered mesoporous SBA-15 was

prepared by sodium silicate solution derived from rice husk with good quality of pore width distribution and pore volume as SBA-15 prepared by commercial silicate solution and TEOS.

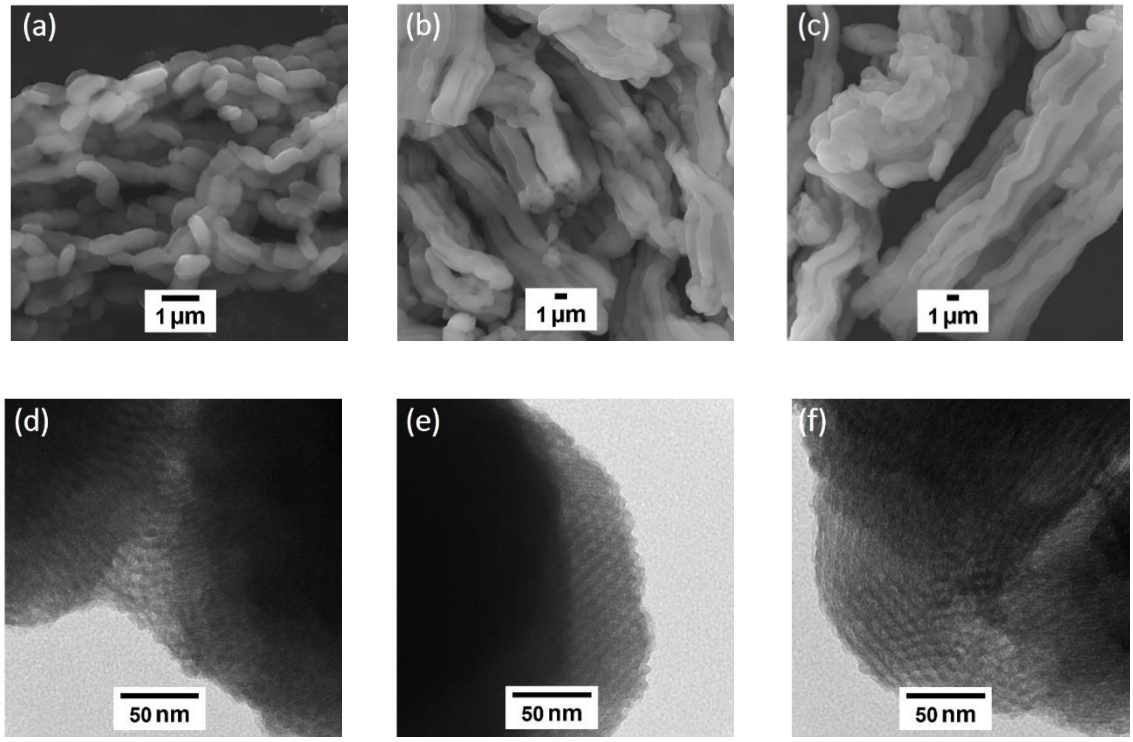

Fig. 22 SEM and TEM images of SBA-15-T-C (a,d), of (b,e) SBA-15-S-C3 and (c,f) SBA-15-RH-C, respectively

The developed methods for the synthesis of SBA-15 with aims of reduction in reaction time in both steps of hydrolysis step and hydrothermal step by using microwave-assisted method as well as using low-cost of RH-SS as silica source were reported in the next part. The textural and morphological properties of mesoporous materials are extremely important for applications. Consequently, the latter part has been studied to control conditions in both synthesis steps. The effect of temperature in hydrothermal step was studied and then the effect of both reaction time in hydrolysis step as well as the effect of reaction time in hydrothermal step were also studied.

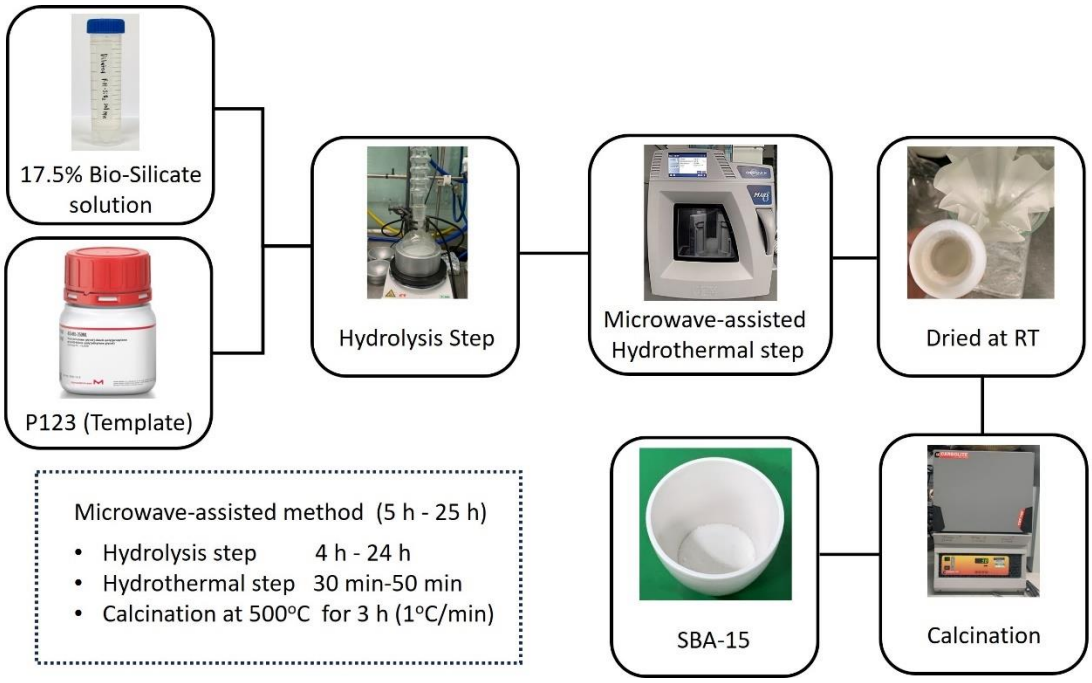

Fig. 23 Schematic overview of the procedures to produce SBA-15 materials via microwave-assisted method

3.3.2 Effect of temperature in hydrothermal step via microwave-assisted method on the structural and physical properties of SBA-15

This part describes the effect of temperature in hydrothermal step. To explore the effect of temperature in hydrothermal step on the structural and physical properties of SBA-15, the various temperatures at 85 ^{O}C (denoted as **MHT-85**), 100 ^{O}C (denoted as **MHT-100**) and 170 ^{O}C (denoted as **MHT-170**) were used for SBA-15 preparation in this part. The schematic overview of the procedures to prepare SBA-15 via microwave-assisted method shown in **Fig. 23**.

The synthesis conditions for preparation of SBA-15 under the microwave-assisted method were performed by using the hydrolysis step at 40 ^{o}C for 6 h, followed by the hydrothermal step under microwave irradiation at various temperatures for 50 min. The conditions for this part shown in **Table 10**.

Table 10 The conditions for preparation of SBA-15 via microwave-assisted method

Sample	Synthesis conditions	
	Hydrolysis step	Hydrothermal step
MHT-85	40 °C for 6 h	85 °C for 50 min
MHT-100		100 °C for 50 min
MHT-170		170 °C for 50 min

3.3.2.1 Brunauer-Emmett-Teller (BET) analysis of SBA-15 prepared via microwave-assisted method

N_2 adsorption-desorption isotherms and pore width distributions of as-prepared SBA-15 illustrated in Fig. 24. Based on IUPAC classification, the isotherms of all samples — in good accordance with the type IV isotherm with a H1 hysteresis loop, indicating that the as-prepared SBA-15 can be identified as mesoporous materials.[268,269]

From these results (Table 11), MHT-170 possess the highest BET surface area of 585 m^2/g, larger pore size (6.26 nm) and has highest total pore volume of 0.92 cm^3/g of all materials. Both MHT-85 and MHT-100 possess pore width of just around 4.4-4.7 nm, and both have quite less amount of total pore volume than MHT170 (0.67 cm^3/g for MHT-85 and 0.72 cm^3/g for MHT-100) as can be seen in Table 11.

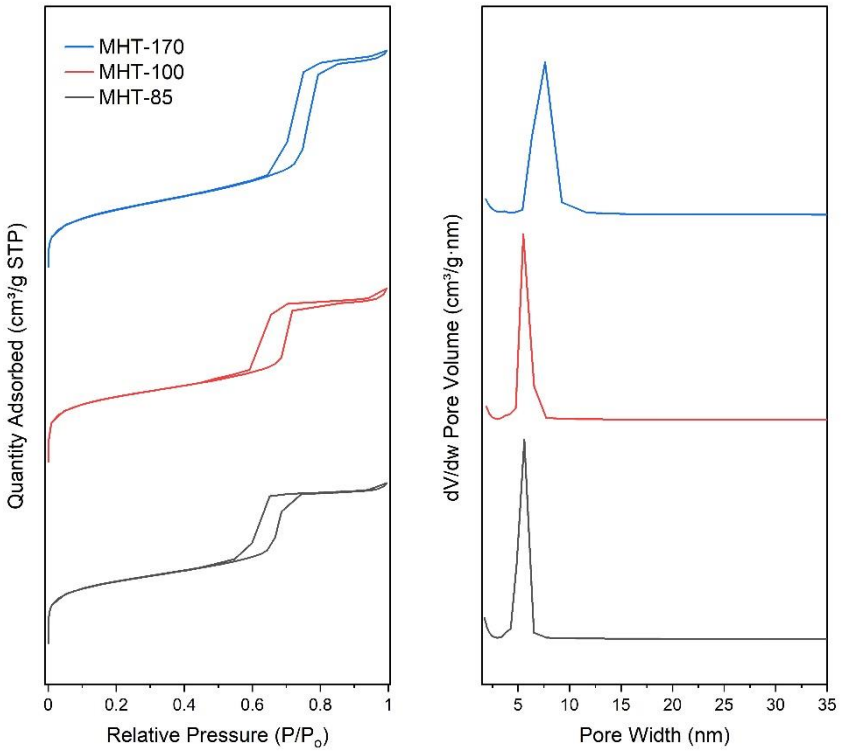

Fig. 24 N_2 adsorption-desorption isotherms and the pore width distributions of SBA-15 synthesised using different hydrothermal temperatures

Table 11 The porosity properties of SBA-15 derived from rice husk using hydrolysis step at 40°C for 6 h and microwave-assisted hydrothermal at different temperatures

Sample	Surface area (m^2/g)			Pore volume (cm^3/g)			D_{BJH} (nm)
	S_{BET}	S_{micro}	S_{meso}	V_{total}	V_{micro}	V_{meso}	
MHT-85	606	168	438	0.67	0.07	0.60	**4.43**
MHT-100	609	162	438	0.72	0.07	0.65	**4.70**
MHT-170	585	180	405	0.92	0.08	0.84	**6.26**

Note: All values of porosity properties were measured and calculated by a single measurement using the Micromeritics® TriStar II plus

It was found that an increase in temperature of hydrothermal step resulted in the increasing of mesopore volume and pore diameter — in accordance with the results reported by Celer *et al.* [72], Juárez-Serrano *et al.*[270], Bai *et al.*[271] and Fulvio *et al.*[272] In the hydrothermal step, after the formation of SBA-15 was occurred, the increasing of temperature in hydrothermal step -resulted in the polyethylene oxide chains of the surfactant become more hydrophobic which leads to the increasing of pore size and the reducing of microporosity.[270]

Apart from the widest pore width, Celer *et al.*[72] described that the thermal stability of as-obtained product synthesised at high temperature (160-180 ^{O}C) in hydrothermal step was enhanced over the thermal stability of those products synthesised at commonly used temperatures under conventional method. So, the condition for preparation of SBA-15 synthesised at 170 ^{O}C (hydrothermal step) was selected for using as a silica support for carbon-silica composite materials preparation in the next step.

3.3.2.2 TEM characterisation of as-synthesised SBA-15 prepared via microwave-assisted method

TEM images (**Fig. 25**) show the morphology of as-synthesised SBA-15, which can be seen the larger pore size of MHT170 (6.26 nm) than others— in good accordance with the pore size data (4.43 nm for MHT-85 and 4.70 nm for MHT-100) as demonstrated in porosity properties (**Table 11**).

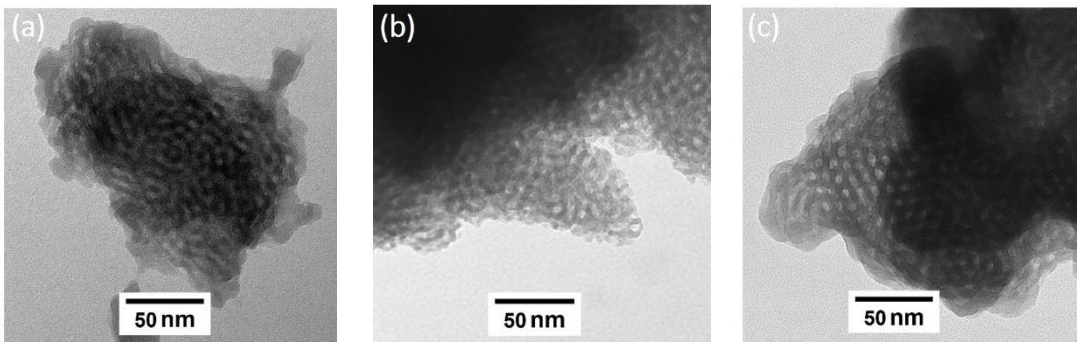

Fig. 25 TEM images of SBA-15 synthesised using different hydrothermal temperatures: MHT-85 (a), MHT-100 (b), and MHT-170 (c), respectively

Thermal stability is beneficial for various applications such as composite materials and catalyst supports.[74,273] As mentioned before, the condition for hydrothermal step at 170 ^{O}C was selected to study the effect of reaction time in hydrolysis step and the reaction time in hydrothermal step which reported in the next part.

3.3.3 Effect of reaction time of hydrolysis and hydrothermal steps on the porosity properties of SBA-15

This part studied the effect of hydrolysis time and hydrothermal time for synthesis of SBA-15. The results of porosity properties of all products shown in Fig. 26, Table 12, and Table 13. The effect of hydrothermal time for the as-synthesised products were investigated at 30 min and 50 min which found that the pore volume and pore diameter tend to increase with the increasing of hydrothermal time, in agreement with the results investigated by Celer *et al.* [72] , Juárez-Serrano *et al.*[270] and Fulvio *et al.*[272] It was also found that an increase in the D_{BJH} of as-obtained product with increasing time (from 5 nm to 6-7 nm) as shown in Table 12 (hydrothermal time for 30 min) and Table 13 (hydrothermal time for 50 min). In this work, the results show that the surface area and total pore volume of SBA-15 products were increased with increasing hydrolysis time (from 4 h to 24 h). These results illustrate that the increasing of hydrolysis time led to the increasing of BET surface area from 532 m^2/g to 730 m^2/g for 30 min of hydrothermal step at 170^{o}C (Table 12) and from 461 m^2/g to 711 m^2/g for 50 min of hydrothermal step (Table 13). A similar trend was also observed in SBA-15 prepared by Shen *et al.*[274]

The average pore width of SBA-15 materials was also increased when prolonging the microwave-assisted hydrothermal periods from 30 min to 50 min which in good accordance with reported by Celer *et al.* [72], Fulvio *et al*.[272] and Newalkar *et al*.[269]

It should be noted that these results indicate it is possible to design (or control) the pore width of SBA-15 to an extent by varying the temperature and time of reaction for various applications via using microwave-assisted hydrothermal routes.

Table 12 The porosity properties of SBA-15 derived from rice husk using different time for hydrolysis and microwave-assisted hydrothermal at 170°C for 30 min

Hydrolysis time (hour)	Surface area (m^2/g)			Pore volume (cm^3/g)			D_{BJH} (nm)
	S_{BET}	S_{micro}	S_{meso}	V_{total}	V_{micro}	V_{meso}	
4	532	130	402	0.69	0.06	0.63	5.19
6	568	151	417	0.72	0.07	0.65	5.07
20	706	108	598	0.92	0.05	0.87	5.19
24	730	314	416	0.92	0.15	0.77	5.03

Note: All values of porosity properties were measured and calculated by a single measurement using the Micromeritics® TriStar II plus

Table 13 The porosity properties of SBA-15 derived from rice husk using different time for hydrolysis and microwave-assisted hydrothermal at 170°C for 50 min

Hydrolysis time (hour)	Surface area (m^2/g)			Pore volume (cm^3/g)			D_{BJH} (nm)
	S_{BET}	S_{micro}	S_{meso}	V_{total}	V_{micro}	V_{meso}	
4	461	72	389	0.88	0.03	0.85	7.64
6	**602**	**178**	**424**	**0.98**	**0.08**	**0.90**	**6.53**
20	606	118	488	1.05	0.05	1.00	6.91
24	711	110	601	1.14	0.05	1.09	6.40

Note: All values of porosity properties were measured and calculated by a single measurement using the Micromeritics® TriStar II plus

In this study, the as-synthesised SBA-15 using a hydrolysis step at 40 °C for 6 h and hydrothermal treatment at 170 °C for 50 min possess high surface area of 602 m^2/g, high total pore volume of 0.98 cm^3/g and large pore width of 6.53 nm, was selected as a silica support to prepare CSC materials in the next step because it is due to the as-synthesised

SBA-15 from this condition obtained from rapid reaction time in both hydrolysis step and microwave-assisted hydrothermal step which possess high surface area and pore volume compared to other conditions. Moreover, it has large pore size which suitable for using as silica support for bio-oil coating to modify the surface area of composite material which will be discussed latter.

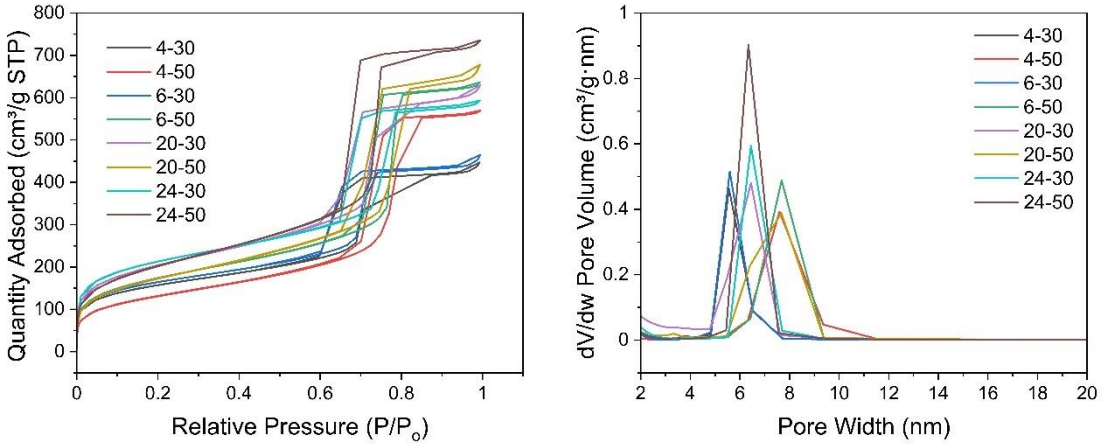

Fig. 26 N_2 adsorption-desorption isotherms and pore width distributions of SBA-15 derived from rice husk using hydrolysis at 40°C using different time for hydrolysis and microwave-assisted hydrothermal at 170°C for 30 min and 50 min

3.3.3.1 SEM and TEM characterisation of SBA-15 synthesised by microwave-assisted method using hydrolysis time at 6 h and 24 h

To investigate the influence of hydrolysis time on the morphology of as-synthesised SBA-15. The morphology of the as-prepared SBA-15 was investigated by SEM (**Fig. 27**). It was found that the similar morphology of rod-like structures formed at 6 h and 24 h of hydrolysis time, but the shorter rods were formed in 24 h of hydrolysis time – in good accordance with the higher BET surface area of 711 m^2/g compared to the as-obtained product at 6 h hydrolysis time (602 m^2/g). However, the pore width of as-prepared products is quite similar size (D_{BJH}) of 6.4-6.5 nm as can be seen in TEM images (**Fig. 27**).

SEM and TEM images revealed similar sizes and shapes for both as-prepared SBA-15. SEM images suggested an average diameter size of 1.0 ± 0.1 µm and 1.0 ± 0.2 µm (100 rods counted) for samples using hydrolysis time at 6 h and 24 h, respectively. This implied that the prolonged hydrolysis time could not have a significant effect on the morphology of the as-prepared product.[73,270]

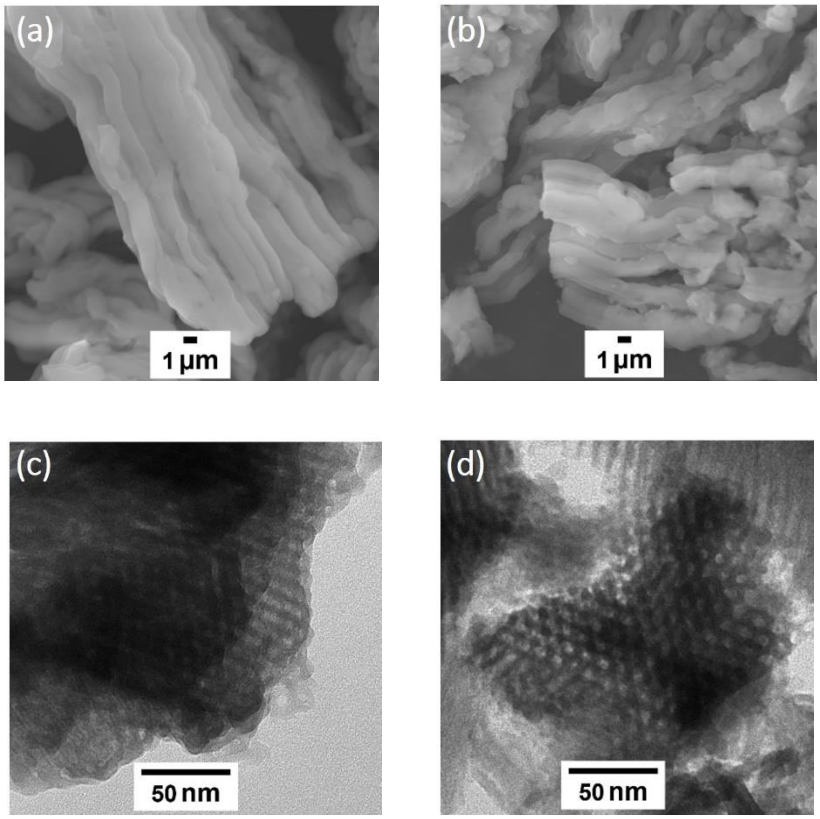

Fig. 27 SEM and TEM images of SBA-15 synthesised for hydrolysis time at 6 h (a,c) and 24 h (b,d), followed by microwave-assisted hydrothermal at 170 oC for 50 min

In summary, this work represents a microwave-assisted method for preparation of well-ordered SBA-15 with high BET surface area and high total pore volume, using a sustainable source of silica (silicate solution derived from rice husk), and proceeds via a microwave-assisted hydrothermal step, which is beneficial in saving time which has advantages for rapid heating to crystallisation temperature, resulting in homogeneous nucleation, and eventually a shorter crystallisation time compared to conventional heating.[269]

3.4 Production of bio-oil derived from rice husk using microwave-assisted pyrolysis

As mentioned in **Chapter 1**, rice husk is an abundant agricultural waste. Many researchers attempt to utilise rice husk via pyrolysis process to obtain bio-oil and bio-char. However, bio-oil from rice husk has unfavourable characteristics such as high moisture content and low energy density.[37] To enhance these inferior characteristics of rice husk, and subsequently the yield and quality of bio-oil produced, more attentions have been extensively explored in three types of pretreatment methods on rice husk, namely, washing, torrefaction (dry and wet), and their combined pretreatments.[20,275]

The objective of the present work is to study an alternative way to utilise the bio-oil derived from rice husk without upgrading process as the carbonaceous phase in carbon-silica composite materials (CSCs). The influences of different pretreatment methods on the characteristics of pretreated rice husk and the subsequent fast pyrolysis in terms of product yields, composition, and chemical properties of the as-produced bio-oil were studied.

Efforts were made to enhance yield and quality of bio-oil for using as a sustainable carbon precursor for preparation of carbon-silica composite materials (CSCs) in the next step because it can provide the functionality for composite materials.[85] The comparison of three bio-oil samples produced via microwave-assisted pyrolysis of raw rice husk (denoted as **BO1**), DI pretreated rice husk (denoted as **BO2**) and HCl pretreated rice husk (denoted as **BO3**) were investigated. The schematic overview of bio-oil derived from rice husk using microwave-assisted pyrolysis method shown in **Fig. 28**.

The composition of complex compounds of all bio-oil samples was investigated prior to preparing CSC materials by using the as-obtained bio-oil as carbon precursor, as described in the next part. The as-obtained bio-char (which is a mixture of silica and carbonaceous residues) from this stage could be used for the preparation of silica materials or activated carbon that could be studied in the future work.

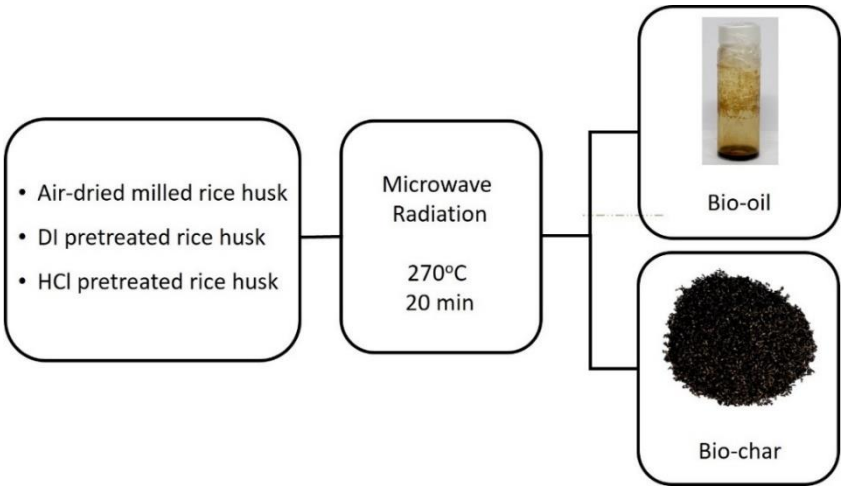

Fig. 28 Schematic overview of the production of bio-oil derived from rice husk using microwave-assisted pyrolysis method

In this work, the as-obtained bio-oil products from this study were carried out via microwave-assisted pyrolysis (CEM Discover SP microwave reactor with round bottom flask (25 ml) and condenser).

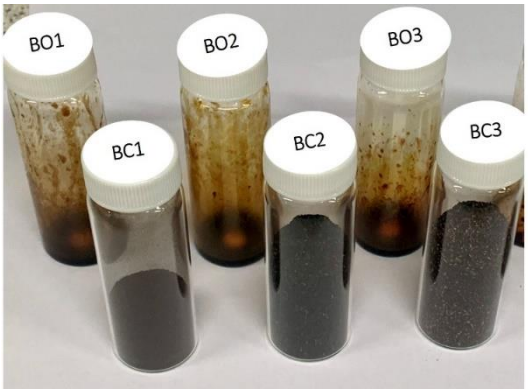

Fig. 29 Bio-oil and Bio-char products produced from rice husk, DI pretreated rice husk and HCl pretreated rice husk via microwave-assisted pyrolysis

The pyrolysis residues, including, the mixture of bio-oil and bio-char, were obtained from this technique represented in Fig. 29. It was found that the mass yield of the three bio-oil samples were found to be 5.38%, 5.68% and 6.62% of BO1, BO2 and BO3, respectively shown in Fig. 30. The highest yield of bio-oil was obtained from BO3 which was pretreated by HCl.

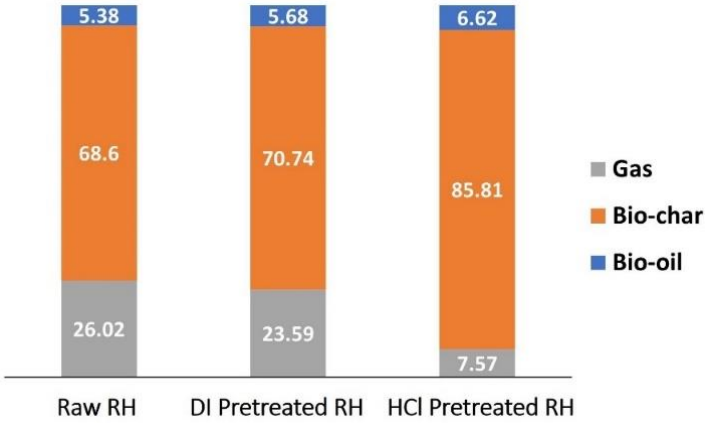

Fig. 30 Yield of the as-obtained bio-oil, bio-char, and gas from raw rice husk, DI pretreated rice husk and HCl pretreated rice husk

Normally, acid or water washing/pretreatment is simple and effective in removing a large amount of water-soluble minerals like K, Na, Cl, and S from rice husk, but it is ineffective in eliminating non-water-soluble minerals like SiO_2, Al_2O_3, and Fe_2O_3.[20]

Interestingly, it was found that the BO2 yield from DI pretreated rice husk generated a similar yield compared to bio-oil from raw rice husk. It should be noted that enhancements of bio-oil yield produced from pretreated DI rice husk might be obtained at higher pyrolysis temperature or could be produced by increasing the temperature of pretreatment step.[30,37]

3.4.1 GC-MS analysis of bio-oil derived from rice husk

The chemical compounds in bio-oil were identified by GC-MS and were compared to the National Institute of Standards and Technology (NIST) library database. Generally, the chemical composition of bio-oils is a very complex mixture of oxygenated compounds and heterocyclic compounds, mainly composed of aromatics, aliphatics, aldehydes, ketones and phenolic compounds with a high viscosity, high oxygen content, high corrosiveness but low heating value and low stability.[21,37,275]

Fig. 31 illustrates GC-MS chromatograms of bio-oil which show that alcohols, furfurals, furans, ketones and aldehydes were found in bio-oil- caused by the decomposition of

cellulose and hemicellulose as well as the existence of aromatics and phenol derivatives i.e. 2-methoxy phenol, 2-methoxy-4-vinyl phenol caused by degradation of lignin.[275] The list of main chemical compounds in the as-obtained bio-oil samples were summarised in Table 14.

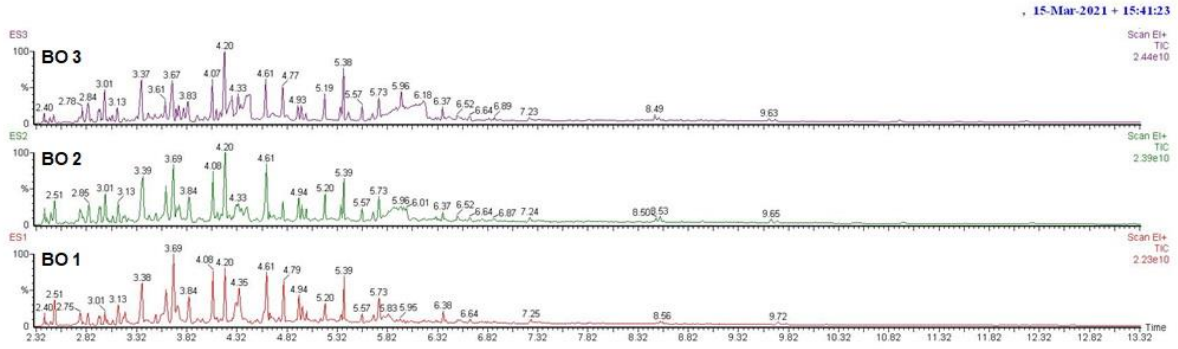

Fig. 31 GC-MS chromatograms of BO1, BO2 and BO3 samples

Overall, the GC-MS chromatograms demonstrate that the composition of the bio-oil is very similar over all three pretreatment conditions. The result of all 3 bio-oil samples shows that the main peak of 2-methoxy-5-methylphenol ($C_8H_{10}O_2$ (at RT = 4.20 min) is phenolic compound in bio-oil. Both BO2 and BO3 have relatively higher content of this compound than BO1. This is a phenylpropanoid formally derived from guaiacol which is produced from lignin pyrolysis – in accordance with the previous report studied by Alvarez *et al*.[275] The only significant change being a broad peak around 5.5-6.5 min which represent the increase in BO3 sample (which higher than BO2 and BO1, respectively).

Table 14 The list of main chemical compounds in bio-oil identified by GC-MS by library match

RT (min)	Compound name	Chemical formula
3.01	2-Furan carboxaldehyde, 5-methyl-	$C_6H_6O_2$
3.37	2-Cyclopenten-1-one	$C_6H_8O_2$
3.69	2-Methoxyphenol	$C_7H_8O_2$
4.08	Phenol, 3-ethyl-	$C_8H_{10}O$
4.20	2-Methoxy-5-methylphenol	$C_8H_{10}O_2$
4.35	Benzaldehyde, 2-methyl-	C_8H_6O
4.61	Phenol, 4-ethyl-2-methoxy	$C_9H_{12}O_2$
4.79	2-Methoxy-4-vinylphenol	$C_9H_{10}O_2$
5.39	Phenol, 2-methoxy-4-(1-propenyl)-, (Z)-	$C_{10}H_{12}O_2$
5.73	2-Propanone, 1-(4-hydroxy-3-methoxyphenyl)-	$C_{10}H_{12}O_3$

3.4.2 FTIR analysis of bio-oil derived from rice husk

According to FTIR analysis, the existence of various compounds such as phenols, ketones, carboxylic acids, and aldehydes was indicated in bio-oil, and could be confirmed by NMR and GC-MS. FTIR spectra of BO1, BO2 and BO3 are shown in Fig. 32 and the list of functional groups is shown in Table 15.

All samples reveal the same pattern of FTIR spectra but there are some signals in the range of 750-1750 cm^{-1} which were found to have different intensities. The broad band centred at 3365 cm^{-1} was assigned to the O-H stretching vibration of hydroxyl groups — showing the presence of water, alcohol, and organic acid.[276] This extends out to ca 2600 cm^{-1} this low frequency tail is indicative of carboxylic acids.

The weak peaks between 3000 and 2800 cm^{-1} are due to C-H stretching vibration, which signify the occurrence of alkyl groups.[277] The peak at 2957 cm^{-1} was attributed to the antisymmetric stretching vibration of aliphatic CH_2 group.[278] The peak at 2927 cm^{-1} was assigned to the-CH stretching vibrations indicating the presence of-CH,-CH_2 (symmetric)

and/or-CH_3 groups which also shown at 1455 cm^{-1} and 1382 cm^{-1} for C-H bending vibrations of alkanes.[277] The peak at 1707 cm^{-1} corresponding to C=O stretching vibration of carboxylic acids, esters, ketones or aldehydes.[21] The signals at 1602 cm^{-1} and 1514 cm^{-1} represent C=C stretching vibration [21] and C=C stretching vibration of alkenes and/or aromatics in bio-oil.[277] The strong peak at 1030 cm^{-1} and 900 cm^{-1} were attributed to stretching vibration of the C-O in ester groups and O-H deformation vibration, which represents the existence of alcohols, carboxylic acids, ethers, esters and phenols. The peak at 880 cm^{-1} was assigned to out-of-plane deformation vibration of C-H of terminal olefins.[278] The weak signals in the region between 900-700 cm^{-1} also related to C-H bending in aromatic compounds which shows a bit stronger intensity for BO3 than BO1 and BO2.[277] As a result, BO3 was selected for using as carbon source of CSCs preparation because BO3 has higher yield of bio-oil compared to other conditions (BO1 and BO2).

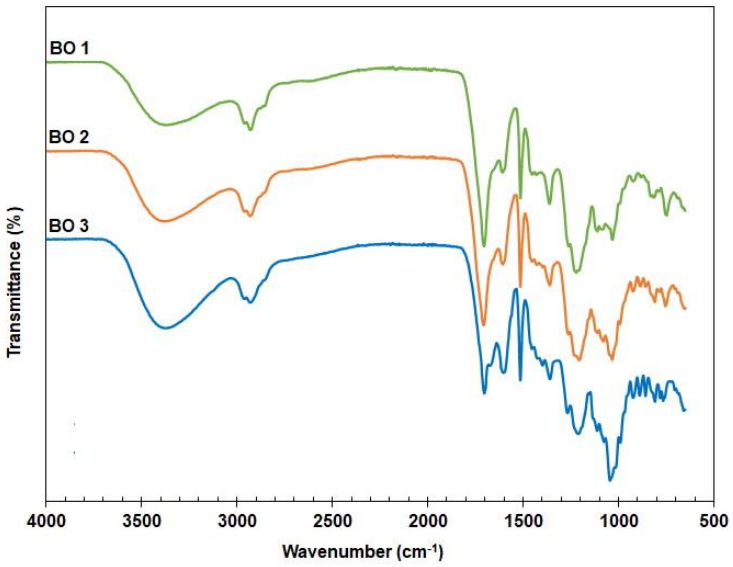

Fig. 32 Infrared spectra of bio-oil BO1, BO2 and BO3 samples

Furthermore, the as-obtained char derived from pretreated HCl rice husk provides the highest yield that can be used for silica preparation by further calcination or activated carbon preparation, this could be studied in the future work.

Table 15 FTIR spectra of the three bio-oil samples

Wavenumber (cm^{-1})	Assignment
3365 (broad band)	O-H stretching vibration of the hydroxyl groups
3000- 2800	C-H stretching vibration of alkyl groups
2957	antisymmetric stretching vibration of aliphatic CH_2 group
2927	-CH stretching vibrations indicating the presence of-CH,-CH_2 and/or -CH_3 groups
2600	Indicative of carboxylic acids
1707	C=O stretching vibration of carboxylic acids, esters, ketones or aldehydes
1602	C=C stretching vibration of alkenes and/or aromatics
1514	C=C stretching vibration of alkenes and/or aromatics
1455	C-H stretching vibrations of alkanes
1382	C-H bending vibrations of alkanes
1030	C-O stretching vibration in ester groups
900	O-H deformation vibration of alcohols, carboxylic acids, ethers, esters and phenols
880	out-of-plane deformation vibration of C-H of terminal olefins
900-700	C-H bending in aromatic compounds

3.4.3 ^{1}H NMR analysis of bio-oil derived from rice husk

^{1}H NMR spectra of the three different conditions of bio-oil derived from rice husk (**Fig. 33**) shows the signals from 9 ppm to 10 ppm are assigned to aldehydes and signals from 6 ppm to 8 ppm are assigned to the aromatics including furans.[21] The olefinic resonances appear in the chemical shift regions of 4-6 ppm.

Signals between 3 and 4 ppm are assigned to the protons adjacent to C-O groups from saccharides, alcohols, ethers, and esters and aromatic bridging methylene protons in bio-oil are also investigated, consistent with the interpretation from FTIR peaks at 3370

cm^{-1} from-OH groups and 1025 cm^{-1} from the C-O bonds, respectively.[29] Signals in the range of 1-3 ppm are assigned to aliphatic protons — in good accordance with the IR spectrum at 2930 cm^{-1} (C-H stretching vibration). These signals are also attributed to the long chain species which include fatty acids or alkyl groups adjacent to carbonyls.[39] Type of hydrogen in ^{1}H NMR results are shown in **Table 16**, illustrates that the aldehyde content of BO3 bio-oil was higher than BO1 and BO2 samples. Moreover, BO3 has stronger peaks at 7.8 ppm and 8.1 ppm which could possibly be due to this condition being more acidic than those conditions (by loss of some alkali type inorganics and maybe some residual acid, then routes to HMF and other dehydration pathways should be favoured). BO3 also shows a stronger peak of HMF at 4.7 ppm, than others.

Table 16 ^{1}H NMR results of the three bio-oil samples

Chemical shift (ppm)	Type of hydrogen
1.0-3.0	Aliphatic protons
3.0-4.0	Protons adjacent to C-O groups from saccharides, alcohols, ethers, and esters and aromatic bridging methylene protons
4.0-6.0	Olefinic resonances
6.0-8.0	Aromatics, including furans
9.0-10.0	Aldehyde

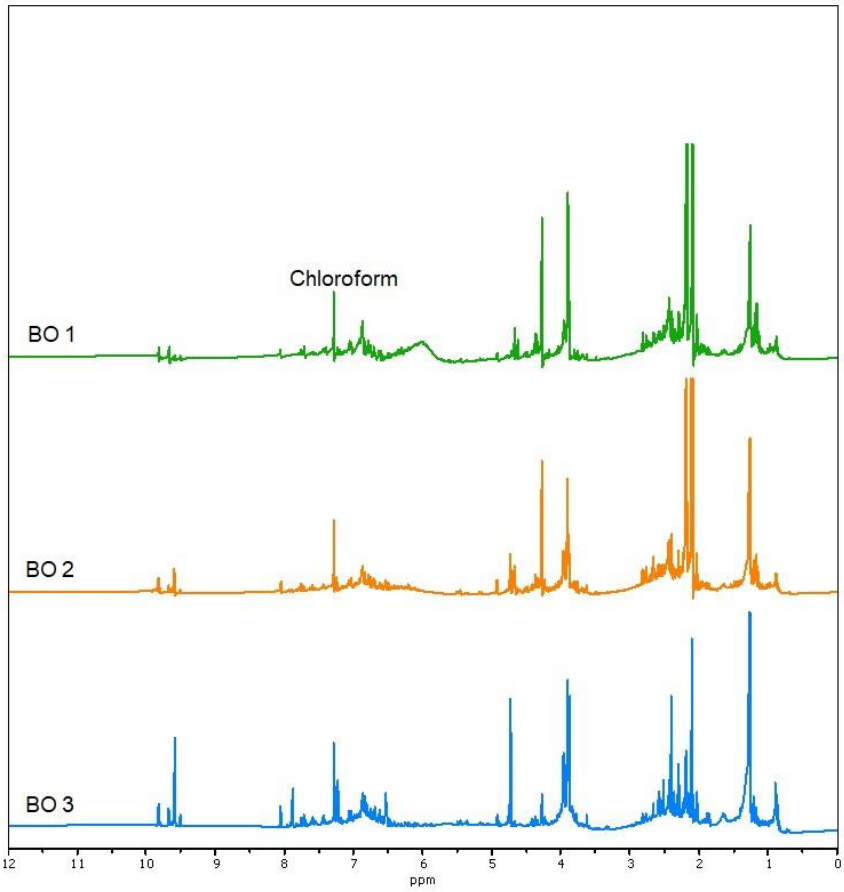

Fig. 33 ^{1}H NMR spectra of BO1, BO2 and BO3 samples

3.4.4 ^{13}C NMR analysis of bio-oil derived from rice husk

^{13}C NMR spectra of bio-oil samples are shown in Fig. 34 and the list of carbon types are represented in Table 17.

The compounds are illustrated from the resonances between 50 ppm and 100 ppm, which is ascribed to the carbon atoms adjacent to an oxygen atom in ethers, or alcohols.[29] The bio-oil contains carbonyl groups but the types are complex, for example, carboxylic acid, esters, ketones and aldehydes which could be reflected from the peaks located from 160 ppm to 210 ppm (>200 are usually ketones, 215-160 ppm for carbonyl carbons, 190-180 aldehydes, 175-260 acids and 160-110 ppm for total aromatic carbons), consistent with ^{1}H NMR results and FTIR spectra pointing to the presence of

aromatics.[279] The region of the ^{13}C NMR spectrum from 1 to 50 ppm consisted of aliphatic carbon region.[29]

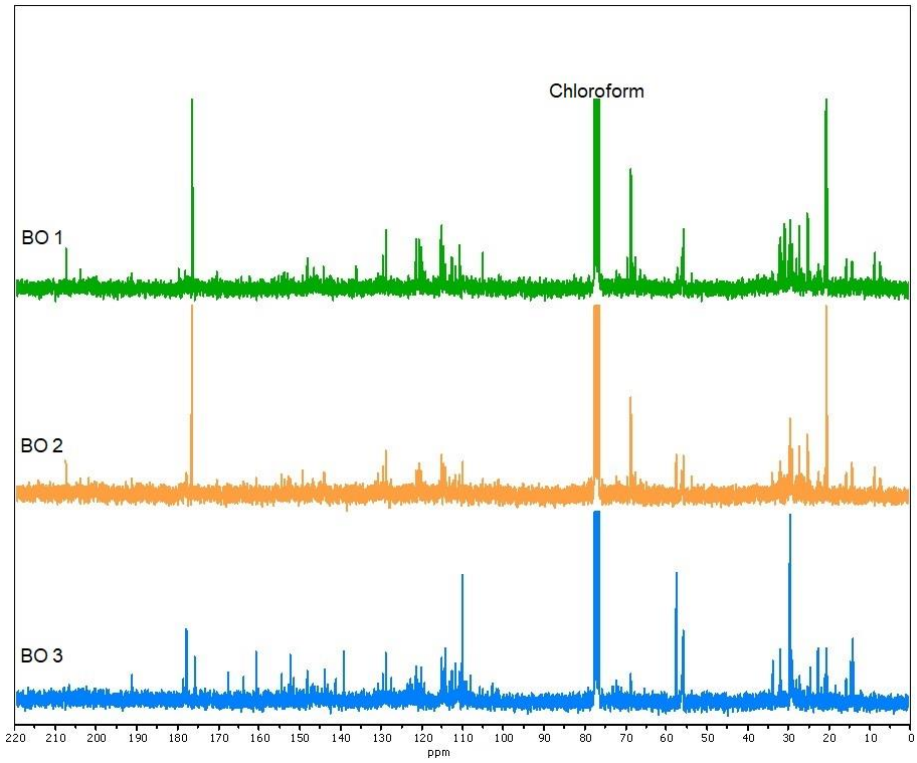

Fig. 34 ^{13}C NMR spectra of BO1, BO2 and BO3 samples

Table 17 ^{13}C NMR results of three bio-oil samples

Chemical shifts (ppm)	Type of carbon
215-160	Carbonyl carbons
160-110	Aromatic carbons
100-50	The carbon atoms adjacent to 1/2 oxygen atom(s) in ethers or alcohols
50-1	Aliphatic carbon

3.4.5 TG analysis of bio-oil derived from rice husk

TG results for the bio-oil shown in **Fig. 35**. The sample was heated up to 625 ^{O}C under (10 ^{O}C/ min) the nitrogen flow. The results indicated that a mass loss of approximately 70-

80% was investigated by 500 ^{O}C for all samples. The weight loss of BO samples before 150 ^{O}C were approximately 37.55% (BO1), 26.2% (BO2) and 18.7% (BO3) due to the evaporation of light volatiles which indicated that BO3 has the least moisture (amount of water) of all samples.[280] The major peak in DTG curve indicated that a significant weight loss during the thermal treatment in nitrogen at approximately 150 ^{O}C for BO1, 190 ^{O}C for BO2 and 230 ^{O}C for BO3, respectively. At the end of process, the mass residue is 17.5% (BO1), 20.5% (BO2), and 25.4% (BO3), respectively.

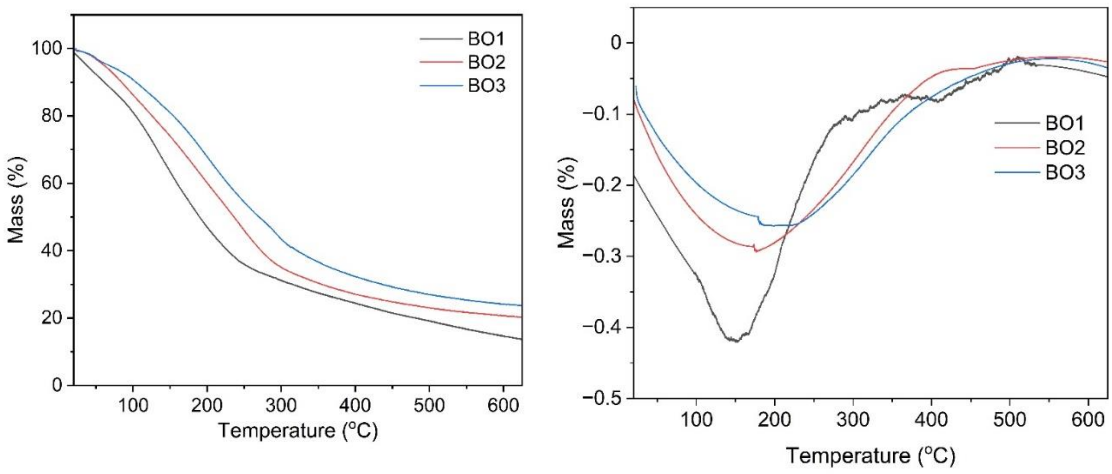

Fig. 35 TG and DTG curves of BO1, BO2 and BO3 samples

From this study, the results could confirm that bio-oil derived from rice husk using microwave-assisted method or thermal decomposition by CEM discover has successfully been produced, allowing its study as a carbon source for the preparation of carbon-silica composites (CSCs) from mesoporous silicas in the following step (Section 3.5).

However, this process could be used to provide the relatively low yield of bio-oil derived from rice husk due to the limitation of equipment. The maximum temperature of CEM discover SP microwave system can be reached at 280^{O}C, this led to losing spill cups regularly to catastrophic melting during pyrolysis reactions and just the small amounts of bio-oil derived from rice husk was produced.

In summary, BO3 is a good candidate for using as carbon source to prepare CSC materials in the next part due to its high contents of complex compounds which can be confirmed

from GC-MS and FTIR results also low amount of water (confirmed by TG). This condition also provides the highest yield of bio-char and the highest amount of inorganic contents that have been effectively removed from this obtained bio-char which also could make it easier to prepare silica material and activated carbon in the next step (as mentioned for the future work).

3.5 Carbon-silica composite (CSC) materials derived from rice husk

There has been great interest from many researchers to study carbon-silica composite materials due to its unique properties from silica and carbonaceous materials. Silica precursors are hydrophilic, biocompatible, and insulating, while carbonaceous materials from bio-oil are hydrophobic, conductive and possess high thermal and chemical stability.[32] Combining the beneficial properties of carbons and silica would be advantageous for many applications.

As previous works reported by Jiang *et al.*[16] and Sotiriou *et al.*[32] which demonstrated a series of reaction conditions for preparation of controllable CSC materials with continuum functionalities ranging from polar hydroxyl groups to aromatic surfaces from bio-oil. Both study using bio-oil from waste office paper which is prepared from microwave fast pyrolysis.

This work describes the first report for preparation of fully bio-based carbon-silica composite material which uses both bio-oil and silica materials generated from rice husk. The challenges in this work are the control of the porosity properties and the tuning of graphitic content of materials.

3.5.1 Optimisation of the SBA-15 and bio-oil ratio for carbon-silica composite preparation

Various conditions for preparation of CSCs materials were investigated due to it is the challenge to prepare CSC materials with tuneable pore size and controlled morphology.[32] From previous section (**section 3.4**), the results indicated that the composition of bio-oil is complex, composed of aromatics, aliphatics, aldehydes, and phenolic. The details

discussion of the bio-oil selected is vital for preparation of CSC materials with tuneable functionalities and surface properties in following part.

In previous work, the silica/bio-oil ratio could significantly affect the pore structure of the as-prepared composite material.[16] As a result, the optimum ratio of silica/bio-oil for the preparation of CSC with uniform mesoporous structure was studied. The ratio of silica/bio-oil was investigated at 1:1, 1:2 and 1:4 for the preparation of CSC materials followed by carbonisation under a nitrogen atmosphere at 500 ^{o}C. These CSC samples are denoted as CSC 1:1, CSC 1:2 and CSC 1:4, respectively. The porosity properties of the as-prepared materials were studied for the optimum ratio for CSC preparation.

3.5.1.1 Brunauer-Emmett-Teller (BET) analysis of SBA-15 and CSC materials derived from rice husk prepared with different ratio of silica/bio-oil

In order to investigate the textural and structural properties of SBA-15 and CSC materials, N_2 adsorption-desorption isotherms have been studied (**Fig. 36**). The N_2 adsorption-desorption isotherms of all as-prepared materials are of type IV, suggesting that they are all mesoporous materials. N_2 adsorption-desorption isotherm of SBA-15 (parent silica) exhibited an H1-type hysteresis loop that indicates the uniform distribution of mesopores. While, CSC1:2 and CSC1:4 led to the uniform mesoporous structure which is similar to ink bottle like (the wider hysteresis loop with narrowing of the pore entrances-H2-type).

The ratio of silica/bio-oil at 1:4 could lead to a narrow hysteresis loop as the pore width decreased due to a large amount of bio-oil filling the mesopores of parent silica, while CSC 1:1 reveals the formation of plugs or corrugated surface and provides a bimodal pore-width distribution (**Fig. 36**) due to an insufficient amount of bio-oil not fully coating the SBA-15 surface.

Additionally, the estimated thickness of carbonaceous layer was calculated by the pore diameter of SBA-15 and CSC materials and the porosity properties of materials are given in **Table 18**. By adjusting the ratio of silica/bio-oil, the thickness of carbonaceous layer in CSC materials could be controlled up to 4.45 nm. BET surface area and pore volume were found to be in the range from 366 to 411 m^2/g and 0.21-0.43 cm^3/g, respectively. For

carbonisation temperature at 500 °C, the as-obtained CSC from the ratio of SBA-15/bio-oil was 1:4 represents the CSC material has 411 m^2/g of specific BET surface area and pore width of 2.08 nm- caused by mostly filled with bio-oil into the silica pores. Where, the as-obtained CSC from the ratio of SBA-15/bio-oil was 1:2 has the uniform of mesoporous structure which is similar to structure of SBA-15.

It is clearly found that as the amount of bio-oil increases from 1 to 4, all the textural properties including pore volume, and pore diameter were decreased. CSC material prepared at ratio of silica/bio-oil = 1:4 (CSC4) shows S_{micro} of 251 m^2/g and V_{micro} of 0.10 cm^3/g which is the highest value of all as-prepared CSC materials. This ratio of silica/bio-oil = 1:4 could be the optimum ratio for CSC preparation at different temperatures (300°C -800°C) in the next step. As the micropore surface area is higher than that of SBA-15, this indicates the optimum of carbonaceous component. Presumably the micropores are at least partly in the carbon layer, as well as the silica mesopores being filled to leave micropores.

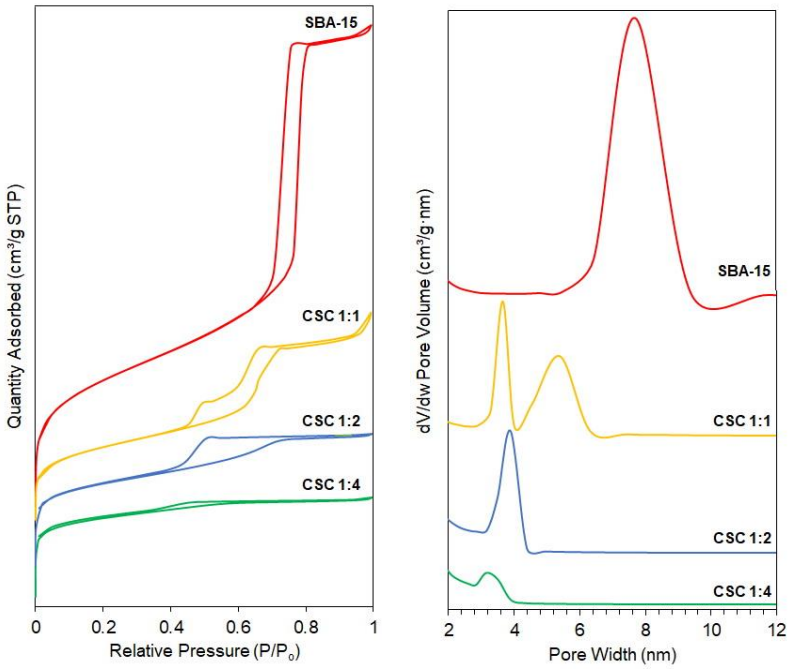

Fig. 36 BET results of the CSC materials prepared with different amounts of the bio-oil

Table 18 Textural properties of SBA-15 and CSC materials prepared with different amounts of the bio-oil

Sample	Silica	Bio-oil	S_{BET} (m^2/g)	S_{micro} (m^2/g)	V_{total} (cm^3/g)	V_{micro} (cm^3/g)	D_{BJH} (nm)	Estimated thickness of carbonaceous layer (nm)
SBA-15	1	-	602	196	0.98	0.08	6.53	-
CSC 1:1	1	1	366	48	0.43	0.02	4.76	0.88
CSC 1:2	1	2	363	174	0.27	0.08	2.97	1.78
CSC 1:4	**1**	**4**	**411**	**251**	**0.21**	**0.10**	**2.08**	**2.22**

Note: All values of porosity properties were measured and calculated by a single measurement using the Micromeritics® TriStar II plus

3.5.2 Effect of temperature on carbon-silica composite preparation

The carbon species in the materials vary significantly based on the carbonisation temperature, resulting in a continuum functionality ranging from polar hydroxyl groups to aromatic surfaces of CSC materials. As can be seen in **Fig. 37**, carbon-silica composite prepared at different temperatures ranging from 300 ^{O}C to 800 ^{O}C show the different shade (brown to black) of the as-obtained CSC materials.

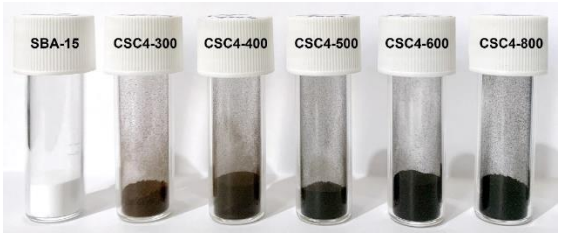

Fig. 37 Carbon-silica composite materials prepared at different temperature

3.5.2.1 Brunauer-Emmett-Teller (BET) Surface Area Analysis of SBA-15 and carbon-silica composite derived from rice husk prepared at different temperatures

Fig. 38 illustrates the nitrogen adsorption isotherm plots which indicate that SBA-15 exhibits a typical type-IV isotherm plot with an H1-type hysteresis loop, and a steep capillary condensation step in adsorption branch implies a uniform mesopore size.

Textural properties of SBA-15 and CSC materials prepared at different temperatures are demonstrated in Table 19, CSC materials prepared at 300 ^{O}C (denoted as CSC4-300) and 400^{O}C (denoted as CSC4-400) could not provide the expected N_2 adsorption-desorption isotherm, possibly due to bio-oil blocking the pore structure of CSC material, supporting the theory that the silica pores have been fully filled with bio-oils and the carbon source has not been removed extensively enough at this temperature (300-400 ^{O}C). This implies that the volume of bio-oil did not change that much at this temperature- in good accordance with textural properties that could not show the N_2 adsorption-desorption isotherms.

CSC materials prepared at 500 ^{O}C (denoted as CSC4-500), 600 ^{O}C (denoted as CSC4-600) and 800 ^{O}C (denoted as CSC4-800) represent H2-type hysteresis loop. This type indicates a complex pore structure consisting of an interconnected network of pores of different shapes and sizes. BET surface area gradually decreased from 411 m^2/g to 336 m^2/g as well as the percentage of V_{meso}/V_{total} decreased (47.6%-26.3%) with the increase of the carbonisation temperature. Whereas the percentage of V_{micro} /V_{total} increased from 52.4% to 73.7% with the increase of the carbonisation temperature, suggesting that the adjustment by carbonisation temperature can be used for easy modification of the surface and pore structure of CSC materials by functionalisation.[30,268]

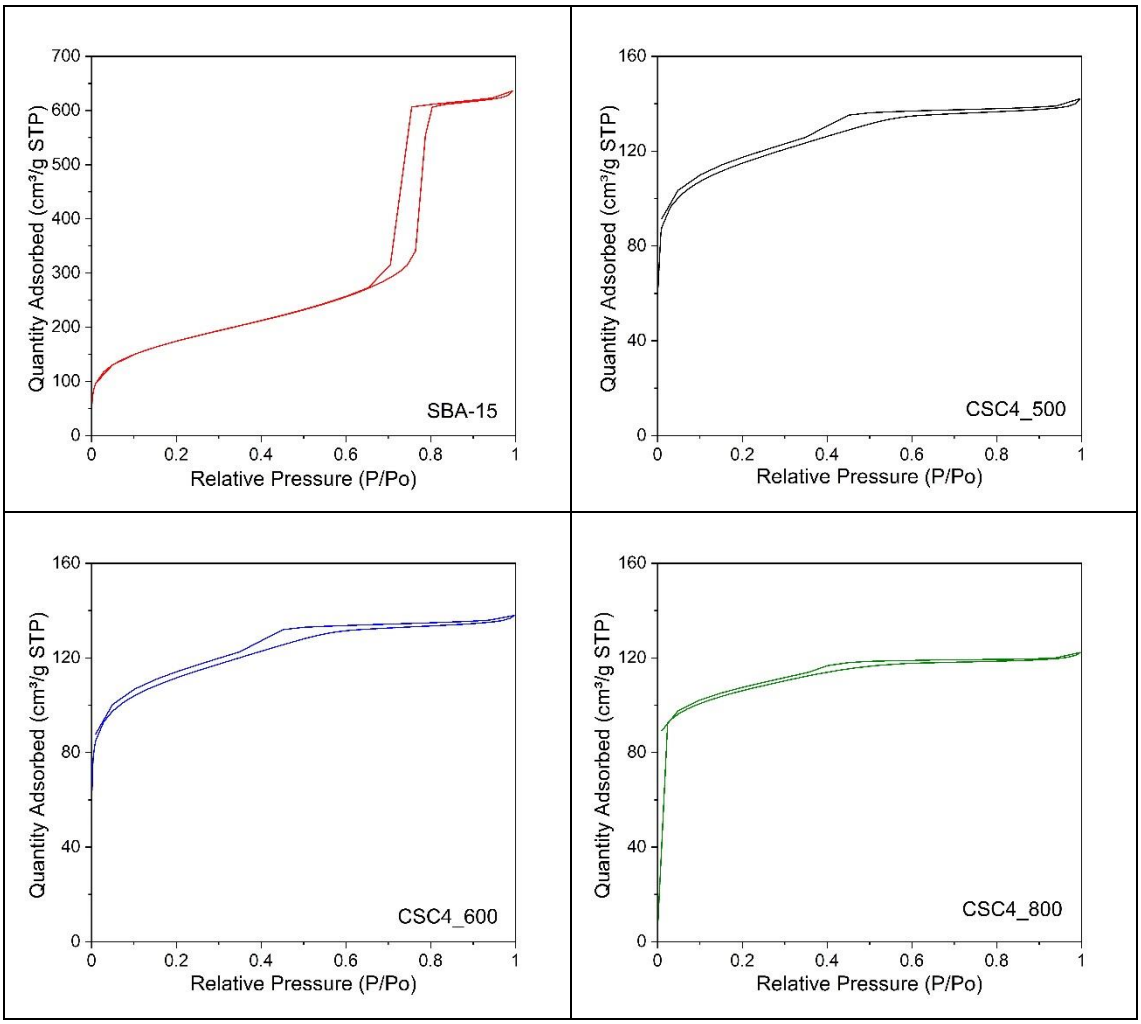

Fig. 38 N_2 adsorption-desorption isotherms of SBA-15, CSC4-500, CSC4-600, and CSC4-800

Table 19 Textural properties of SBA-15 and CSC materials prepared at different temperatures

Sample	Surface area (m^2/g)			Pore volume (cm^3/g)			V_{micro}/V_{total} (%)	V_{meso}/V_{total} (%)	D_{BJH} (nm)	Estimated thickness of carbonaceous layer (nm)
	S_{BET}	S_{micro}	S_{meso}	V_{total}	V_{micro}	V_{meso}				
SBA-15	602	196	406	0.98	0.08	0.90	8.20	91.8	6.53	-
CSC4-300	-	-		-	-	-	-	-	-	-
CSC4-400	-	-		-	-	-	-	-	-	-
CSC4-500	411	251	160	0.21	0.11	0.10	52.4	47.6	2.08	2.22
CSC4-600	355	266	89	0.21	0.14	0.07	66.7	33.3	2.40	2.06
CSC4-800	336	284	52	0.19	0.14	0.05	73.7	26.3	2.25	2.14

Note: All values of porosity properties were measured and calculated by a single measurement using the Micromeritics® TriStar II plus

3.5.2.2 SAXS analysis of SBA-15 and carbon-silica composite derived from rice husk prepared at different temperatures

The SAXS patterns of as-prepared CSC and SBA-15 (silica parent) provide evidence that the inorganic structure of the SBA-15 silica remains intact after bio-oil modification process. As shown in **Fig. 39**, SAXS patterns of CSC materials match well with parent SBA-15 which can be indexed to a hexagonal lattice.

Besides, the intensities of the peaks in SAXS pattern increase with the increasing of temperature. The highest intensity of peak can be observed for the 700 ^{o}C material, suggesting that the increasing of temperature has a positive effect on the composite structural ordering.[16]

The significant increase of intensities is described by the removal organic species from the inside of the mesopores and the formation of a more uniform carbonaceous layer. The pores of the materials were filled with organic compounds at lower temperature. Then, some of organic species could decompose with the increase of temperature and a

uniform layer containing the chemically stable compounds formed, coating with silica surface, confirming that the SAXS analysis could strongly support the validity of successful fabrication of CSC materials.

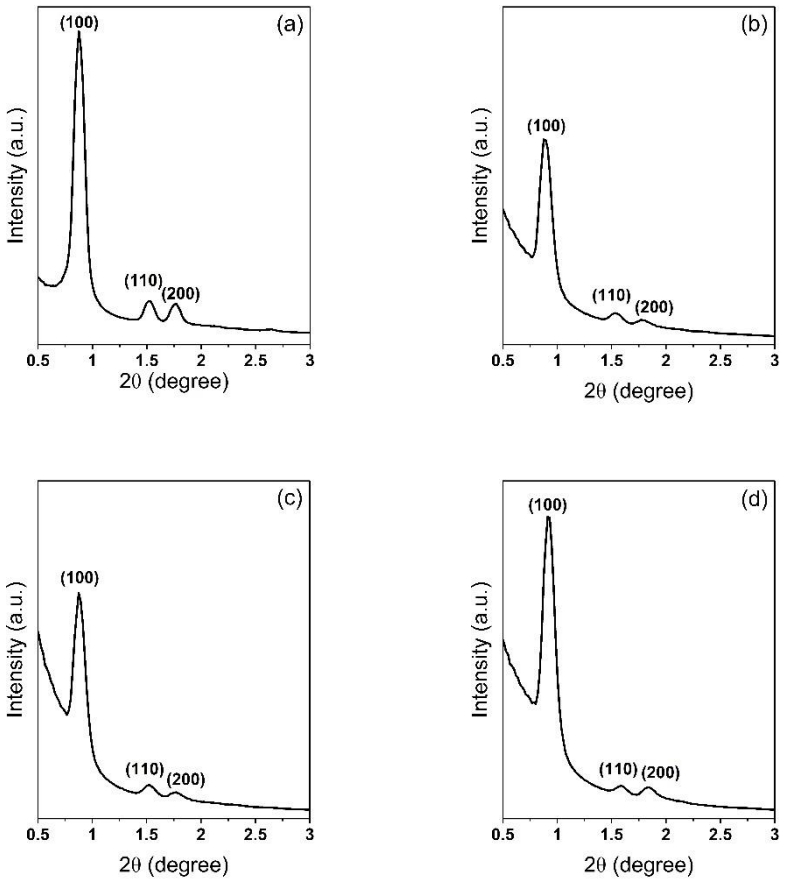

Fig. 39 SAXS spectra of SBA-15, CSC4-300, CSC4-500, and CSC4-700

3.5.2.3 SEM and TEM characterisation of SBA-15 and carbon-silica composite derived from rice husk prepared at different temperatures

SEM and TEM characterisation were carried out to investigate the morphology and size of the as-prepared CSC4-400, CSC4-500, CSC4-600 and CSC4-800. SEM images suggested an average diameter size of 1.2 ± 0.1 µm for CSC4-400, 1.2 ± 0.3 µm for CSC4-500, 1.1 ± 0.2 µm for CSC4-600 and 1.0 ± 0.1 µm for CSC4-800. SEM (**Fig. 40**) also showed similar morphology of rod-like structures formed in all samples. However, the rough surface of

CSC4-400 (**Fig. 40 (a)**) was represented- caused by the bio-oil coated onto the surface of CSC and the carbon source not being removed significantly at this temperature, in good agreement with textural properties. Whereas, smaller size of diameters and clearer surface of materials were investigated in CSC4-600 and CSC4-800. The increasing of temperature led to the clean surface of structures being demonstrated in CSC4-500, CSC4-600, and CSC4-800 (**Fig. 40 (b-d)**) because the strong interactions between oxygenated compounds existing in bio-oil and residual silanol groups in silicas, the organic compound not in close contact with silica surface. This could be more easily changed by increasing temperature resulted in a carbonaceous layer coating the interior of silica pores which could be further confirmed by XPS.

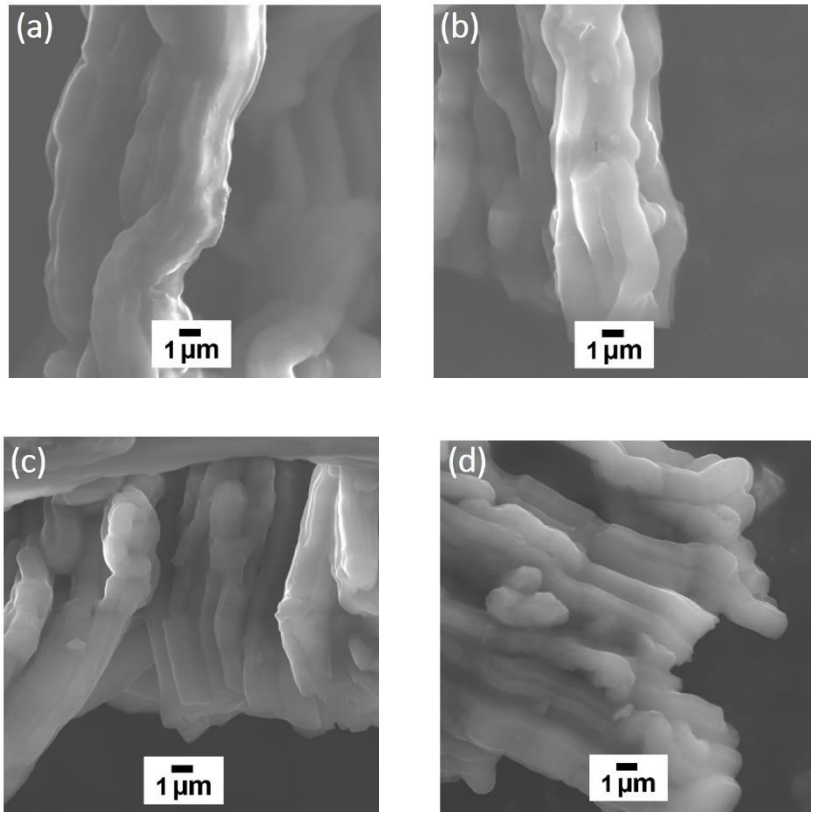

Fig. 40 SEM images of CSC4-400, CSC4-500, CSC4-600, and CSC4-800

TEM image (**Fig. 41 (a)**) of CSC4-400 represented that bio-oils were coated onto SBA-15 material, which is in good accordance with the information from SEM and porosity properties. As mentioned before from textural properties data, the pore structure of as-prepared material could not be seen at low temperature. Then, pore structures of as-prepared CSC materials could be seen from TEM image after carbonisation at higher temperature (500 ^{O}C- 800 ^{O}C). The small pore width (D_p) could be seen from TEM images (**Fig. 41 (b-d)**) of CSC4-500, CSC4-600, and CSC4-800 (approximately 2 nm) which implies that some of organic species could decompose with the increase of temperature and a uniform layer containing the chemically stable compounds formed by coating with SBA-15 surface.

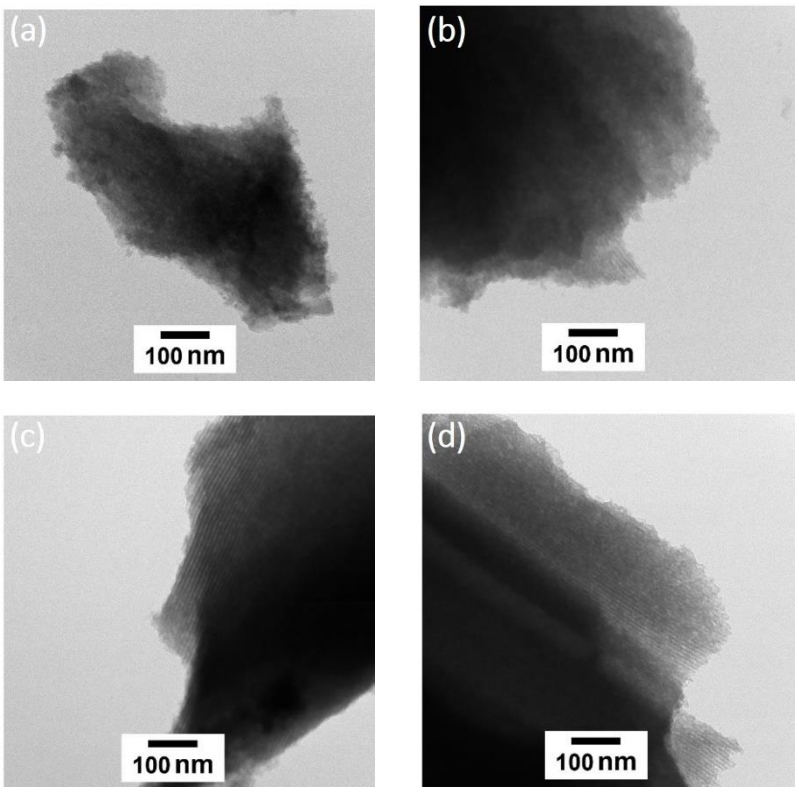

Fig. 41 TEM images of (a) CSC4-400, (b) CSC4-500, (c) CSC4-600, and (d) CSC4-800

3.5.2.4 XPS analysis of carbon-silica composite derived from rice husk prepared at different temperatures

XPS is a technique which analyses the chemical bonding state by irradiating x-rays on the samples surface of CSC samples, and measuring the kinetic energy of the photoelectron emitted from the CSC surface.[183] XPS was carried out to determine the elemental content on the CSC surface. Notably, most changing molecules are composed of elements such as C, N and O can be precisely distinguished by this technique.[281] XPS C1S data illustrates that C=C (aromatic), C-C (aliphatic), C-O (C-O-C or C-O-H) and COO (COOH/COOR) groups on the surface of CSC materials at 284.2 eV, 285.0 eV, 286.8 eV and 288.2 eV binding energy, respectively.[183,281]

XPS spectra (**Fig. 42 (a)**) indicate that CSC4-400 carbon surface still displays the COO group of ester and carboxylic group from bio-oil – in good according with the interpretation by FTIR, ^{1}H NMR and ^{13}C NMR analysis.[30]

As a significant loss in the proportion of hydrophilic compounds containing oxygen is observed upon heating to higher temperatures (500-800^{O}C) the disappearance of COO group can be observed in CSC4-500 (**Fig. 42 (b)**), CSC4-600 (**Fig. 42 (c)**) and CSC4-800 (**Fig. 42 (d)**) mateirials. These oxygenated carbon functionalities decompose with increasing temperature, showing an increase in aromatic character and a significant loss of hydrophilic and aliphatic compounds containing oxygen.

As can be seen the dominant peak in these samples is assigned to C=C group. The intensity of the C=C peak tends to increase with the increasing of temperature (from 9.59% to 43.41%), whereas C-C group tends to decrease (from 25.79% to 5.69%) as the increase of temperature –caused by the loss of aliphatic compounds. Moreover, the as-prepared CSC4-800 prepared at 800 ^{O}C, C-O group is disappeared – in good according with the previous report.[183]

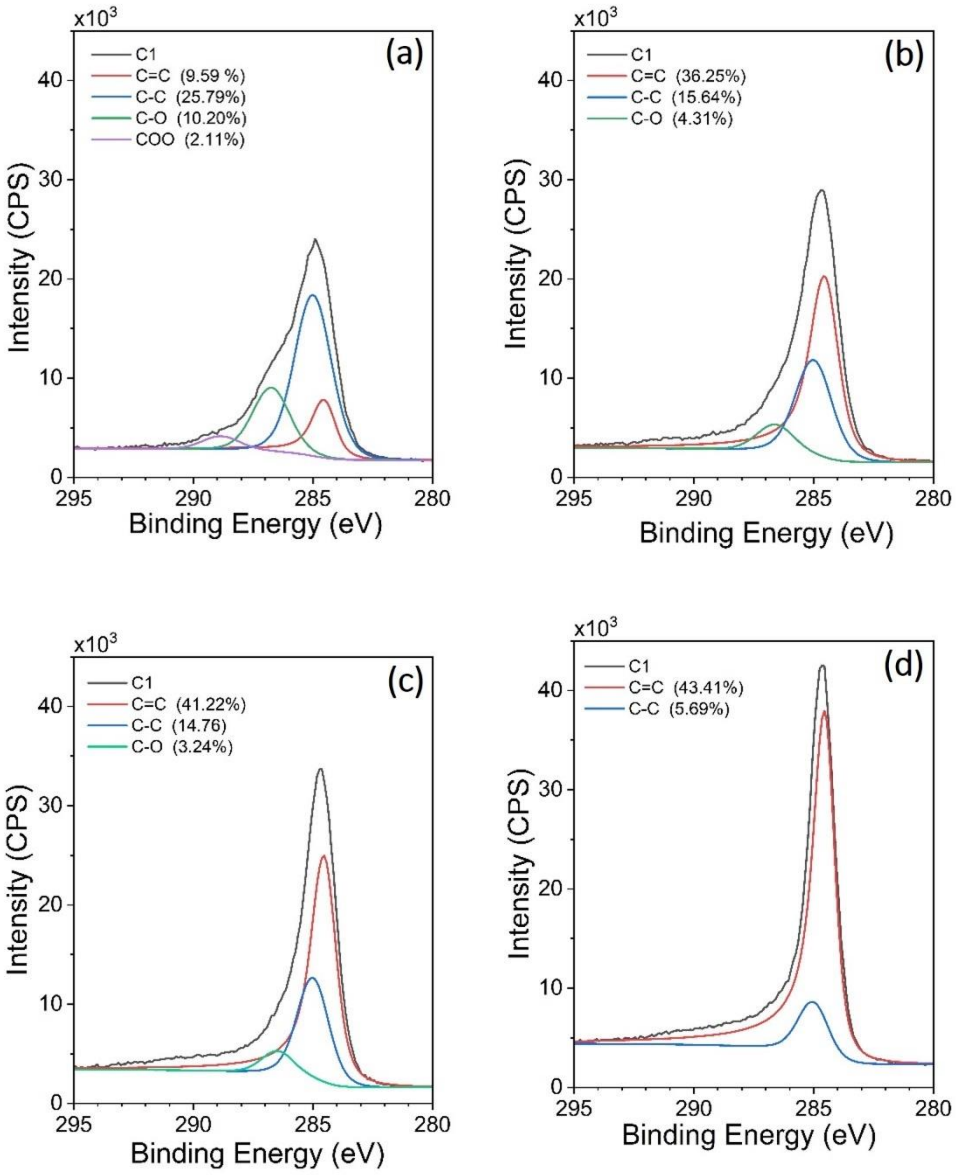

Fig. 42 XPS spectra of CSC materials (a) CSC4-400, (b) CSC4-500, (c) CSC4-600 and (d) CSC4-800 after carbonisation at 400 ^{O}C, 500 ^{O}C, 600 ^{O}C and 800 ^{O}C

3.5.2.5 FTIR analysis of carbon-silica composite derived from rice husk prepared at different temperatures

FTIR spectra of all CSC materials before carbonisation, after carbonisation at 500^{O}C, 600 ^{O}C and 800 ^{O}C are represented in (**Fig. 43**) FTIR spectra illustrate a peak at 1602 cm^{-1}, indicating the C=C stretching which matches with C=C bond in bio-oil.[307] The characteristic peaks at 1100 cm^{-1} and 960 cm^{-1} in the spectra of CSC were assigned to asymmetric Si-O-Si stretching vibration and symmetric Si-OH stretching vibrations — in good accordance with the synthesised SBA-15. Disappearance of the peak at 2930 cm^{-1} was assigned to CH stretching indicates that the aliphatic chains in bio-oil decompose completely at 500 ^{O}C.[16] The existence of C=O groups from acid, ester, ketone or aldehyde could be confirmed by the peak at 1720 cm^{-1}. It was found that this peak disappears after carbonisation, indicating the decomposition of C=O containing species at high temperature.[183]

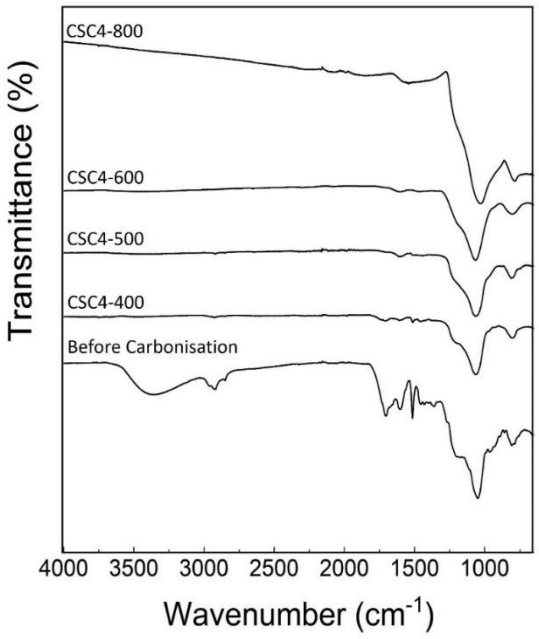

Fig. 43 FTIR spectra of CSC-before carbonisation, CSC4-400, CSC4-500, CSC4-600 and CSC4-800

3.5.2.6 ^{13}C solid-state NMR analysis of carbon-silica composite derived from rice husk prepared at different temperatures

^{13}C solid-state NMR spectra of CSC materials prepared at 300 ^{O}C, 400 ^{O}C, 500 ^{O}C and 600 ^{O}C are represented in **Fig. 44**. CSC material prepared at 800 ^{O}C (CSC4-800) could not be analysed because of the high conductivity of the material, resulting in the inability to properly tune the probe. This phenomenon implies that CSC material prepared at high temperature could be applied in electrochemistry, chemical sensor and nano-electronic applications.[63] ^{13}C solid-state NMR spectra of all CSC materials represent aromatic group in a range of 150-110 ppm which are a value consistent with the predominantly aromatic character of the material. ^{13}C solid-state NMR spectrum of only CSC4-300 reveals variety of functional groups such as carboxylates (acids/esters) at ca. 175 ppm, aromatics at ca. 150-110 ppm, aliphatics at ca. 30 ppm, and alcohols at ca. 55 ppm.[282] These functional groups carboxylates (acids/esters) at 175ppm are almost absent at 400^{o}C and then disappear at 500^{o}C and 600 ^{o}C also furanic at 150 ppm and phenolic at 110 ppm have disappeared at higher temperature (CSC-500 and CSC-600) which indicated the decomposition of aliphatics and alcohols. It should be noted that the NMR and FTIR results specified that the organic functionality of CSC materials was altered by the adjustment of carbonisation temperature.[16]

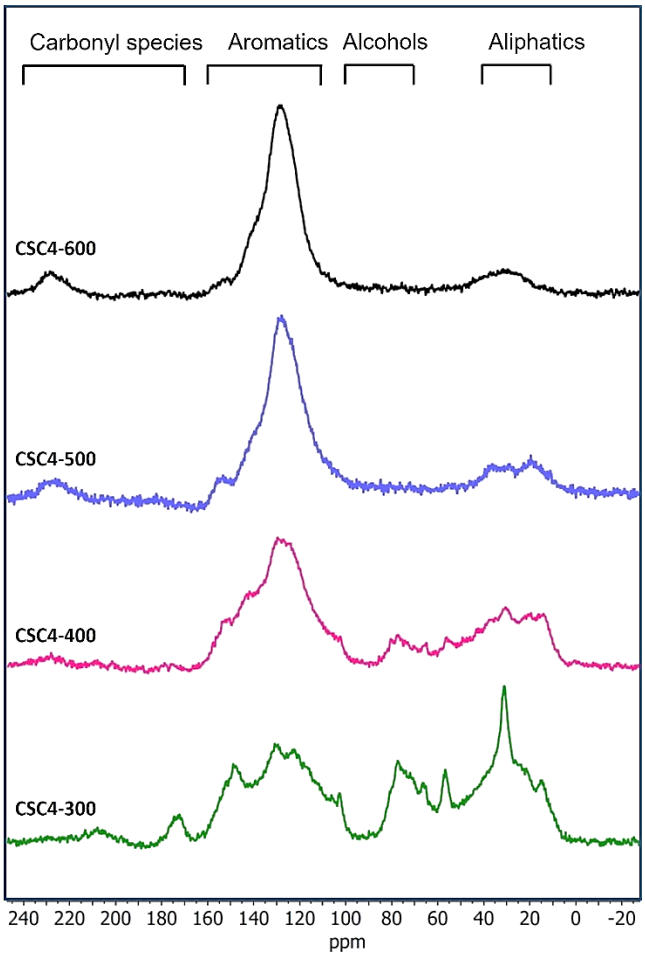

Fig. 44 ^{13}C solid-state NMR spectra of the CSC materials prepared at different temperatures

To the best of our knowledge there are no reports on fully bio-based carbon-silica composite material from rice husk being successfully synthesised from bio-oil derived from rice husk via microwave-assisted pyrolysis (as carbon source) and SBA-15 (as parent silica), also synthesised under the microwave-assisted irradiation from silicate solution derived from rice husk with controllable functionality and surface properties.

This mild condition with the simple approach allows the composite to retain the porosity characteristics of parent silica by attaching a thin carbonaceous film on the surface, giving great control over the surface polarity. Moreover, the surface properties of the fully bio-based carbon-silica composite material can be simply tuned by the variation of

preparation temperatures – causing a continuum of functionalities ranging from polar hydroxyl rich surfaces to carbonaceous aromatic surfaces which can be confirmed by ^{13}C solid-state NMR, FTIR and XPS.[37] In addition, these materials will be studied for methylene blue removal in the next part.

3.6 Study of methylene blue adsorption by as-synthesised mesoporous materials derived from rice husk

Previous parts demonstrated the synthesis of mesoporous materials. In this part, the application of as-synthesised mesoporous materials derived from rice husk from the previous part including SiO_2, SBA-15 and CSC materials for MB adsorption were investigated. The as-synthesised materials derived from rice husk which possess the high BET surface area, pore volume and optimum pore width were selected as adsorbent for removal of MB in aqueous solution. In this section, SiO_2 (surface area of 322 m^2/g and D_{BJH} of 4.05 nm), SBA-15 (surface area of 602 m^2/g and D_{BJH} of 6.53 nm), and CSC4-600 (surface area of 355 m^2/g and D_{BJH} of 2.40 nm) were used to investigate MB adsorption.

The adsorption technique is an effective and simple method for wastewater treatment, but there are several disadvantages such as high cost of adsorbents and difficulty in regeneration, which increase the cost for wastewater treatment. Thus, production of low-cost adsorbent with high efficiency as well as a sustainable abundant source is still a challenge for water remediation.[283] This work was curtailed due to time lost during Covid. This section reports MB adsorption efficiency, kinetic study, isotherm study as well as thermodynamic study of MB adsorption by the as-prepared bio-derived mesoporous materials.

3.6.1 UV-Vis quantification of methylene blue

In this part, a series of concentrations (1, 2, 4, 6, 8, 10 ppm) of methylene blue were prepared in DI water. In terms of kinetics, isotherms and thermodynamics study, the calibration curve of MB dye was prepared for UV-Vis quantification in the linear range and R^2 of 0.9996 as shown in **Fig. 45**. This calibration curve used for the determination of MB

adsorption onto as-prepared materials. Each mixture was determined with the UV-Vis method, with maximum absorption at 664 nm.

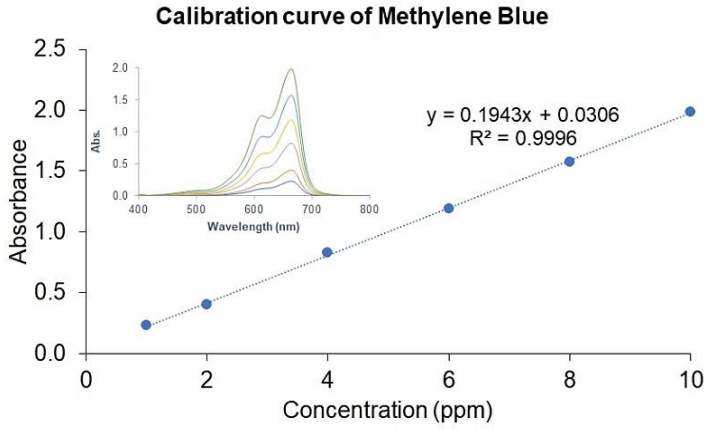

Fig. 45 Calibration curve of methylene blue for UV quantification

As described in section 2.4.6, Fig. 46 illustrates a schematic diagram of the methodology for methylene blue adsorption by as-synthesised mesoporous materials derived from rice husk. Batch adsorption experiments were carried out and a small amount of mix solution was withdrawn at different time intervals and then subjected to UV-Vis analysis. The adsorption capacity at each time point was calculated and plotted against time.[256] The adsorption capacity at each time q_t (mg/g) was calculated, and pseudo-first order model and pseudo-second order model were investigated for the kinetic adsorption. The isotherms are analysed by adsorption models which include Langmuir isotherm and Freundlich isotherm. All adsorption operations were carried out by shaking the solution containing dose of adsorbent 0.5 g/l in the desired concentration of MB, shaking at 150 rpm until concentration equilibrium was reached as can be seen in Fig. 46. Finally, the influence of temperature on the MB adsorption isotherm onto as-synthesised materials at different temperatures were investigated. The kinetics adsorption, Isotherms and thermodynamic adsorption results will be discussed in detail in a subsequent section.

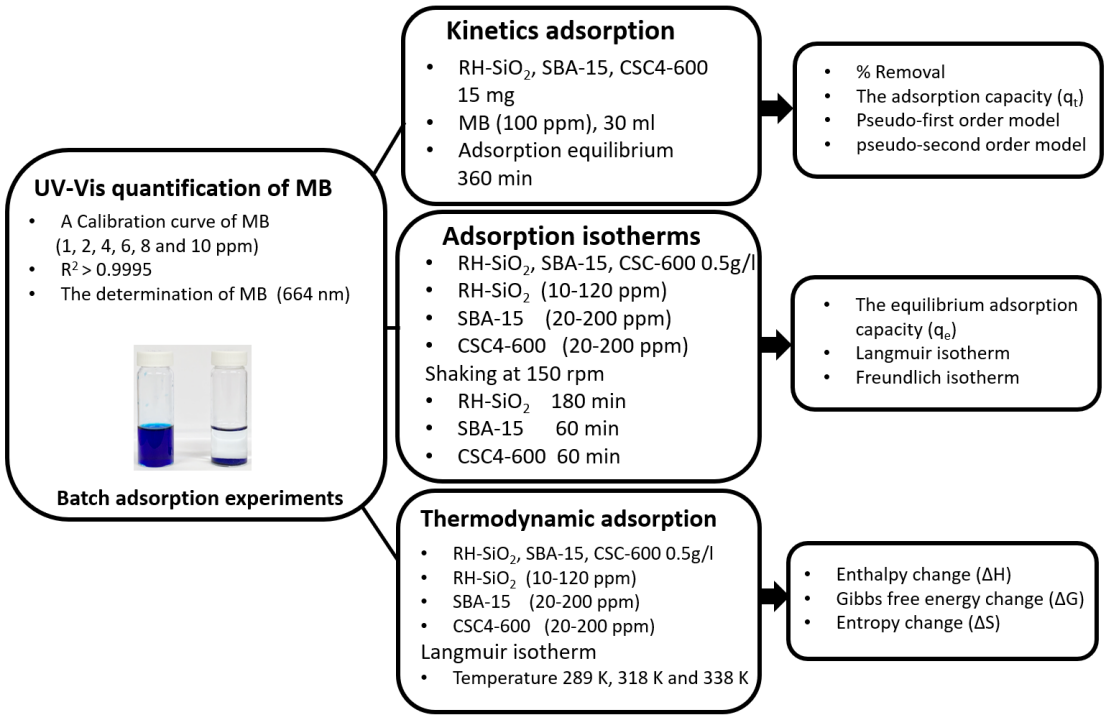

Fig. 46 A schematic diagram of the methodology for methylene blue adsorption by as-synthesised mesoporous materials derived from rice husk

3.6.2 Kinetics of methylene blue adsorption by as-synthesised mesoporous materials derived from rice husk

The rate of methylene blue adsorption by adsorbent was one of the significant factors that define the efficiency of adsorption. From these results represent that SBA-15 shows the highest removal rate of all materials (98.15%) within an hour, CSC can remove methylene blue dye (78.30 %) and SiO_2 can only remove 43.22% of the methylene blue dye in an hour as can be seen in Fig. 47. It is clearly revealed that the removal rates for all materials are fast, especially in the initial stage. Due to MB molecules at high concentration for the initial stage, providing higher driving force to overcome the mass transfer resistance of MB molecules from aqueous solution to adsorbent.[284]

The determination of kinetic models of MB adsorption on the as-synthesised mesoporous materials was investigated including, pseudo-first order and pseudo-second-order models. The pseudo-first-order and pseudo-second-order models are shown in Fig. 48

and the kinetic parameters for SiO_2, SBA-15 and CSC are listed in **Table 20.** The kinetics analysis showed that the overall adsorption process was successfully fitted with the pseudo-second-order kinetic model according to the better coefficient of determination ($R^2 > 0.99$) specifically, the correlation coefficient (R^2) for pseudo-second-order kinetic model of SiO_2, SBA-15 and CSC was found to be 0.9991, 0.9999 and 0.9998 represented in **Fig. 49**. In contrast, R^2 values for pseudo first order model are 0.9017, 0.9512 and 0.9734, respectively. This suggests that a strong attractive force occurred between the dye molecules and the sorbent, and with an increase in contact time, the remaining vacant surface sites are difficult to be occupied owing to saturation occurring.[283] This could be due to the deficient number of available sorption sites at the end of the sorption process, thus the removal efficiency remained almost constant after 60 min.

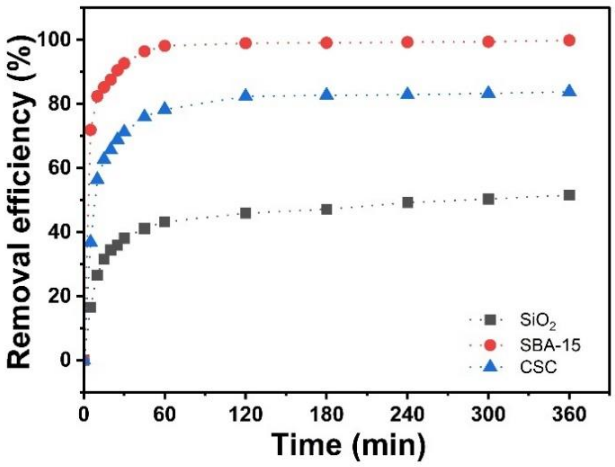

Fig. 47 Removal efficiency (%) of methylene blue by SiO_2, SBA- 15 and CSC materials

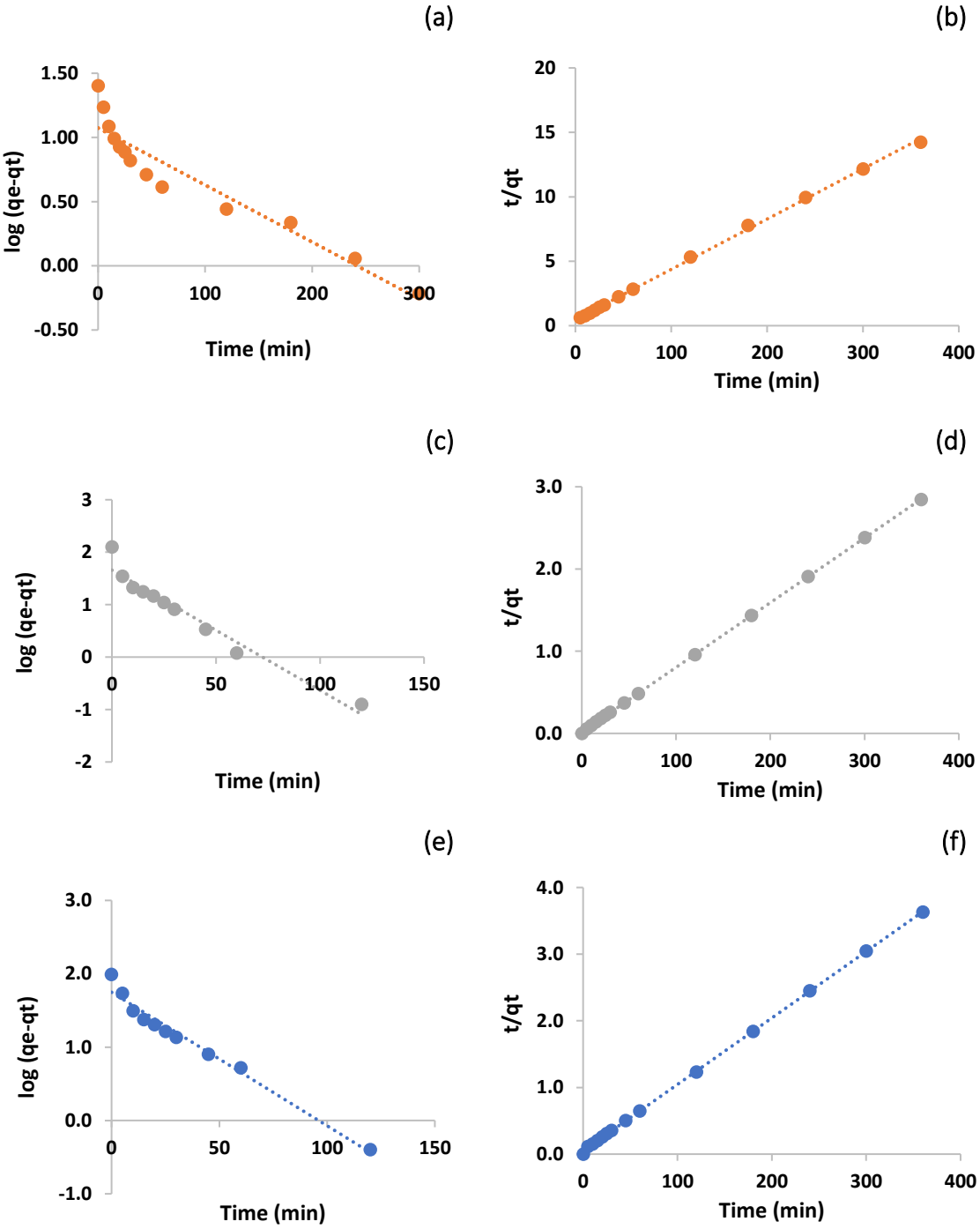

Fig. 48 Pseudo-first-order adsorption kinetic and Pseudo-second-order adsorption kinetic for the adsorption MB onto SiO_2 (a,b), SBA-15 (c,d) and CSC4-600 (e,f), respectively

Table 20 Kinetic parameters of methylene blue adsorption onto SiO_2

Adsorbent	Pseudo-first order			Pseudo-second order		
	$q_{e\ cal}$ (mg/g)	k_1 (1/min)	R^2	$q_{e\ cal}$ (mg/g)	k_2 (mg /g·min)	R^2
SiO_2	11.83	0.010	0.9017	25.64	0.0032	0.9991
SBA-15	45.47	0.053	0.9512	126.58	0.0040	0.9999
CSC4-600	55.95	0.042	0.9734	100.00	0.0021	0.9998

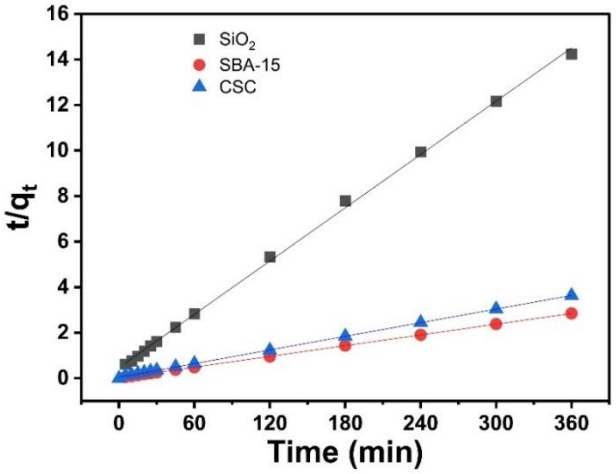

Fig. 49 Pseudo-second-order adsorption kinetic for the adsorption MB onto SiO_2 SBA-15 and CSC

3.6.3 Adsorption isotherms for methylene blue removal by as-synthesised mesoporous materials derived from rice husk

Methylene blue adsorption mechanism on mesoporous materials have been studied by adsorption isotherm models include Langmuir isotherm and Freundlich isotherm to describe the type of interaction between MB dye and the surface as-prepared materials.[79]

Adsorption capacity demonstrating how much absorbent is reasonable to enrich an adsorbate from a given solution is an important factor. Langmuir isotherm describes monolayer formation on the homogeneous surface of mesoporous materials with the limitation of surface-active sites while Freundlich isotherm describes that MB multilayers can be formed on the surface of mesoporous material.[79,285]

The adsorption process both of Langmuir isotherms and Freundlich isotherms of MB onto SiO_2, SBA- 15 and CSC4-600 materials are shown in **Fig. 50**. The correlation coefficient of Langmuir isotherms for SiO_2, SBA- 15 and CSC materials was found to be 0.9969, 0.9997 and 0.9990, respectively.

Due to the correlation coefficient determined from Langmuir isotherms (R^2>0.99) of all materials are higher than that calculated from Freundlich model which are also summarised in **Table 21**, thus these steps fitted better with the Langmuir isotherms, and are plotted in **Fig. 51** rather than Freundlich isotherm (**Fig. 50 b,d,f**). This suggested that the equilibrium adsorption capacity increases with increasing initial concentration of MB, which derives from the larger mass transfer driving force and better diffusion process at the higher initial concentration.[283]

Table 21 Isotherm parameters of MB adsorption onto SiO_2, SBA-15 and CSC at 25 ^{O}C

Adsorbent	Langmuir				Freundlich		
	q_m (mg/g)	k (L/mg)	R_L	R^2	1/n	k_f	R^2
SiO_2	37.74	0.1540	0.051-0.238	0.9969	0.268	11.55	0.8902
SBA-15	149.25	1.5227	0.003-0.015	0.9997	0.120	93.80	0.8478
CSC	107.50	0.4627	0.012-0.052	0.9990	0.079	74.08	0.9395

The related parameters are calculated and given in **Table 21.** These results show the highest q_m value was found to be 149.25 mg/g of SBA-15, has higher value than the q_m of SiO_2 (37.74 mg/g) and CSC (107.50 mg/g). Moreover, the q_m value of as-prepared SBA-15 also has higher value than q_m reported by Abboud et al.[286] This suggesting that SBA-15

with uniform pore diameter and higher surface area than CSC and SiO_2, hold a promising adsorption property for cationic dyes.

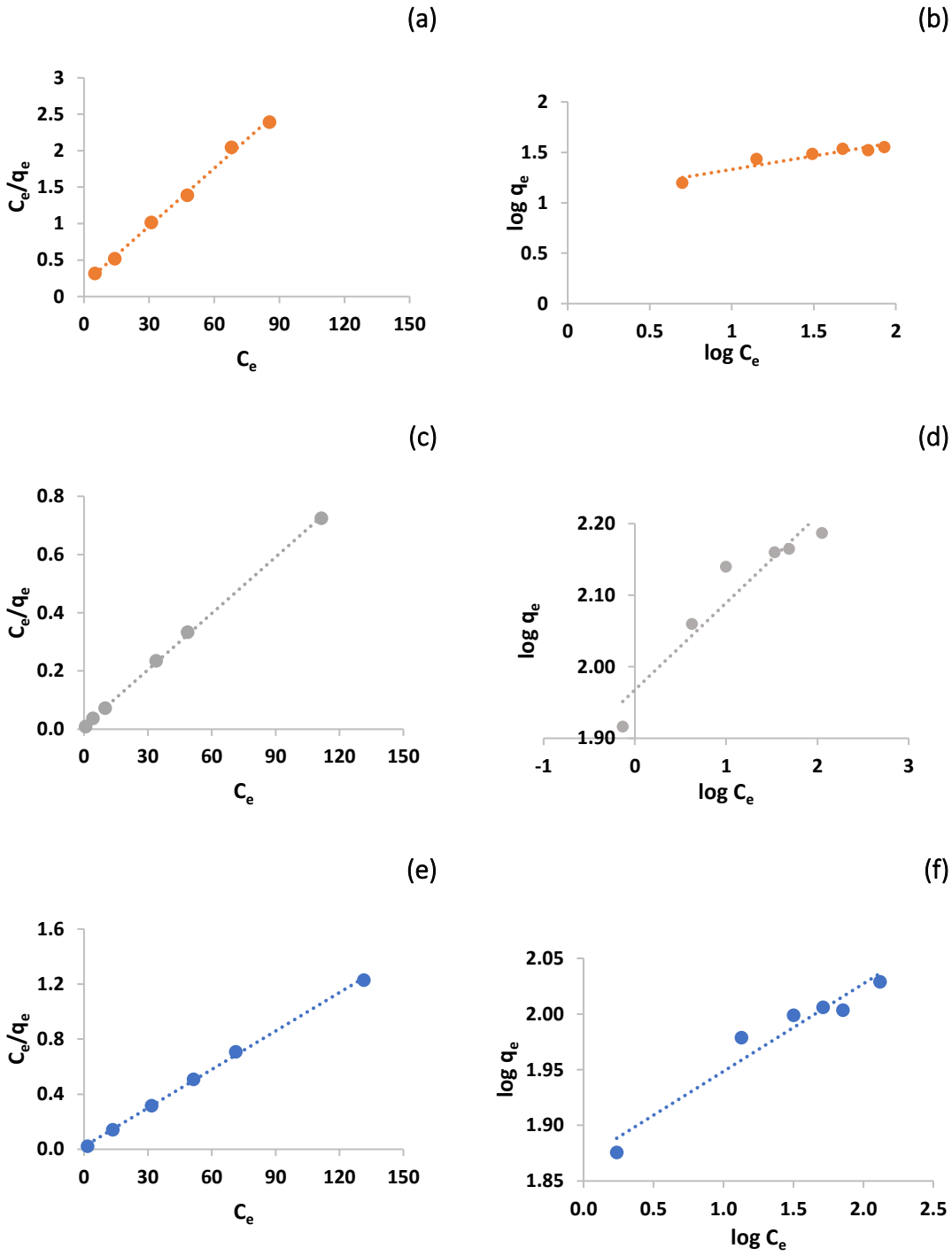

Fig. 50 Adsorption isotherms: Langmuir isotherm and Freundlich Isotherm for the adsorption MB onto SiO_2 (a,b) , SBA-15 (c,d) and CSC (e,f), respectively

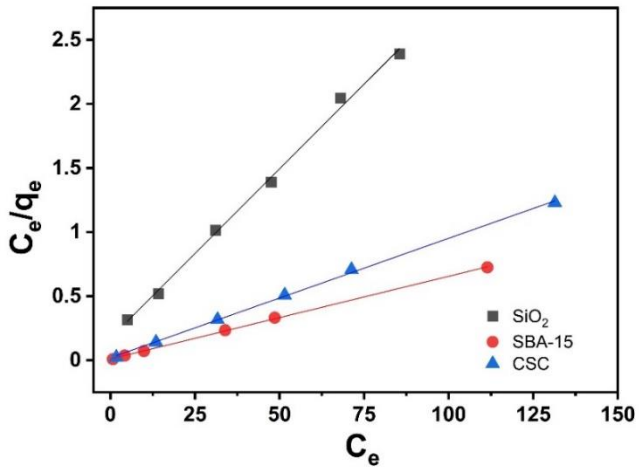

Fig. 51 Langmuir isotherm of MB adsorption onto RH-SiO_2, SBA-15 and CSC, respectively

3.6.4 Thermodynamic adsorption study

To investigate the influence of temperature on the adsorption of MB onto as-synthesised materials, the different temperatures at 298 K, 318 K and 338 K were studied for MB adsorption isotherms. Thermodynamic parameters including, enthalpy change (ΔH), Gibbs free energy change (ΔG) and entropy change (ΔS) were also calculated from thermodynamic adsorption study. The results data of adsorption isotherm from the previous part were specified that MB adsorption onto all materials is fitted with Langmuir isotherm thus this section, Langmuir isotherm used for study on thermodynamic adsorption at different temperature.

3.6.4.1 Thermodynamic adsorption study of SiO_2 derived from rice husk

For this study, the q_m is increased with the increasing of temperature from 298 K to 338 K which indicated that the high temperature is beneficial for MB adsorption onto SiO_2.[310] Thermodynamic parameters for the MB adsorption by SiO_2 are: ΔG = − 1.62 kJ/mol,-2.56 kJ/mol and −3.80 kJ/mol at 298 K, 318 K and 338 K, respectively; ΔH = 14.57 kJ/mol and ΔS = 54.15 kJ/mol K. Langmuir isotherm for MB adsorption onto SiO_2 at different temperature (298 K, 318 K and 338 K) is shown in Fig. 52 and isotherm parameters of methylene blue adsorption onto SiO_2 at different temperature are given in Table 22. The plot of I_n kc against 1/T for the determination of thermodynamic parameters of SiO_2 is

illustrated in **Fig. 53** and the positive value of ΔH (**Table 23**) can confirm that the MB adsorption onto SiO_2 was an endothermic process.[287] The adsorption was favourable at higher temperature and MB molecules were orderly adsorbed on the surface of SiO_2 which in good accordance with the results reported by Wu *et al*.[284], Zirak *et al.*[287] and Nassar *et al*.[283] The negative value of ΔG indicated that the feasibility and spontaneity of MB adsorption onto SiO_2.

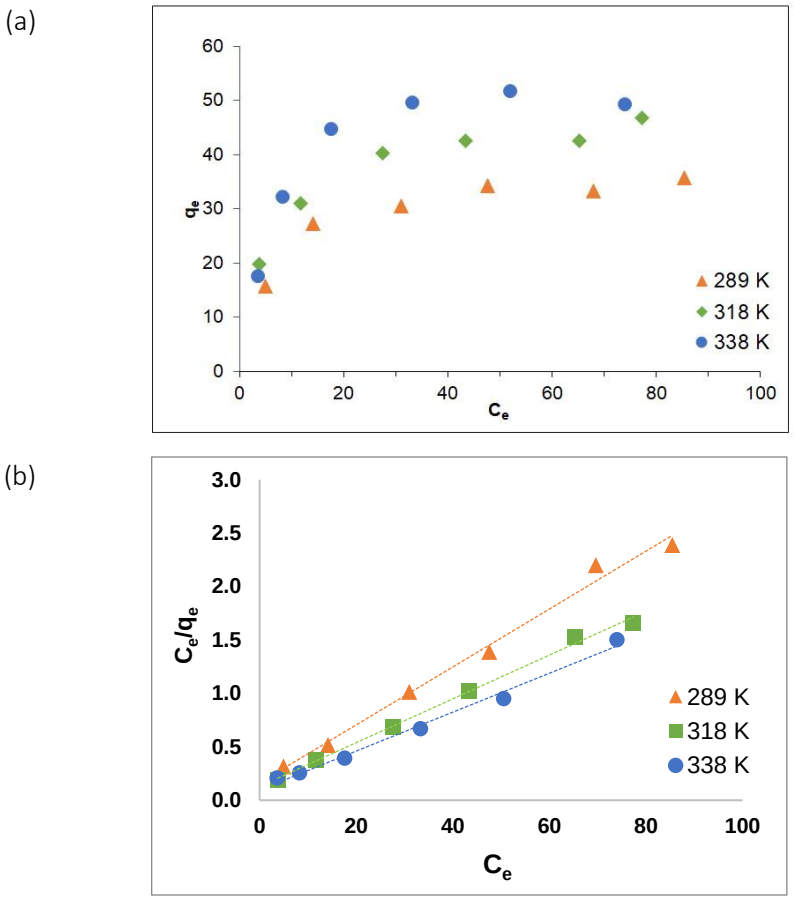

Fig. 52 The plot of q_e against C_e (a) and Langmuir isotherm (b) for MB adsorption onto RH-SiO_2 at different temperature

Table 22 Isotherm parameters of methylene blue adsorption onto SiO_2 at different temperature

Temperature (K)	q_m (mg/g)	k (L/mg)	R_L	R^2
298	37.74	0.1540	0.051-0.238	0.9969
318	48.78	0.1587	0.048-0.211	0.9954
338	54.64	0.1896	0.041-0.199	0.9933

Table 23 The thermodynamic parameters of methylene blue adsorption onto SiO_2 at different temperature

Temperature (K)	k_c	ΔG (kJ/mol)	ΔH (kJ/mol)	ΔS (J/mol K)
298	1.93	-1.62	14.57	54.15
318	3.24	-2.56		
338	3.87	-3.80		

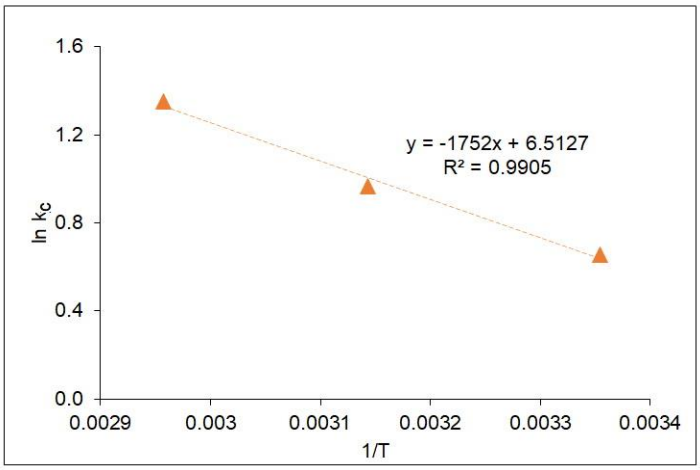

Fig. 53 The plot of In k_c against 1/T for the determination of thermodynamic parameters of SiO_2

3.6.4.2 Thermodynamic adsorption study of SBA-15 derived from rice husk

The isotherm study of MB adsorption onto SBA-15 was fitted with Langmuir isotherm. As a result, Langmuir isotherms were plotted at different temperatures (298 K, 318 K and 338 K) to study thermodynamic adsorption of SBA-15 shown in **Fig. 54**. The increasing of temperature led to the increasing of q_m value which are summarised in **Table 24**. It was found that the adsorption was favourable at higher temperature as can be concluded from the calculated value of ΔG = − 3.33 kJ/mol at 298 K, ΔG =-4.07 kJ/mol at 318 K and ΔG =-4.86 kJ/mol at 338 K, respectively. The thermodynamic parameters of the SBA-15 adsorption system are summarised in **Table 25.**

The plot of I_n kc against 1/T for the determination of thermodynamic parameters of SBA-15 also shown in **Fig. 55**. which used to calculate thermodynamic parameters for the removal of MB. The thermodynamic parameters calculated from Van 't Hoff equation were ΔH =8.03 kJ/mol and ΔS = 38.10 kJ/mol K. The positive value of enthalpy change identifies an endothermic process and increased adsorption capacity of SBA-15 for MB with temperature may be due to the mobility of the MB molecules and enables their penetration within the adsorbent — in accordance with results reported by Abboud *et al.*[286], Bardajee *et al.*[288] and Qiang *et al.*[289]

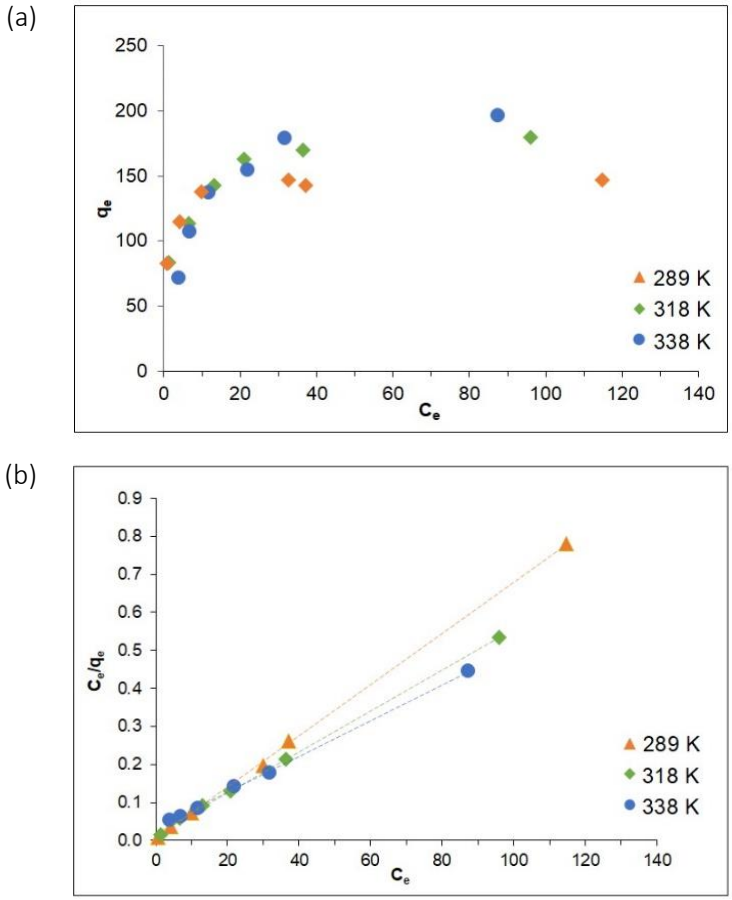

Fig. 54 The plot of qe against Ce and Langmuir isotherm for MB adsorption onto SBA-15 at different temperature (289 K, 318 K and 338 K)

Table 24 Isotherm parameters of methylene blue adsorption onto SBA-15 at different temperature

Temperature (K)	q_m (mg/g)	k_L (L/mg)	R_L	R^2
298	149.25	1.5227	0.003-0.015	0.9997
318	185.19	0.3176	0.017-0.068	0.9993
338	212.77	0.1420	0.037-0.151	0.9993

Table 25 The thermodynamic parameters of methylene blue adsorption onto SBA-15 at different temperature

Temperature (K)	k_c	ΔG (kJ/mol)	ΔH (kJ/mol)	ΔS (J/mol K)
298	3.84	-3.33	8.03	38.10
318	4.66	-4.07		
338	5.64	-4.86		

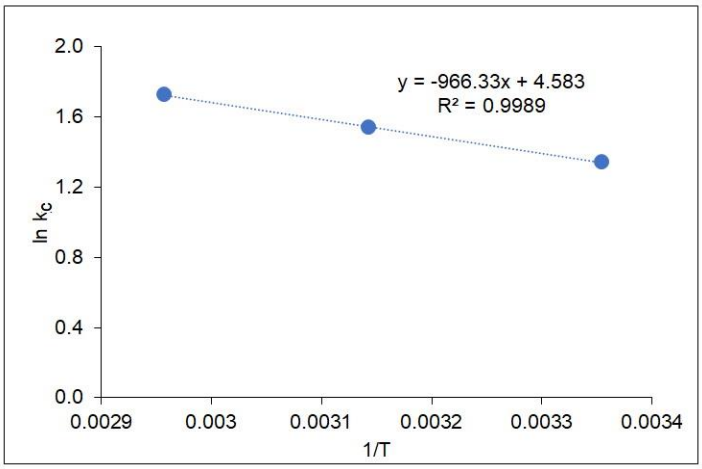

Fig. 55 The plot of In k_c against 1/T for the determination of thermodynamic parameters of SBA-15

3.6.4.3. Thermodynamic adsorption study of CSC material derived from rice husk

Langmuir isotherms were plotted at different temperatures (298 K, 318 K and 338 K) to study thermodynamic adsorption of CSC materials illustrated in **Fig. 56** and the q_m values are represented in **Table 26**. The increase of q_m value with the increase of temperature indicated that the high temperature is beneficial for MB adsorption onto CSC materials like SiO_2 and SBA-15.

The thermodynamic parameters of the CSC adsorption system are summarised in **Table 27**.

The thermodynamic parameters, based on Gibbs free energy change for the MB dye adsorption onto CSC are: ΔG =-4.28kJ/mol,-5.40kJ/mol and-5.98 kJ/mol at 298 K, 318 K and 338 K, respectively. The negative value of ΔG at various temperatures indicated that the adsorption processes are spontaneous.[288]

Moreover, endothermic process and increase of randomness during the adsorption of MB was identified by both positive values of ΔH = 3.52 kJ/mol and ΔS = 28.08 kJ/mol K, respectively which can be calculated from the slope and intercept of linear plot (**Fig. 57**) of ln Kc versus 1/T.[287]

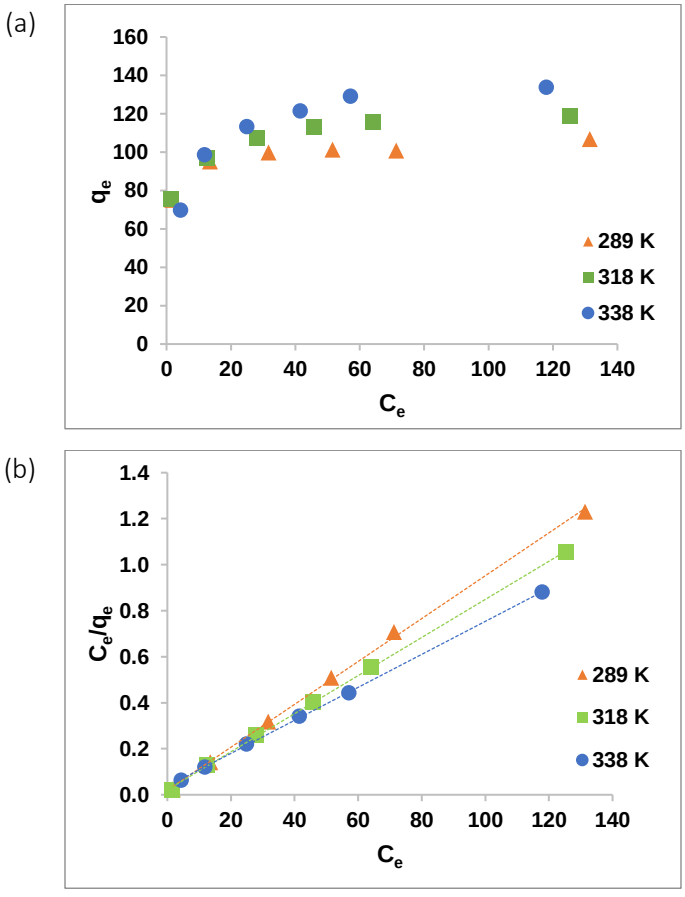

Fig. 56 The plot of q_e against C_e and Langmuir isotherm for MB adsorption onto CSC different temperature (289 K, 318 K and 338 K)

Table 26 Isotherm parameters of methylene blue adsorption onto CSC at different temperature

Temperature (K)	q_m (mg/g)	k (L/mg)	R_L	R^2
298	107.50	0.4627	0.012-0.052	0.9990
318	120.50	0.3897	0.019-0.078	0.9995
338	138.90	0.1809	0.030-0.128	0.9997

Table 27 The thermodynamic parameters of methylene blue adsorption onto CSC at different temperature

Temperature (K)	k_c	ΔG (kJ/mol)	ΔH (kJ/mol)	ΔS (J/mol K)
298	7.08	-4.28	3.52	28.08
318	7.70	-5.40		
338	8.38	-5.98		

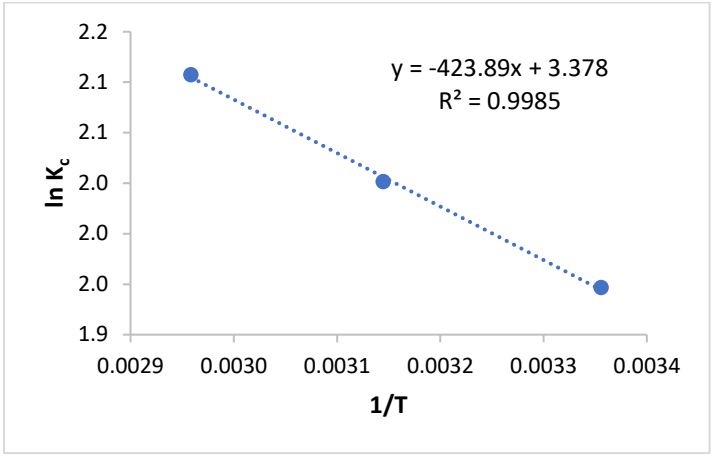

Fig. 57 The plot of In k_c against 1/T for the determination of thermodynamic parameters of CSC material

In this thermodynamic study, the positive value of ΔH can be confirmed the endothermic nature of MB adsorption onto SiO_2, CSC and SBA-15 and the adsorbed amount increased with temperature. Moreover, the negative value of ΔG indicated that the adsorption of MB onto the SiO_2, SBA-15 and CSC was spontaneous.[283,287] It should be noted that the removal of MB dye by adsorption procedure could be processed with low-cost materials in ambient temperature and simple method because it is not necessary to control the temperature during water treatment.

3.7 Conclusion

Project 1: Microwave-assisted synthesis of bio-derived mesoporous materials from rice husk for methylene blue removal

In this part, the development of greener routes for valorisation of rice husk using microwave-assisted methods (microwave-assisted biomass pretreatment, microwave-assisted hydrothermal and microwave-assisted pyrolysis) to produce bio-derived mesoporous materials were reported. Microwave-assisted method was performed through almost all processing steps to reduce significant reaction time and to save energy with the design method to maximize incorporation of all materials used in the process into the final product which defined as close-to-zero waste production.

Bio-derived mesoporous materials using silica along with carbonaceous components from rice husk to generate high surface area mesoporous materials, including silica, SBA-15 and carbon-silica composite were successfully prepared under microwave-assisted method for methylene blue removal.

SiO_2, CSC and SBA-15 were successfully prepared for MB adsorption. The as-synthesized materials exhibited relatively high BET surface area of 322 m^2/g, 602 m^2/g and 355 m^2/g for SiO_2, SBA-15 and CSC material, respectively, all materials exhibit type IV isotherms typical for mesoporous structure. SBA-15 has H1 hysteresis loop, confirming the uniform pore size distribution of cylindrical mesopores and a highly ordered hexagonal pore structure with arrays of uniform channels as can be investigated by TEM image. Meanwhile, CSC material represents H2 type hysteresis loop and TEM image revealed the CSC material still possessed pore arrangement as parent silica. The results for MB adsorption demonstrated that SBA-15 can remove nearly 100% of methylene blue (MB) within an hour (98.15%), CSC can remove 78.30% of MB while SiO_2 can remove only 43.22% of MB. The adsorption isotherms of all materials were fitted with the Langmuir isotherm and the highest q_m of SBA-15 was found to be 149.25 mg/g. In addition, SBA-15 possesses the highest $q_{e,cal}$ value of 126.58 mg/g, suggesting that mesoporous SBA-15 with uniform pore diameter and higher surface area than CSC and SiO_2, hold the most promising adsorption property for cationic dye (MB). Even though, CSC was not as good as the SBA-15, this may be due to it could be a good adsorbent for anionic dye adsorption such as Congo red which will be studied for future application. The positive value of enthalpy change also identifies an endothermic process and increased adsorption capacity of bio-derived mesoporous materials which suggesting that the adsorption procedure could be processed with cost-effective in ambient temperature and simple procedure because it is not necessary to control the temperature during wastewater treatment.

3.8 Future work

Project 1: Microwave-assisted synthesis of bio-derived mesoporous materials from rice husk for methylene blue removal

This work has investigated bio-derived mesoporous materials from rice husk synthesised by greener methods. However, some further work is still needed.

- Preliminary of preparation and characterisation of activated carbon and silica derived from rice husk biochar after microwave-assisted pyrolysis to yield bio-oil is still need to investigate in future work in order to design close-to-zero-waste production of rice husk waste biomass.
- Although the as-prepared bio-derived mesoporous materials were applied as promising adsorbent materials for methylene blue (cationic dye) removal in aqueous solution in this research, it is worth introducing these ordered bio-derived mesoporous materials with high surface area to get bio-derived catalyst support.
- It is well demonstrated that bio-derived mesoporous SBA-15 has high removal efficiency for MB removal. Reusability is important to reduce waste and this material is not be disposed of after their several use for wastewater treatment.

Chapter 4

Rice husk-derived cellulose microfibres/nanofibres for bio-composite film preparation

4.1 Organosolv fractionation of rice husk using microwave-assisted method

Over the last decades, biorefineries are increasingly focused on integrated process design for maximised valorisation of fractionated biomass components for a spectrum of various products. Consequently, utilisation of renewable lignocellulosic biomass like rice husk has received great attention. Various approaches based on chemical or thermal processes, or combinations of both have been reported, for example solvent extraction, alkaline treatment, organosolv pretreatment, and ionic liquid extraction.[111,194,236,290-292] Among the biomass fractionation methods, organosolv fractionation is an effective method, and has been applied for the highly selective dissolution of lignin and hemicelluloses and to separate cellulose from lignocellulosic materials and also recovers high purity of three parts.[193,237,293]

Typically, organosolv fractionation was used for cellulose, hemicellulose and lignin isolation by using a variety of organic solvents such as ethanol, acetone, methanol, organic acids (i.e., formic acid, acetic acid and sulfuric acid), inorganic and organic bases, ketones, ethylene glycol, esters and combined solvents with and without catalysts (acid, alkaline, etc.).[192,290,293] Organic solvents reduce the viscosity of the pretreatment medium, resulting in better penetration into the biomass, facilitating a more efficient removal of lignin.[238] Formic acid also exhibits a good ability to dissolve the lignin, and led to the recovered cellulose from the process being easy to hydrolyse.[294] Moreover, ethanol and water are highly effective in microwave energy absorption, the combination of an organosolv process together with microwave heating can offer an interesting new technology for the utilisation of lignocellulosic biomass.[167]

As mentioned above, the organosolv method can be used for the fractionation of biomass components into three fractions. However, most researches have been using organosolv process for delignification of lignocellulosic biomass, particularly in isolation of lignin which is a value-added product.[192,194,290] In other words, removal of lignin from lignocellulosic biomass exposes the purer cellulose fibre leading to a wide range of applications. Thus, this work was mainly focused on the cellulose fibre extracted from rice husk using organosolv fractionation process combined with microwave-assisted methods

since the ethanol organosolv-fractionation method can recover high-purity cellulose from biomass.[290,293,294] The various reaction parameters such as ethanol concentration and reaction temperature were also studied.

A schematic overview of production and application of cellulose fibres derived from rice husk and lignin fraction from organosolv fractionation is illustrated in Fig. 58. Apart from the cellulose-rich solid fraction, other two parts of lignin-rich solid fraction and hemicellulose-rich fraction will be studied in further work.

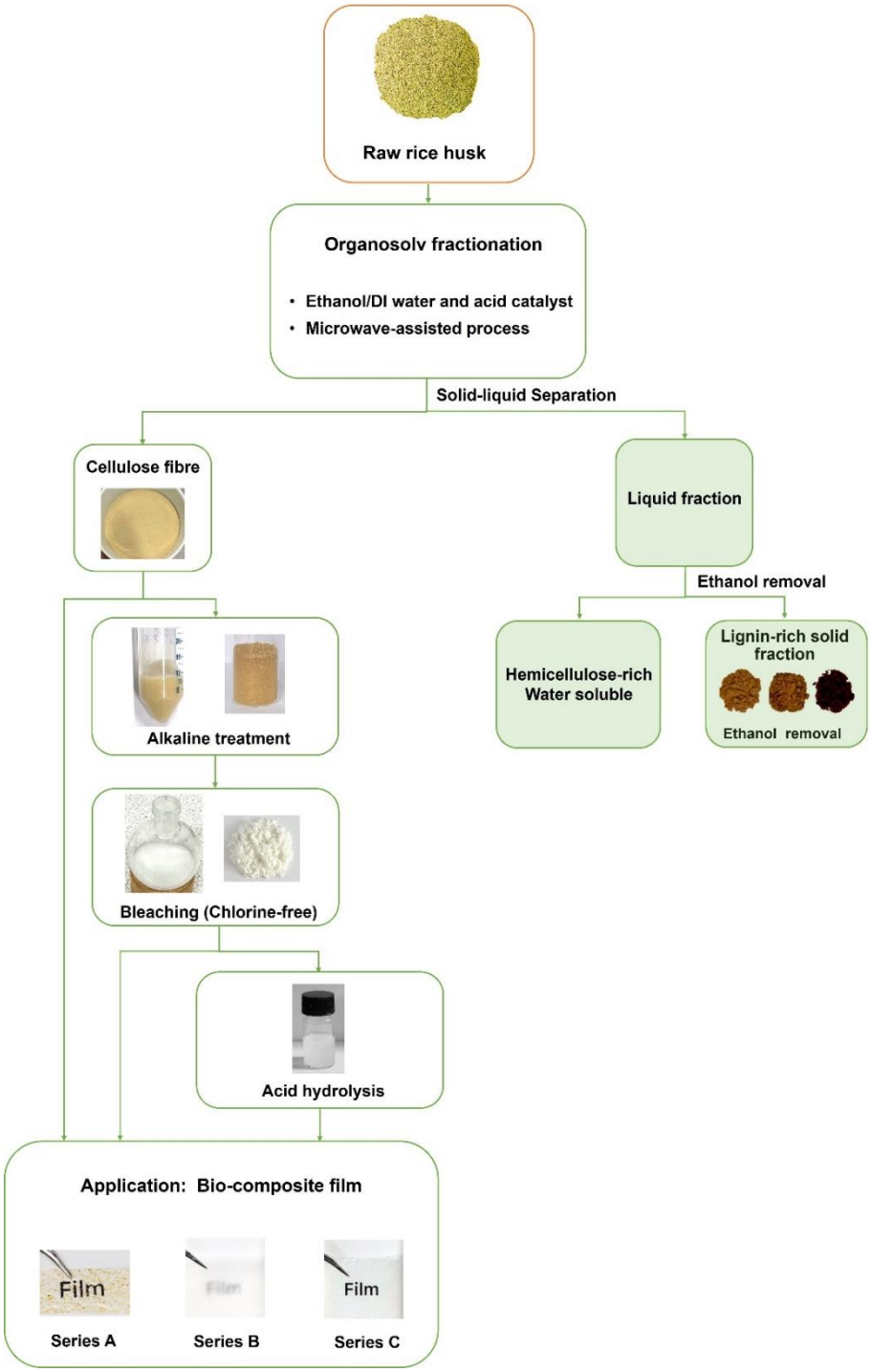

Fig. 58 Schematic overview of the production and the application of cellulose fibres derived from rice husk from organosolv fractionation
(the green rectangles are further works)

4.1.1 Optimisation conditions for organosolv fractionation of rice husk using microwave-assisted method

This section describes the combination of organosolv fractionation by using ethanol and DI water in the presence of diluted formic acid as acid promoter with microwave-assisted heating for the isolation of cellulose-rich fraction from rice husk. To achieve the optimum condition in organosolv process, (i) an appropriate combination of solvent ratio and (ii) reaction temperature should be explored.

4.1.2 Effect of ethanol concentration for organosolv fractionation of rice husk on cellulose-rich fraction

From previous report investigated by Li et al.[195] described aqueous-organic systems perform better than single solvent systems and ethanol/DI water organosolv system catalysed by formic acid can efficiently fractionate bamboo into relatively high purity lignin and cellulose. In this part, the effect of ethanol concentration on the cellulose-rich fraction obtained from organosolv fractionation of rice husk in the presence of diluted (5%) formic acid was investigated and the optimum ratio of ethanol:DI water determined. This can be seen in **Table 28.** The as-obtained cellulose-rich solid fraction are denoted C1 to C4.

Table 28 Various ratio of ethanol/DI water for orgasolv fractionation of rice husk using microwave-assisted method

	Method		Cellulose-rich solid fraction
Condition	Ethanol	DI water	
OS1	45	55	C1
OS2	55	45	C2
OS3	30	70	C3
OS4	70	30	C4

4.1.2.1 Degree of crystallinity (CrI) and yield of cellulose-rich solid

Degree of crystallinity (CrI) and yield of cellulose-rich solid of C1-C4 obtained from organosolv fractionation under various conditions are presented in **Table 29**.

In this comparison, four different cellulose-rich solid samples were analysed via XRD spectrometer and CrI values calculated, which assume to be related to removal of hemicellulose, lignin, and other impurities of cellulose materials. As can be seen in **Fig. 59**, the CrI of raw rice husk is 40.98% then the CrI increased from 51.53% to 55.69% as the ethanol ratio increased from 30 to 70. Condition OS3 provided the highest yield of cellulose-rich solid (60.35%) but the lowest value of CrI (51.53%). While C2 has CrI% = 55.28% which is almost the same value as OS4 which revealed the CrI of 55.69% as well as the almost the same percentage of yield. This suggested that at the high ethanol concentrations, the exposure of the amorphous part increased owing to the dissolution of a large amount of lignin, and hence, cellulose could be increasingly dissolved.[290]

However, considering economic demands, the reaction using lower ethanol concentration-condition OS2 (ethanol/DI water = 55/45) would be the most preferable due to its cost-effective and easier recovery ethanol to be reused by distillation.

Table 29 The yield and CrI of C samples from organosolv process under different conditions

Condition	Cellulose-rich solid		
	Sample	Yield (%)	CrI (%)
OS1	C1	59.87	53.20
OS2	**C2**	**58.37**	**55.28**
OS3	C3	60.35	51.53
OS4	C4	57.03	55.69

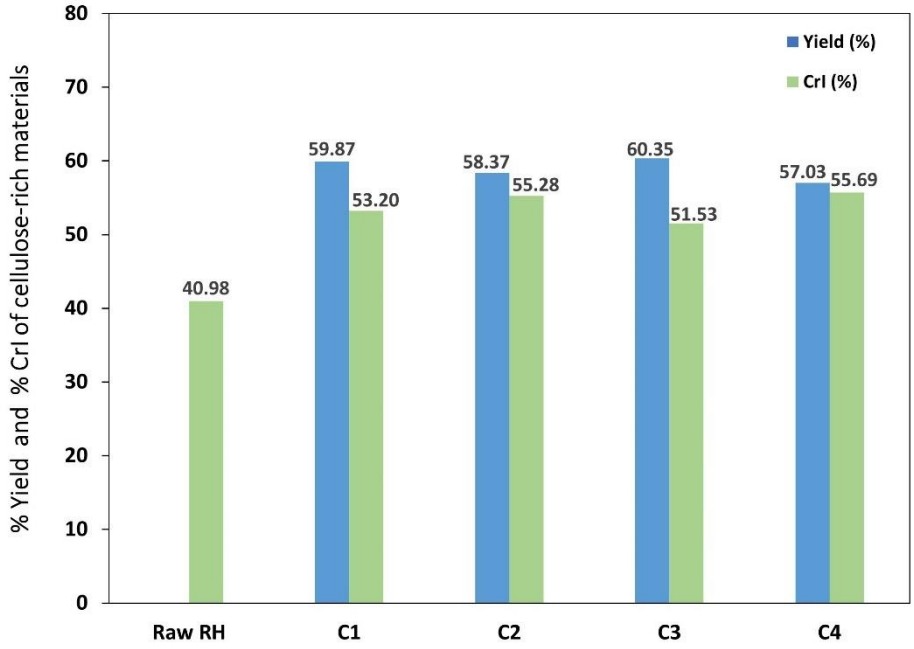

Fig. 59 The yield and CrI of cellulose-rich solid obtained from organosolv process under different conditions

4.1.2.2 XRD characterisation of rice husk and cellulose-rich solids obtained from organosolv process

XRD patterns of cellulose-rich solids which were obtained from the organosolv process under various conditions and RAW-RH were shown in Fig. 60. All XRD patterns of cellulose-rich solids from four conditions exhibited the characteristic diffraction peaks at 15.5°, 22° and 35° corresponded with (110), (200) and (004) planes, which confirmed the characteristic of cellulose crystal structure.[58,142] The major peak was found to be at 22°, indicating the crystalline polymorph of cellulose I.[142]

The CrI values were calculated from Segal method based on XRD pattern of cellulose-rich solid fraction at higher concentrations of ethanol such as C2 and C4 also reveal high value due to the higher concentrations of ethanol cause the exposure of amorphous cellulose through the increased removal of other components such as hemicellulose and lignin, dissolving amorphous cellulose into a liquid, leaving only the more crystalline parts.[290]

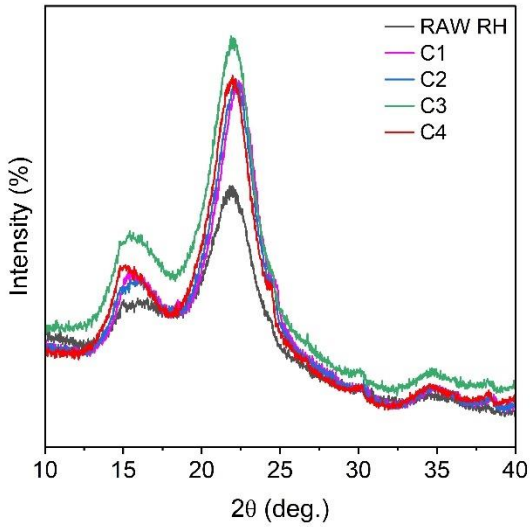

Fig. 60 XRD pattern of RAW-RH and cellulose-rich solid obtained from organosolv process under different conditions

4.1.3 Effect of temperature for organosolv fractionation of rice husk on cellulose-rich solid

As mentioned before, the OS2 condition (ethanol/DI water = 55/45) in the presence of 5% formic acid was selected for organosolv fractionation of rice husk as an optimum ratio of solvent. Many researches revealed that the temperature of organosolv process has significant effect for delignification while the increasing reaction time has a slightly effect on lignin yield.[194,236,290,295]

Then, the effect of reaction temperature (170°C, 190°C and 210°C) was also investigated for the most effective organosolv pretreatment against delignification, hemicellulose removal and cellulose recovery in this part.

4.1.3.1 Degree of crystallinity (CrI) and yield of cellulose-rich solid

Degree of crystallinity (CrI) and yield of cellulose-rich solid (C170, C190 and C210) obtained from organosolv fractionation under various conditions are illustrated in **Table 30** and **Fig. 61**. Increasing of reaction temperatures, leading to an increase in the CrI

values from 51.80% (C170) to 56.26% (C210), whereas a decrease in yield from 60.21% of C179 to 55.52% of C210.

As the same reason as described in the previous part (see **Section 3.1.2**) then, the optimum reaction temperature in this work was found to be 190^{o}C.

Table 30 The yield and CrI of cellulose-rich (C samples) obtained from organosolv process at different temperatures

Condition	Cellulose-rich solid		
	Sample	Yield (%)	CrI (%)
OS170	C170	60.21	51.80
OS190	**C190**	**58.37**	**55.28**
OS210	C210	55.52	56.27

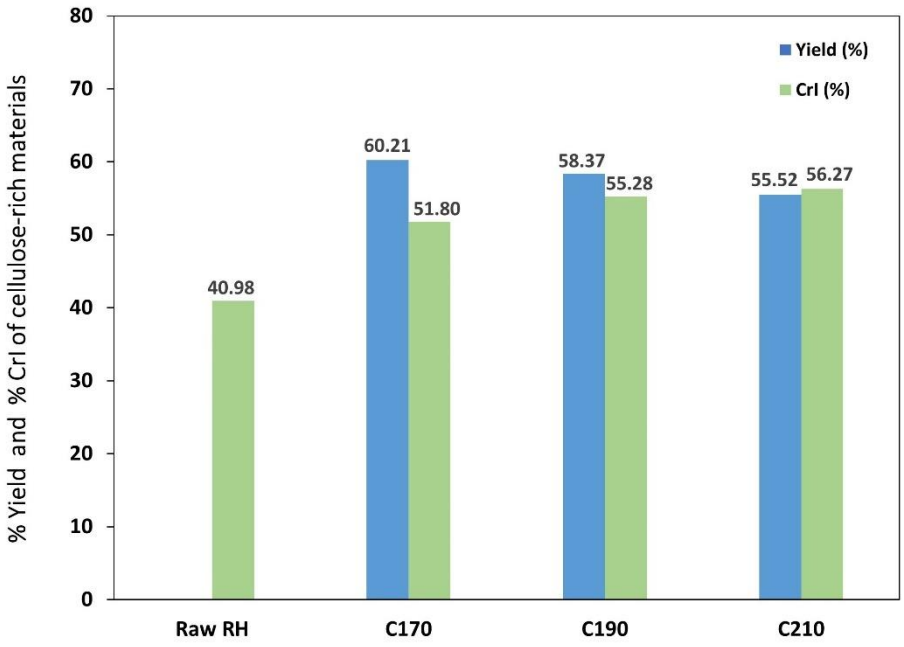

Fig. 61 The CrI and Yield of C170, C190 and C210 of cellulose rich products from organosolv process at different temperatures

4.1.3.2 XRD characterisation of rice husk and cellulose-rich fractions

The XRD patterns of the Raw-RH and cellulose-rich fractions from organosolv process at different temperatures were observed by XRD. **Fig. 62** shows XRD patterns of C170, C190 and C210 which illustrates that diffraction peaks at 2θ = 15.5°, 22° and 35° which can be assigned to 110, 200 and 004 planes, which confirmed that a characteristic of cellulose crystal structure.[100,142] According to the Segal method, the crystallinity index (CrI) of C170 was calculated to be 51.80%, while the CrI of C190 and C210 were calculated to be 55.28% and 56.27%, respectively. There was an increasing tendency of CrI values of all samples with increasing reaction temperatures indicating that hemicellulose/lignin were gradually removed from cellulose during the microwave treatment.

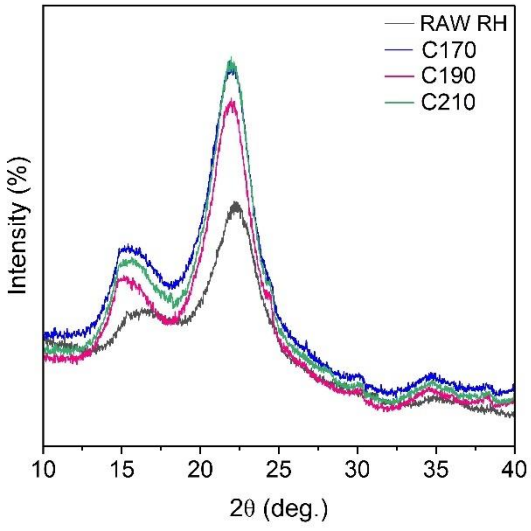

105

Fig. 62 XRD pattern of RAW-RH, C170, C190 and C210 from organosolv fractionation at different temperatures

4.1.3.3 Thermal properties of rice husk and cellulose-rich fractions

Thermal stability of RAW-RH and cellulose rich products from organosolv process at different temperatures (170°C-210°C) was investigated by differential thermogravimetric analysis (DTG) are shown in **Fig. 63**.

The DTG curves represent that there were differences in decomposition temperature in the RAW RH, C170, C190 and C210. The initial weight loss was found in all samples in the around 100°C attributed to the evaporation of moisture/water because of the hydrophilic character of the lignocellulose fibres. [115,290,296] RAW-RH sample represents the broad peak from 200-400 °C in DTG curve due to the presence of lignin and hemicellulose in raw fibres.[257] While, C170 fibre from organosolv treatment at 170 °C resulting in the sharper peak in the temperature in the range of 250-400 °C with a small shoulder peak this might be due to some residual lignin and hemicellulose.[296] This result indicates that 170°C might be not enough to fractionate the purer cellulose fibre compared to higher temperatures at 190 °C and 210 °C.

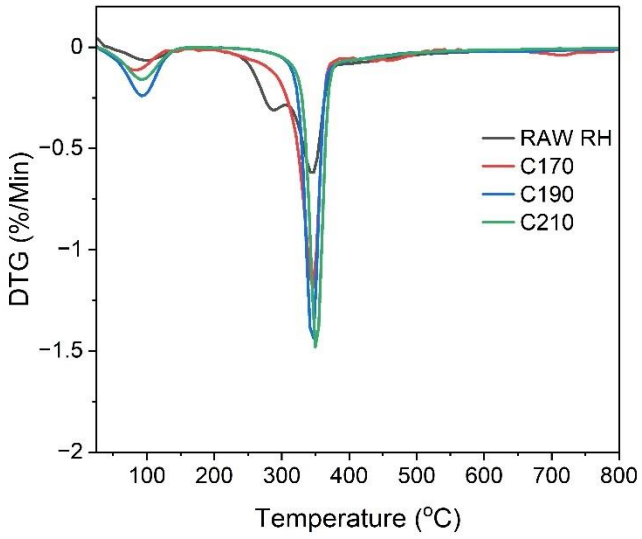

Fig. 63 The derivative thermogravimetric (DTG) curves of RAW-RH, C170, C190 and C210 from organosolv fractionation at different temperatures

The DTG curves of 190 ^{O}C and 210 ^{O}C show sharper peaks in the range of 300-400 ^{O}C without a shoulder, this might imply that the removal of lignin and hemicellulose and also might be due to the increasing crystallinity of C190 and C210 samples, as evidenced by XRD pattern.[226,297] This could suggest that an increase of organosolv fractionation temperature at 190 ^{O}C and 210 ^{O}C led to purer cellulose.

From these results, the optimum condition for organosolv fractionation of rice husk using microwave-assisted method was OS2 condition, using a solvent system consisting of 55% EtOH/45% H_2O (vol/vol) in the presence of formic acid (5%v/v) as a homogeneous catalyst under the microwave radiation at 190^{o}C.[125,298,299]

The cellulose-rich fraction derived from this condition (denoted as OS) was used as reinforcing agent for bio-composite film in following step (see Section 4.4)

Moreover, alkaline treatment, bleaching process and acid hydrolysis were also studied for producing high-purity micro and nanofibre from these cellulose-rich fraction.

4.2 Chemical treatment of cellulose-rich fraction from rice husk after organosolv fractionation

Chemical treatment is one of the most important steps to alter its composition and structure of biomass which can also remove lignin and hemicellulose.[300,301] Alkali treatment is the most common method due to its ability to increase cellulose accessibility and lignin removal capability.[112,113] The pretreatment process also resulted in an increase in the degree of crystallinity because of the swelling of lignocellulose material that eventually leads to the elimination of amorphous parts.[300-302] Bleaching treatment is also an important step to further remove colour ed lignin in fibres and hemicellulose after alkaline treatment. Acid hydrolysis is most widely used for the extraction of nanocellulose from biomass fibres due to it requiring shorter reaction time than other processes.[110,136,258]

In this work, the alkaline and bleaching treatment as well as acid hydrolysis were performed to produce high-purity cellulose in micro and nano scale of cellulose fibres derived from rice husk after organosolv treatment.

4.2.1 Alkaline treatment of cellulose-rich fraction from rice husk after organosolv

As mentioned before, cellulose-rich fraction from optimum condition of organosolv process was subsequently treated with 5% of sodium hydroxide solution to purify the cellulose by removing residue of lignin and hemicellulose from rice husk fibres to provide purer fibres (denoted as OS-alkaline). Besides, some minerals such as silica were also removed during alkali treatment.[94]

4.2.2 Bleaching process of fibres from rice husk after alkaline treatment

After alkaline treatment, OS-alkaline fibres were subsequently bleached by bleaching process with chlorine-free method using mild condition of (2.5%) H_2O_2 acidified by acetic acid to completely remove lignin, resulting in almost pure cellulose fibres (denoted as Organosolv-Alkaline-Bleached). The as-obtained OS, OS-alkaline and Organosolv-Alkaline-Bleached fibre are shown in Fig. 64. The colour of the OS fibre is brown and changes to dark brown after alkaline treatment (OS-alkaline). The bleached fibre (Organosolv-Alkaline-Bleached) is clearly different and appears completely white. These colour changes are due to the removal of non-cellulosic materials (such as lignin and hemicelluloses) also other impurities after each stage of chemical treatment of the rice husk.[118,259]

Fig. 64 The OS, OS-alkaline and Organosolv-Alkaline-Bleached fibre

The comparison of degree of crystallinity, surface chemistry and thermal properties of the RAW-RH and treated fibres which include OS, OS-alkaline, Organosolv-Alkaline-Bleached samples were observed by XRD pattern, FTIR analysis and TGA technique and discussed in the following part.

4.2.2.1 Degree of crystallinity (CrI) and XRD characterisation of rice husk fibres after different chemical treatment stages

X-ray diffraction (XRD) analysis was completed to evaluate the crystallinity of the rice husk fibres after different chemical treatment stages and illustrated in **Fig. 65**. All samples showed characteristic peaks at 2θ of around 15.5°, 22° and 35° corresponding to the cellulose I, crystallographic planes 110, 200 and 004, respectively.[66,156] Which in good agreement with the XRD pattern from alkali-treat fibres and bleached fibres from rice husk reported by Varshney *et al*.[58] The intensity of these crystalline peaks tended to increase due to the removal of hemicellulose, lignin also amorphous cellulose, after each stage of treatments. This suggested that the chemical treatments do not affect the crystal structure of cellulose.[117]

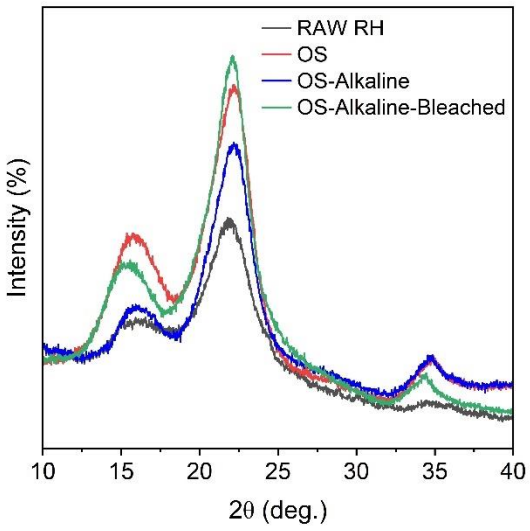

Fig. 65 XRD pattern of Raw RH, OS, OS-alkaline, and OS-Alkaline-Bleached

The crystallinity index was determined for the various samples and the results are summarised in **Table 31**. The highest value (58.16%) corresponds to OS-Alkaline-Bleached, which also displayed the strongest and sharpest peak at 2Θ = 22°. The increase in CrI from Raw-RH to OS-Alkaline-Bleached fibre is ascribed to the progressive removal of amorphous non-cellulosic materials (hemicellulose, lignin, and other impurities).[205,303]

The subsequent increase of the CrI value upon bleaching step of purified cellulose rice husk fibres is indicative of the dissolution of amorphous cellulosic domains as discussed above.[94,304]

This increase in CrI of cellulose fibres was also expected to increase their stiffness and rigidity, and therefore strength. Thus, it was assumed that the potential mechanical properties and reinforcing capability of treated fibres increased.

Table 31 The CrI of RAW-RH, OS, OS-alkaline, and OS-Alkaline-Bleached samples from organosolv process

Sample	CrI (%)
Raw rice husk	40.98
Organosolv	52.70
Organosolv-Alkaline	54.84
Organosolv-Alkaline-Bleached	58.16

4.2.2.2 FTIR analysis of rice husk, cellulose-rich fraction at various stages of treatment and commercial cellulose

To study changes in functional groups of fibres at various stages of treatment. FTIR technique was performed and FTIR spectra of Raw RH, OS, OS-alkaline, OS-Alkaline-Bleached and Commercial Cellulose are illustrated in Fig. 66.

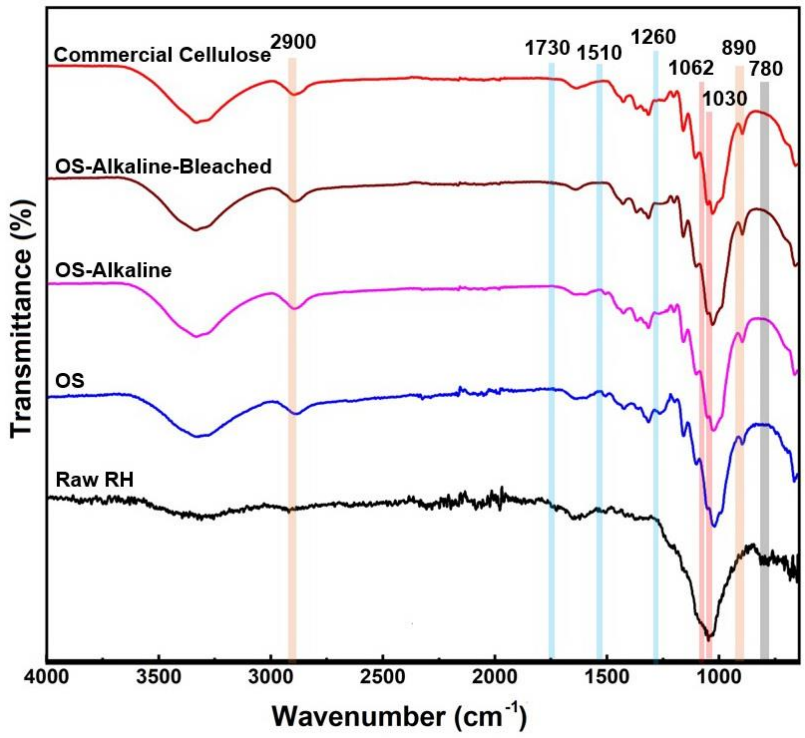

Fig. 66 FTIR spectra of Raw RH, OS, OS-alkaline, OS-Alkaline-Bleached and Commercial Cellulose

The broad peak between 3300 cm^{-1} and 3400 cm^{-1} and peak at 2900 cm^{-1} were assigned to the stretching vibrations of O-H and C–H groups in cellulosic materials, respectively. The peak at 1638 cm^{-1} was assigned to the bending vibration of absorbed water.[100]

The peak at 1160 cm^{-1} was attributed to C–O–C asymmetric stretching vibration of the cellulose. The peak at 890 cm^{-1} was assigned to C–O–C stretching vibration of β-(1→4)-glycosidic linkages. The peak at 1062 cm^{-1} was assigned to C–O stretching vibration in cellulose and asymmetric stretching of Si-O-Si and peak at 780 cm^{-1} was assigned to Si–O–Si symmetric stretching of silica.[53,166,305]

In addition, the three peaks which corresponding to the existence of hemicellulose and lignin in the raw rice husk fibres were also observed such as the peak at 1730 cm^{-1} was assigned to the acetyl groups of hemicelluloses and ester linkage in the phenyl propionic alcohols of lignin, the peak at 1510 cm^{-1}, and 1260 cm^{-1} were attributed the C=C

stretching vibration from aromatic ring and C-O out of plane stretching vibration of aryl group in lignin and hemicellulose was assigned to These three peaks were rarely observed after alkaline treatment and completely disappeared after bleaching process indicating the removal of most of lignin and hemicellulose.[118]

While the three peaks above (1730 cm^{-1}, 1510 cm^{-1} and 1260 cm^{-1} for lignin and hemicellulose) were disappeared, the increase in the intensity of peak at 1160 cm^{-1} (which corresponded to C–O–C asymmetric stretching vibration of the cellulose) could also confirmed the increase in cellulose content after the chemical treatments. The list of functional groups of as-obtained samples is also shown in Table 32.

Table 32 Assignment of FTIR spectra of Raw RH, OS, OS-alkaline, OS-Alkaline-Bleached and Commercial Cellulose

Wavenumber (cm^{-1})	Assignment
3300-3400	O–H stretching vibrations and hydrogen bonding in phenolic and aliphatic structures
2900	C–H groups in cellulosic materials
1730	C=O stretching vibration in acetyl groups of hemicellulose or ester linkage in carboxylate derivatives in ferulic and p-coumeric acids of lignin
1510	C=C stretching of aromatic skeleton in lignin molecules
1260	C-O out of plane stretching vibration of aryl group in lignin and hemicellulose
1160	C–O–C asymmetric stretching vibration of the cellulose
1062	C–O stretching in cellulose and asymmetric stretching of Si-O-Si
1030	C–C stretching vibration in cellulose
890	C-H deformation of anhydroglucose unit in cellulose and hemicellulose of lignocellulosic biomass materials
780	The symmetric stretching modes of Si–O–Si group

4.2.2.3 Thermal properties of rice husk, cellulose-rich fraction at various stages of treatment

Thermal properties of RAW-RH, OS, OS-alkaline and OS-Alkaline-Bleached were investigated by TGA technique. TG and DTG curves are represented in **Fig. 67**. The initial weight loss observed were found in all samples in the range of 50–150 ^{O}C due to the evaporation of moisture.[115,290,296] DTG curve of RAW-RH illustrates the broad peak at 200-400 ^{O}C with a shoulder because RAW-RH fibres mainly consisted of cellulose, lignin and heimicellulose.[257]

After chemical pretreatment, the DTG curves of OS, OS-alkaline and OS-Alkaline-Bleached become narrower in the range of 300-400 ^{O}C due to the removal of lignin and hemicellulose.[296] However, TGA curve of OS-Alkaline-Bleached show the narrowest peak without shoulder in the range of 300-380 ^{O}C this implied that purer cellulose fibre was obtained after bleaching step due to the completely removal of lignin with in good agreement with XRD spectra.[306-309]

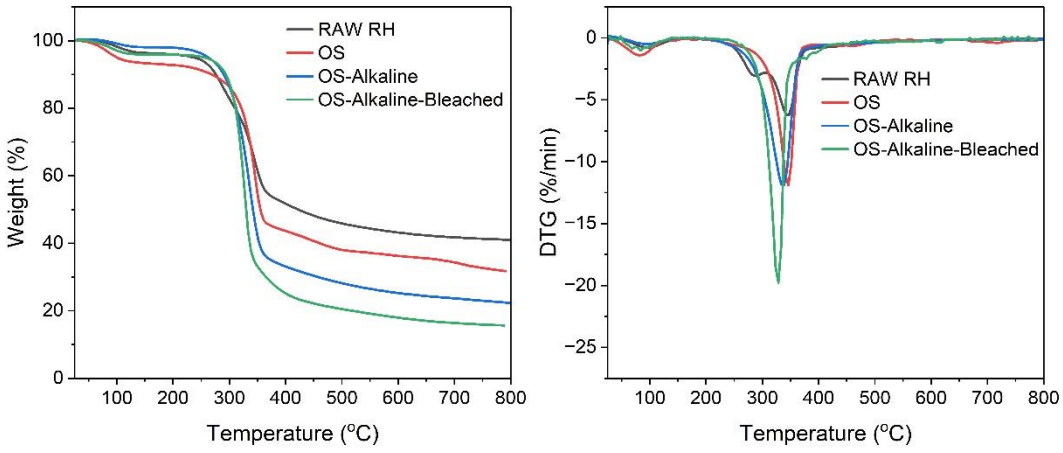

Fig. 67 TGA thermogram of Raw-RH, OS, OS-alkaline, OS-Alkaline-Bleached and Commercial Cellulose

4.2.2.4 SEM characterisation of rice husk and cellulose fibres from rice husk after bleaching process

The chemical treatments used for cellulose purification from the rice husk are also expected to induce morphological changes. The SEM images show the ground RAW-RH (**Fig. 68 (a)**) had relatively large size of particles, this might be due to lignin, hemicellulose, and other non-cellulosic impurities act as binders cover cellulose fibres and form a dense structure.[297] SEM images (**Fig. 68 (b,c)**) also illustrate that after bleaching step, OS-Alkaline-Bleached fibres bundles separate into individual fibres compared to raw rice husk and a reduction of average size of diameter of fibres (3.8 µm ± 1.5 µm).[297,304] This might be due to this bleaching step being able to completely remove lignin and other impurities in fibres.[310]

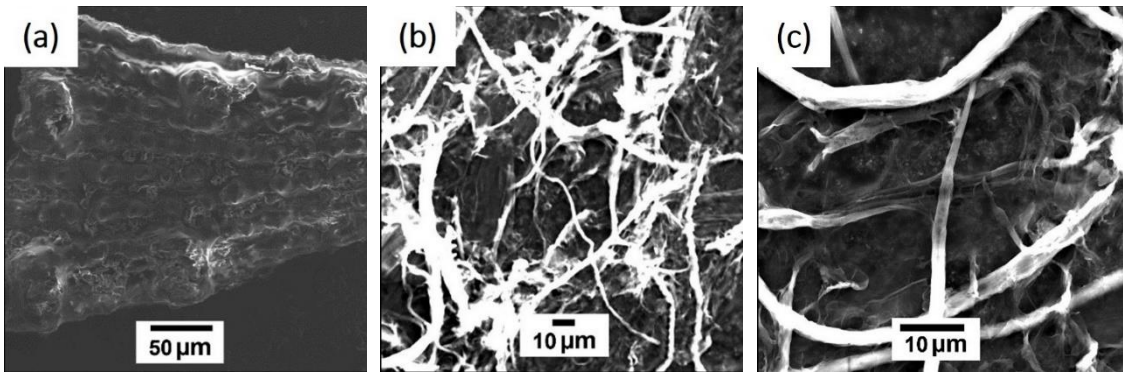

Fig. 68 SEM images of (a) Raw-RH and (b-c) OS-Alkaline-Bleached

4.2.3 Acid hydrolysis for the extraction of nanocellulose fibres

The production of nanocellulose is attained by a three-step process. In the first step, the organosolv pretreatment process of native cellulose biomass is done which provides cellulose fibres (OS fibre). Then the second step, pretreated cellulose fibres were obtained after alkaline and bleaching treatment (OS-Alkaline-Bleached fibre). The third step pretreated cellulose fibres are converted into nanocellulose fibre using various techniques. Acid hydrolysis is most widely used for the extraction of nanocellulose fibre from biomass fibres.[110,187] It is easily hydrolysed into the disordered regions of cellulose. In this process, sulfuric acid is commonly employed for the acid hydrolysis.[190,258]

This part reported the production of nanocellulose fibre by acid hydrolysis and the as-obtained samples denoted as OS-Alkaline-Bleached-AH.

4.2.3.1 TEM characterisation of cellulose fibres from rice husk after acid hydrolysis step

The morphology and size of OS-Alkaline-Bleached-AH after acid hydrolysis was observed by TEM as shown in **Fig. 69**. The TEM images reveal the nanostructures of rice husk celluloses in the form of nanorod/needle-like particles in the range of 100-500 nm, with an average length of 415 nm ± 142 nm and an average diameter of 9.12 nm ± 4.43 nm (100 particles counted), were obtained after acid hydrolysis. This indicated that the much smaller size of cellulose nanostructures could be isolated from acid hydrolysis step.

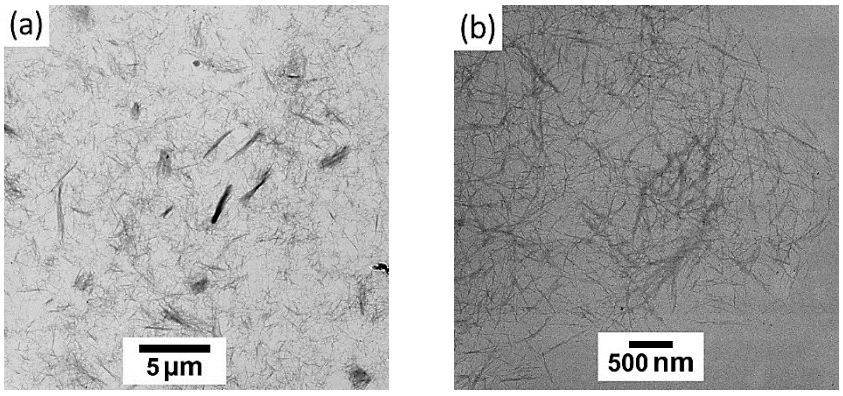

Fig. 69 TEM images (a) and (b) with different magnification of OS-Alkaline-Bleached-AH

4.3 Mechanical treatment

The mechanical treatment by homogenisation was carried out for defibrillation of cellulose in suspension.[260,300] After homogenisation, the morphology of the homogenised fibre was observed by TEM analysis The fibres were then used as reinforcing agent for bio-composite film in latter part.

Cellulose fibres derived from rice husk by the organosolv fractionation (OS fibre) and subsequently by chemical pretreatment (OS-Alkaline-Bleached fibre) were fibrillated into cellulose micro/nanofibres through a subsequent homogenisation.[126]

4.3.1 Homogenisation of OS fibre for defibrillation of cellulose fibres from rice husk

Cellulose fibres derived from rice husk by organosolv fractionation at 190 ^{O}C (OS fibre) subsequently by homogenisation for 1 h prior to prepare bio-composite film.

4.3.1.1 SEM and TEM characterisation of cellulose-rich fibres from rice after homogenisation

The morphology and size of fibres obtained from organosolv fractionation subsequently by homogenisation for 1 h (denoted as OS-H) were characterised by SEM and TEM images. Due to OS fibres obtained from organosolv fractionation being too rigid, they could not mix well with the PVA solution used to prepare bio-composite film. Thus, the homogenisation was performed to reduce the size of fibres (or disperse the fibres) by mechanical treatment to form the homogenous dispersion of cellulose fibres prior to preparing bio-composite films (Series A). The as-obtained fibres exhibit more homogeneous phase of defibrillated celluloses compared to the as-obtained fibres from organosolv fractionation and could be mixed with a mixture for film preparation in the following part (see Section 4.4.1). The morphology of OS-H is shown in Fig. 70. The form of OS-H is more homogenous than OS derived from organosolv fractionation obtained after homogenisation for 1 h. SEM image suggested an average diameter size of 4.9 µm ± 1.2 µm for OS-H fibres. This appears to be caused by the encouraging effect of homogenisation process in detaching of the hydrogen bonds of microfibrils cohesion and splitting the amorphous region.[300,303]

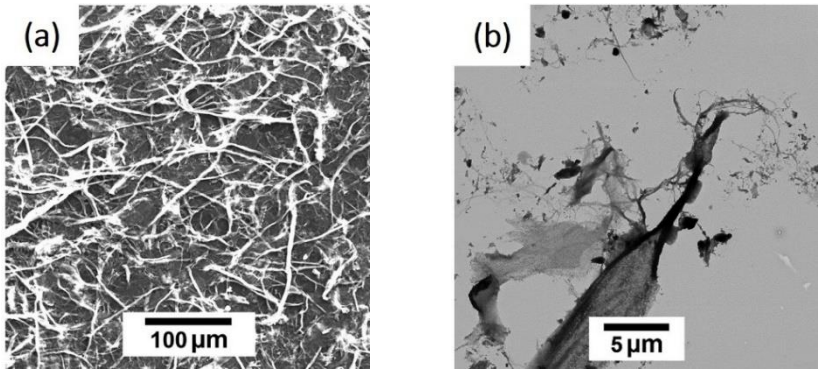

Fig. 70 SEM (a) and TEM (b) images of OS-H

4.3.2 Homogenisation of OS-Alkaline-Bleached

In order to prepare the homogenous form of cellulose fibres derived from chemical treatments (OS-Alkaline-Bleached), the homogenisation process was applied for 15 min.

4.3.2.1 TEM characterisation of cellulose fibres derived from rice husk after homogenisation

The morphology of OS-Alkaline-Bleached-H obtained after bleaching step and homogenisation for 15 min was investigated by TEM analysis. As can be seen in Fig. 71, mixed phases of micro and nanofibres with diameter in a range of 10-20 nm (an average diameter of 19.9 nm ± 9.83 nm), with the length of 1-5 microns (an average length of 2.30 ± 0.95 µm (100 fibres counted), were found after homogenisation. However, the diameter and length of the as-obtained fibres from this step were obviously larger than those OS-Alkaline-Bleached-AH fibres obtained from acid hydrolysis step (see Section 4.2.3, Fig. 69)

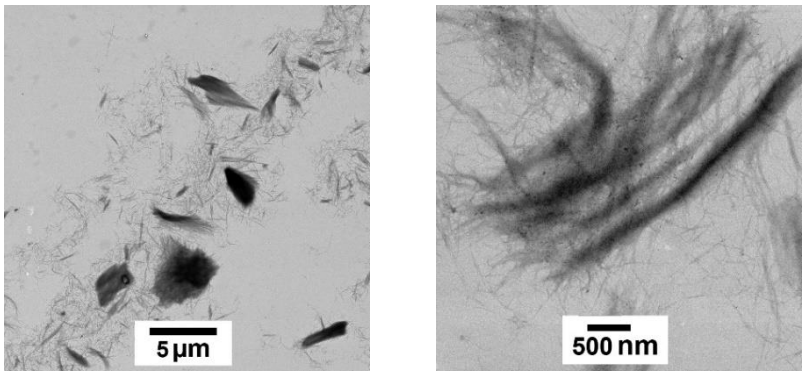

Fig. 71 TEM images at different magnification of OS-Alkaline-Bleached-H

Morphological observations of the treated fibres revealed that after homogenisation may accelerate the fibrillation process resulting in the easier fibrillation of cellulose to generate microfibre.[126]

In this study, the as-prepared cellulose microfibres/nanofibres derived from rice husk, were mixed with PVA. The mixture was cast and regenerated to form bio-composite cellulose film. The properties of the bio-composite film such as transparency, tensile strength, and thermal stability were also studied.

4.4 Bio-composite film preparation from biodegradable polymer using cellulose fibres from rice husk as reinforcing agent

Biodegradable film packages are thin layers previously formed as plastic films. As an alternative to films produced with conventional materials, many studies have been performed using biodegradable, biocompatible and renewable sources to develop films that avoid polluting the environment.[116,208]

Among the synthetic polymers, PVA is widely used for food packaging because of its biodegradability, cost-effectiveness, good film-forming ability, water processability, and ready availability which make it a good promising polymer used for film preparation.[213,299,311,312]

From literature, the optimum condition for film preparation was used at 5% PVA (w/v) due to the as-prepared film from this concentration provide the relatively high transmittance value and good physical property as reported by Fong *et al*.[313] and Bahrami

et al.[314] Thus, bio-composite film prepared in this work was used at this concentration.[259,311,315] However, PVA polymer film is rather brittle and inflexible.[212] Plasticisers can be introduced to improve film flexibility while maintaining relatively good mechanical properties (tensile strength).[212] Blending the plasticiser with polymer materials increases the interchain distance resulting in free volume in polymer materials, which in turn leads to the enhancing of the macromolecular mobility of polymer chains. The resulting polymer becomes less dense which is related to the improvement of chain flexibility.[316,317] Glycerol is commonly used owing to its low molecular weight, low volatility, and good compatibility with the host polymer such as PVA.[237,317] The optimum content of glycerol in the film preparation used at 2% (v/v) results in a film which exhibits more flexibility and less brittleness than the pure PVA film. However, higher concentrations of glycerol in the film formulation can cause a greasy film and a decrease of film toughness.[318] Thus, in this part the glycerol concentration of 2% (v/v) blended in 5% (w/v) of PVA was used for bio-composite film preparation.

Moreover, natural fibres can be used to reinforce composite structures for creating composite structures from bio-based materials with superior mechanical properties.[211,318] Depending on the different size of cellulose fibres, these can exhibit different thermal, optical, and mechanical properties so this part studied bio-composite film preparation by using different type of rice husk fibres.[303,306] Schematic diagram of cellulose fibres and bio-composites films production is shown in Fig. 72.

The aims of this part were to develop biodegradable films based on blending with glycerol and poly (vinyl alcohol) and reinforcing agents like micro/nano cellulose fibres from rice husk were also investigated to measure their impact on mechanical and thermal properties of the bio-composite films.

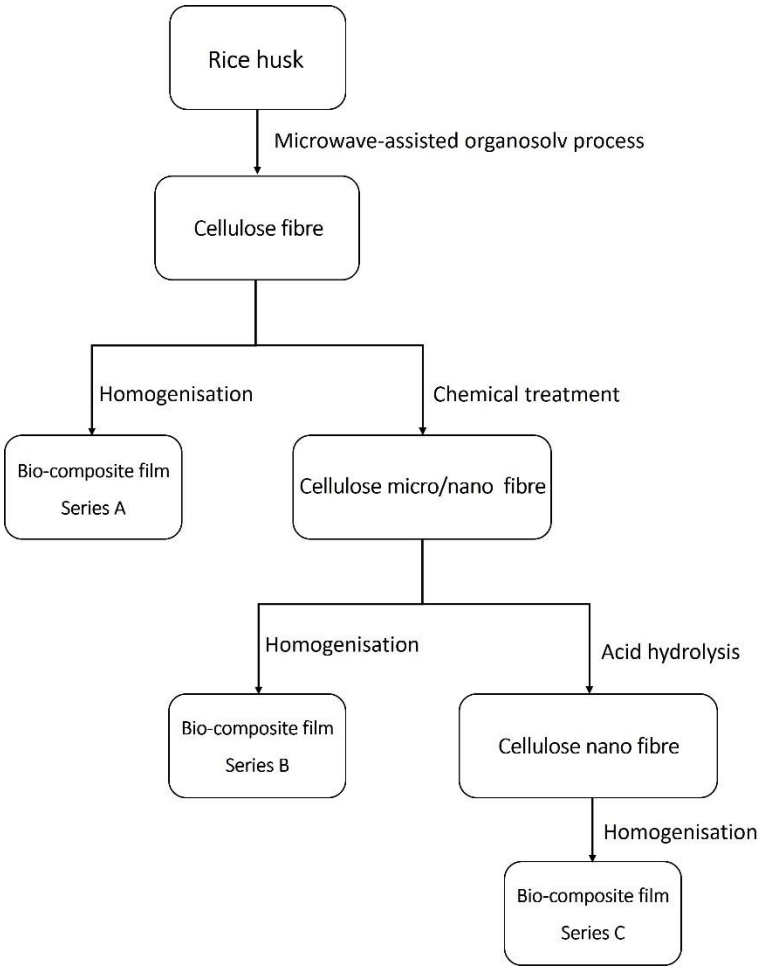

Fig. 72 Schematic diagram of cellulose fibres and bio-composites films production

Bio-composite films contained the different types of cellulose fibres (1-5%) including, Series A prepared from OS-H (cellulose fibres from organosolv fractionation subsequently by homogenisation), Series B prepared from OS-Alkaline-Bleached-H (cellulose fibres after bleaching step subsequently by homogenisation), and Series C prepared from OS-Alkaline-Bleached-A (cellulose nanofibres after acid hydrolysis step), all films were mixed with mixture of PVA and glycerol. Then, optical properties and mechanical properties by tensile analysis were investigated and discussed in the latter part.

4.4.1 Bio-composite film preparation: Series A

As-prepared cellulose fibres from organosolv fractionation possess rigid particles that could not be used for film preparation. In order to prepare the homogenous phase of

mixture, cellulose fibres from organosolv fractionation were subsequently homogenised for 1 h (OS-H) prior to being used for film preparation with the optimum content of (2%v/v) glycerol addition. The effect of various content of cellulose fibres on the optical and mechanical properties of bio-composite films series A was studied.

A0 A1 A2 A3 A4 A5

Fig. 73 Bio-composite films: Series A

4.4.1.1 UV-visible transmittance (transparency) of bio-composite films series A

UV-visible transmittance of the bio-composite films series A, containing different content of cellulose fibres from rice husk shown in Fig. 74. The optical transmittance influenced by various factors including, the dispersibility and film thickness.[319,320]

The transparency curve shown in the range of 200–800 nm. As-prepared film PVA mixed with glycerol without cellulose denoted as A0, is the most transparent of all films. The as-prepared films by adding 1%, 2%, 3%, 4% and 5% v/v of OS-H were denoted as A1, A2, A3, A4 and A5, respectively. The transmittance spectra were acquired using air as background.

Light transmittance of the bio-composite films was observed in the visible light wavelength range (400-800 nm). The transmittance of the pure PVA film blended with 2% (v/v) of glycerol was very stable in the visible light region with a wavelength of 400–800 nm, especially as high as 98.2 % at a wavelength of 500 nm. At 500 nm, the light transmittance tends to decrease from 98.2% to 61.6% with the increasing in the

concentration of OS-H addition in film preparation. The light transmittance of the bio-composite films series A are summarised in Table 33.

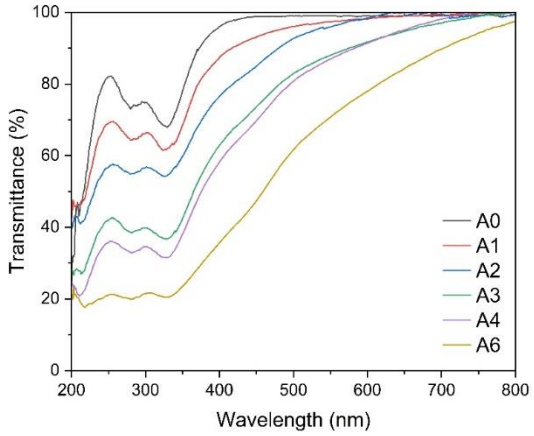

Fig. 74 Optical properties of bio-composite films: series A in UV- visible range

As can be seen in Fig. 73, PVA blended with glycerol (A0) film shows a poor UV-shielding property as it could not absorb/block UV radiation at wavelengths from 200 to 400 nm, having high UV transmittance of 80%. However, in the UV region of 200–400 nm, the light transmittance of the bio-composite films decreases sharply with a decrease in wavelength, which indicates that these as-prepared films have good absorption of UV light. An increase of OS-H led to the increase in performance of UV-shielding from 70% UV transmittance of A1 to 20% of A5. This suggested that the high content OS-H of 5% added in bio-composite films could provide good performance of UV-protection. Due to the as-obtained A5 being a light brown film (Fig. 73) it also is less transparent than those films.

Table 33 The light transmittance of the bio-composite films: Series A

Series A	Cellulose content (%)	Optical transmittance (%) at 500 nm
A0	0	98.2
A1	1	96.1
A2	2	92.7
A3	3	82.9
A4	4	80.8
A5	5	61.6

4.4.1.2 Thermal property of bio-composite films series A

TGA and DTG curves of the bio-composite films series A, containing different content of cellulose fibres from rice husk shown in Fig. 75.

The DTG curves can be divided into three stages. The initial mass loss at around 200 ^{O}C was attributed to the evaporation of water and glycerol. [321] The second stage consists of major weight losses observed in the range of 220-350 ^{O}C.[315] These might be caused by the evaporation of glycerol and the degradation of side chain in PVA molecules. The third stage occurred at around 450 ^{O}C which caused by the degradation of the main chains of PVA molecules.[322] Compared with the A0 (PVA mixed with glycerol), the composite films (A1, A3 and A5) represent the higher weight loss temperatures by approximately 280-430 ^{O}C dehydration and chain scission, respectively, due to their enhanced thermal stability.[317]

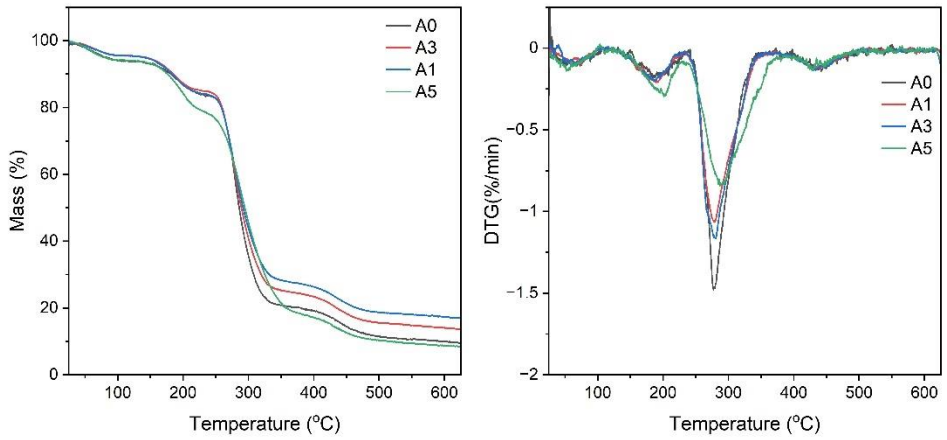

Fig. 75 TGA (a) and DTG (b) curves of bio-composite films: series A

4.4.1.3 Mechanical testing of bio-composite films series A

The tensile properties of the as-prepared films were investigated by using an Instron® 3367 Universal Testing machine shown in Fig. 76 also summarised in Table 34.

Table 34 Tensile properties of as-prepared films: Series A

Series A	Tensile strength (MPa)	Elongation at break (%)
A0	30.4 ± 0.2	335.7 ± 6.7
A1	31.4 ± 1.1	293.0 ± 19.1
A2	27.4 ± 1.7	226.8 ± 25.8
A3	31.8 ± 1.8	99.9 ± 14.5
A4	31.5 ± 1.0	36.7 ± 3.3
A5	26.5 ± 2.5	25.2 ± 7.7

The A1 film shows a little more tensile strength of 31.4 MPa, whereas A2 reveals a lower value of 27.4 MPa than A0 film. This might be caused by the concentration (1-2%) of OS-H fibres not being well dispersed in mixture and could be forming the agglomeration in film preparation. Although 3-4% of OS-H fibres added in film preparation led to a slight increase of tensile strength- 31.8 MPa and 31.5 MPa, respectively.

However, a dramatic decrease in elongation at break by 70% and 89% for A3 and A4 film respectively, compared to A0 film. Besides, A5 film exhibits a brittle film and broke at the lowest strength of all films (26.5 MPa). This might be due to the excess of cellulose fibres agglomerated on films and non-nanoscale fibres precipitated during film preparation.

From this series, the as-obtained fibres could not be mixed well with the mixture for bio-composite preparation resulted in brittle films with less flexible which may be caused by heterogenous phase of regular shapes fibres being poorly dispersed in as-prepared films.[315] These fibres hinder its homogeneous dispersion in PVA and weakens the hydrogen bond interaction between fibres and PVA matrix, resulting in the polymer molecular chains not being compactly stacked, and the defects are easily formed. [116]

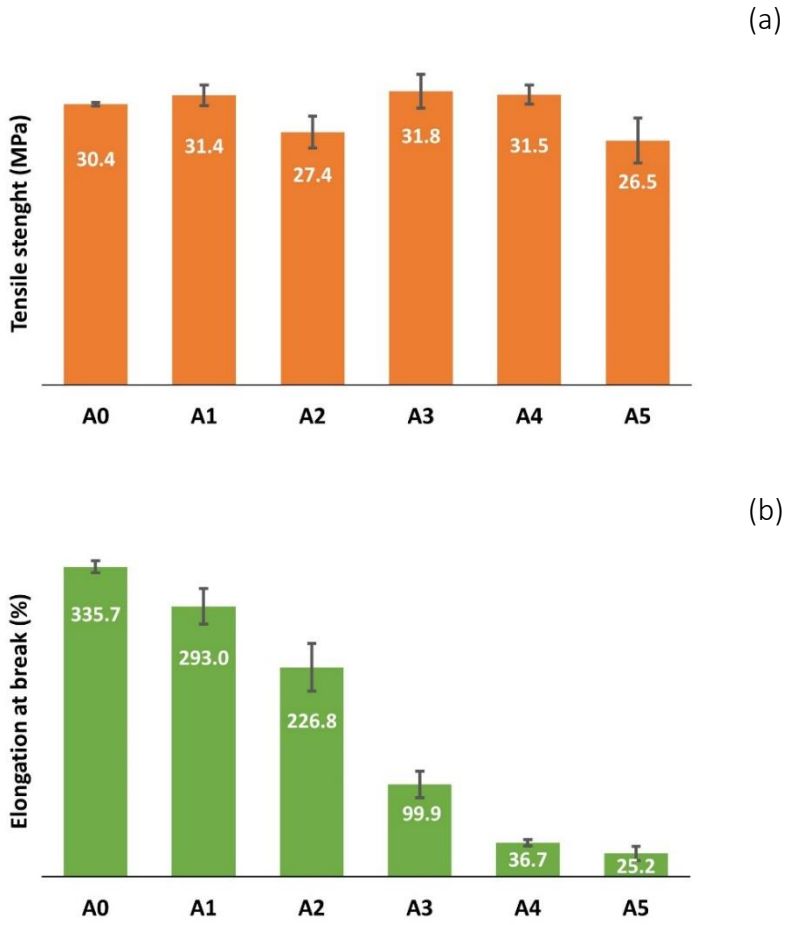

Fig. 76 Tensile strength (a) and elongation at break (b) of bio-composite films: Series A

4.4.2 Bio-composite film preparation: Series B

This part described the bio-composite film preparation from OS-Alkaline-Bleached fibres subsequently by homogenisation for 15 min (OS-Alkaline-Bleached-H). In order to well-mix with glycerol and PVA mixture, OS-Alkaline-Bleached-H was used for film preparation rather than OS-Alkaline-Bleached. The as-obtained films with 0%, 1%, 2%, 3%, 4% and 5% of OS-Alkaline-Bleached-H fibres were denoted as B0, B1, B2, B3, B4 and B5, respectively. Bio-composite films: Series B shown in Fig. 77.

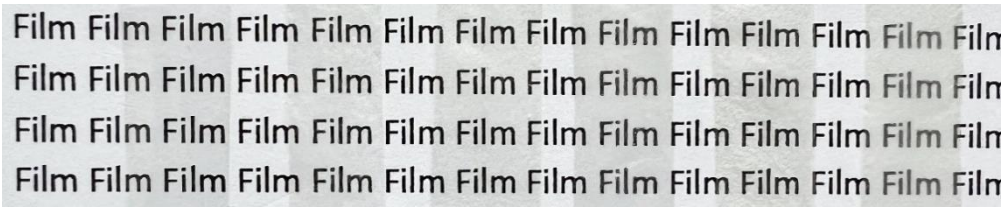

Fig. 77 Bio-composite films: Series B

4.4.2.1 UV-visible transmittance (transparency) of bio-composite films series B

The UV-visible spectra of all films (series B) at the wavelength range 200–800 nm are shown in **Fig. 78**. Also, the % transmittance at 500 nm of the bio-composite films series B are summarised in **Table 35**. The transmittance decreased from 98.2% to 93.4% with the increase in OS-Alkaline-Bleached-H content addition in bio-composite film preparation. This suggested that the bio-composite films series B have a good performance in visible region. While the transmittance in the UV region (200-400 nm) of the as-prepared series B bio-composite films reveal a decreasing tendency of transmittance from 80% to 50%. This means that the UV-shielding performance increased with the increasing of OS-Alkaline-Bleached-H content.

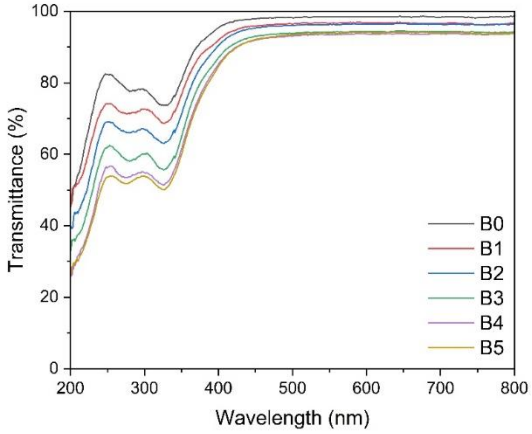

Fig. 78 Optical properties of bio-composite films: series B in UV- visible range

Table 35 The light transmittance of the bio-composite films: Series B

Series B	Cellulose content (%)	Optical transmittance (%) at 500 nm
B0	0	98.2
B1	1	96.5
B2	2	96.0
B3	3	93.8
B4	4	93.1
B5	5	93.4

4.4.2.2 Thermal property of bio-composite films series B

The thermal property of bio-composite films series B using different concentration of cellulose fibres (OS-Alkaline-Bleached fibres) was investigated by TGA and DTG curves as can be seen in Fig. 79.

DTG curves of the bio-composite films series B also indicated three major weight loss (as described above in series A).[321] In the second stage was at around 220-350 ^{O}C which caused by the degradation of side chain in PVA molecules.[322] These results revealed that all peaks of bio-composite films (B1, B3 and B5) moved to higher temperatures after the addition of cellulose fibres compared to B0 film. The thermal stability of bio-composite films tends to increase with the increasing of OS-Alkaline-Bleached fibres content in film preparation. This suggested that micro/nanocellulose fibres addition in film preparation improved the thermal stability of bio-composite films.[315,323]

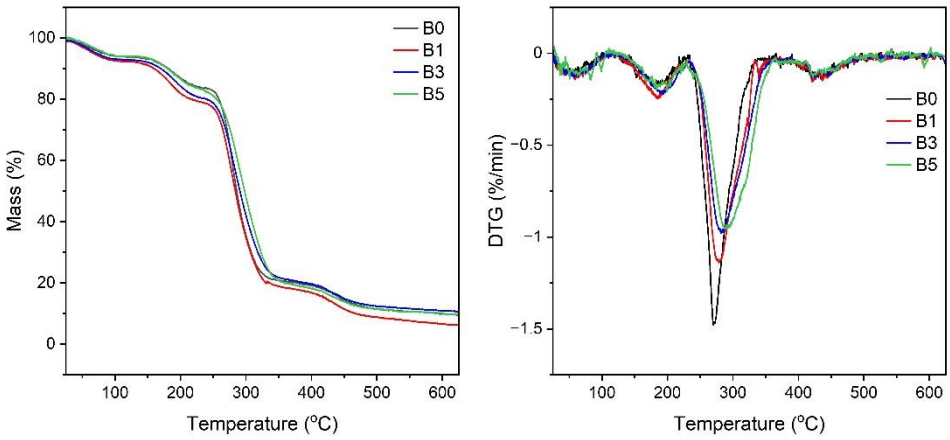

Fig. 79 TGA (a) and DTG (b) curves of bio-composite films: series B

4.4.2.3 Mechanical Properties of bio-composite films series B

The mechanical properties of all film's series B were performed by the tensile test are summarised in Table 33 and also shown in Fig. 80.

Table 36 Tensile properties of as-prepared films: Series B

Film series B	Tensile strength (MPa)	Elongation at break (%)
B0	30.4 ± 0.21	335.7 ± 6.70
B1	31.9 ± 0.61	363.7 ± 5.15
B2	32.9 ± 0.72	300.3 ± 8.75
B3	35.8 ± 0.69	319.2 ± 6.57
B4	37.7 ± 0.42	283.4 ± 7.77
B5	38.5 ± 0.48	104.6 ± 7.77

The addition of 1% of OS-Alkaline-Bleached-H fibres in as-prepared film increased the tensile strength of bio-composite film as well as the strain of as-prepared film was also improved by approximately 8% compared to B0 film. A 26.5% improvement in the tensile strength of bio-composite film (B5) was obtained with 5% OS-Alkaline-Bleached adding in

film preparation. This bio-composite film was more rigid than the B0 film and broke at strain of 104%. The increasing of OS-Alkaline-Bleached-H content led to an increase of tensile strength while the elongation at break tended to decrease. This result suggested that the addition of OS-Alkaline-Bleached-H had stronger and stiffer composite film compared to the B0 film. From series B, B3 provides both relatively high value of tensile strength of 35.8 MPa and elongation at break of 319.2%.

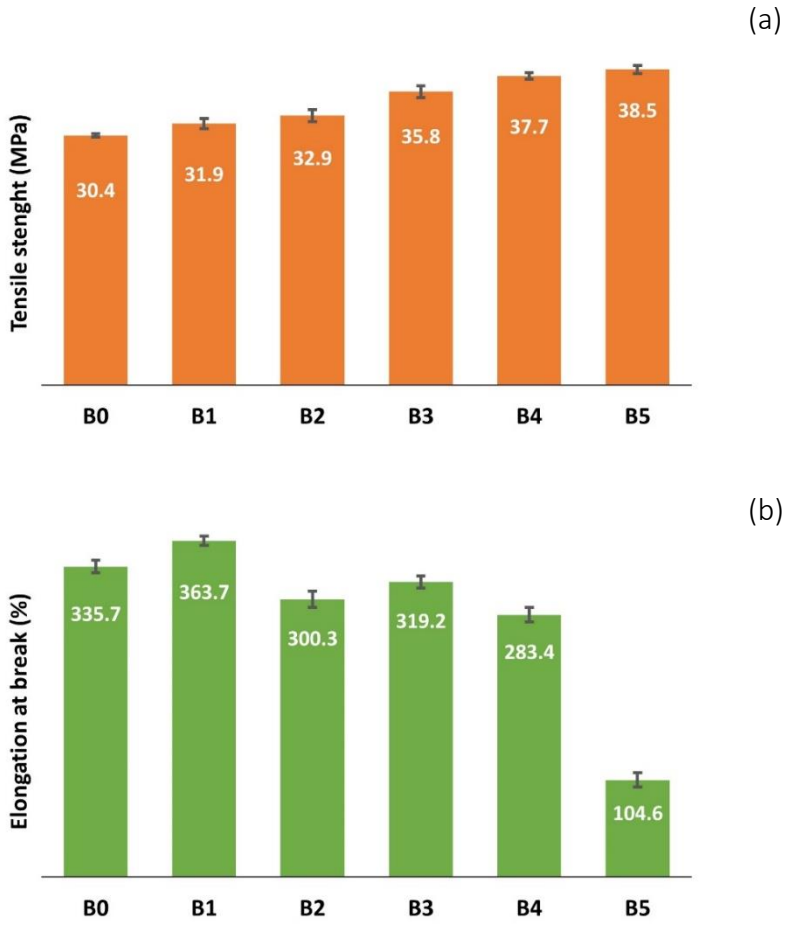

Fig. 80 Tensile strength (a) and elongation at break (b) of bio-composite films: Series B

4.4.3 Bio-composite film preparation: Series C

Nanocellulose has received great interest, particularly in polymer composite material preparation as a reinforcement or nanofiller because it can improve mechanical properties for film preparation due to the formation of a network structure by hydrogen bonding to form connection with others. Thus, this part described the bio-composite film preparation from OS-Alkaline-Bleached-A. The as-obtained films with 0%, 1%, 2%, 3%, 4% and 5% of OS-Alkaline-Bleached-A were denoted as C0, C1, C2, C3, C4 and C5, respectively as can be seen in **Fig. 81**.

Fig. 81 Bio-composite films: Series C

4.4.3.1 UV-visible transmittance (transparency) of bio-composite films series C

The UV-Vis spectra of the bio-composite films performed in the UV-Visible light wavelength range 200-800 nm are illustrated in **Fig. 82** and % Transmittance of all as-prepared films series C at 500 nm are summarised in **Table 37**.

A slight decrease in light transmittance at 500 nm from 98.2% to 93.4% with the increasing of OS-Alkaline-Bleached-H loading in bio-composite film preparation was investigated in film series C.

As the content of nanocellulose increased, the light transmittance of the composite films did not change significantly due to the nanoscale dispersion of nanocrystal (CNC) within the PVA matrix. The nanofibre added in bio-composite films illustrated the best optical transmittance of all series (better optical performance than series A and series B). This is

thought to be due to nanocellulose in bio-composite films exhibiting a better alignment, resulting in a good degree of homogeneity of nanocellulose film.[259,324]

Furthermore, a decrease of transmittance in UV range (200-400) was observed with an increase of nanofibres addition in film preparation from 80% of C0 to 58% of C5.

Table 37 The light transmittance of the bio-composite films: Series C

Series C	Cellulose content (%)	Optical transmittance (%) at 500 nm
C0	0	98.2
C1	1	96.9
C2	2	95.5
C3	3	95.7
C4	4	95.1
C5	5	95.1

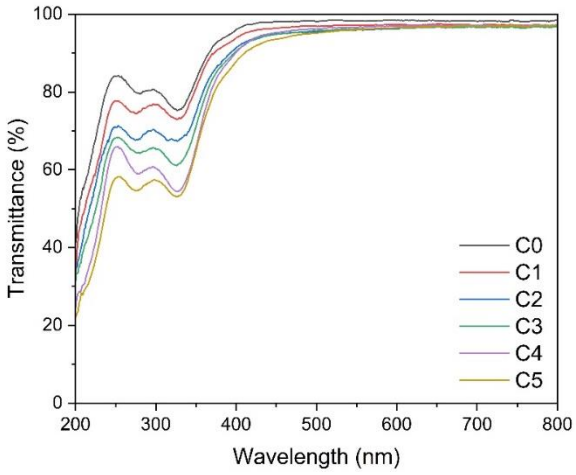

Fig. 82 Optical properties of bio-composite films: series C in UV- visible range

4.4.3.2 Thermal property of bio-composite films series C

The decomposition of bio-composite films with the addition of nanocellulose in film preparation was illustrated by DTG curves. As can be seen in **Fig. 83**, there were three stages in the thermal degradation of as-prepared films which relating to the evaporation of water and glycerol in films in the first stage.[315] The second stage of degradation of side chain in PVA molecules and the third stage of degradation of the main chains of PVA molecules also shown in this series (the same pattern with series A and series B). [298,321]

In this case, a small shoulder at around 350 ^{O}C was observed in C1, C3 and C5, indicating the decomposition of cellulose which could be suggested that a slight increase in thermal stability of C1, C3 and C5 bio-composite films.[325]

From these results, it should be noted that the thermal stability of bio-composite films could be improved by nanocellulose addition in film preparation.[322]

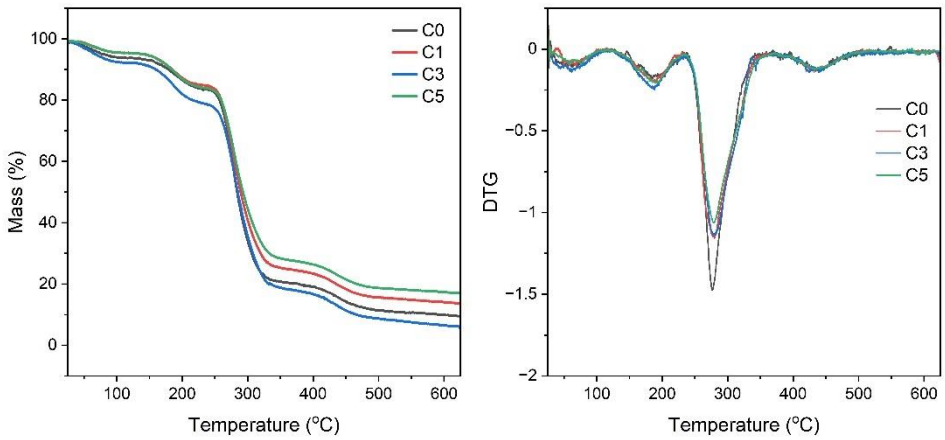

Fig. 83 TGA (a) and DTG (b) curves of bio-composite films: series C

4.4.3.3 Mechanical Properties of bio-composite films series C

The mechanical properties of the as-prepared bio-composite films-PVA blended with different content of OS-Alkaline-Bleached-A (1-5%). The reinforcing effect of nanocellulose fibre in the soft chain of PVA polymer matrix was reported in this part. A significant increase of tensile strength with the increased addition. It was found that the

tensile strength increases of 48.4% for as-prepared C5 film (45.2 MPa), compared to 0% OS-Alkaline-Bleached-A addition (30.4 MPa). Tensile properties of as-prepared films: Series C are summarised in Table 38.

Table 38 Tensile properties of as-prepared films: Series C

Series C	Tensile strength (MPa)	Elongation at break (%)
C0	30.4 ± 0.2	335.7 ± 6.7
C1	34.4 ± 0.4	462.4 ± 4.2
C2	37.4 ± 0.4	349.3 ± 5.6
C3	39.3 ± 0.5	333.3 ± 8.0
C4	44.7 ± 0.3	410.8 ± 6.0
C5	45.2 ± 0.4	388.6 ± 5.9

A gradual increase of tensile strength with the increase of OS-Alkaline-Bleached-A content could be seen in Fig. 84. However, percentage of elongation at break reveals that 1% and 4% of OS-Alkaline-Bleached-A content in film preparation provided the relatively high values of 464.4% and 410.8%, compared to C0 film. As the amount of NFC increased from 1% to 3%, the tensile strength of the bio-composite films increased whereas elongation at break decreased. However, the addition of 4%-5% could show the same trend of tensile strength for all series but elongation at break of C4 and C5 were found to be 410.8% and 388.6% which more than C0 film. Compared to all films of series C, C4 provides both high value tensile strength of 44.7 MPa and elongation at break of 410.8%.

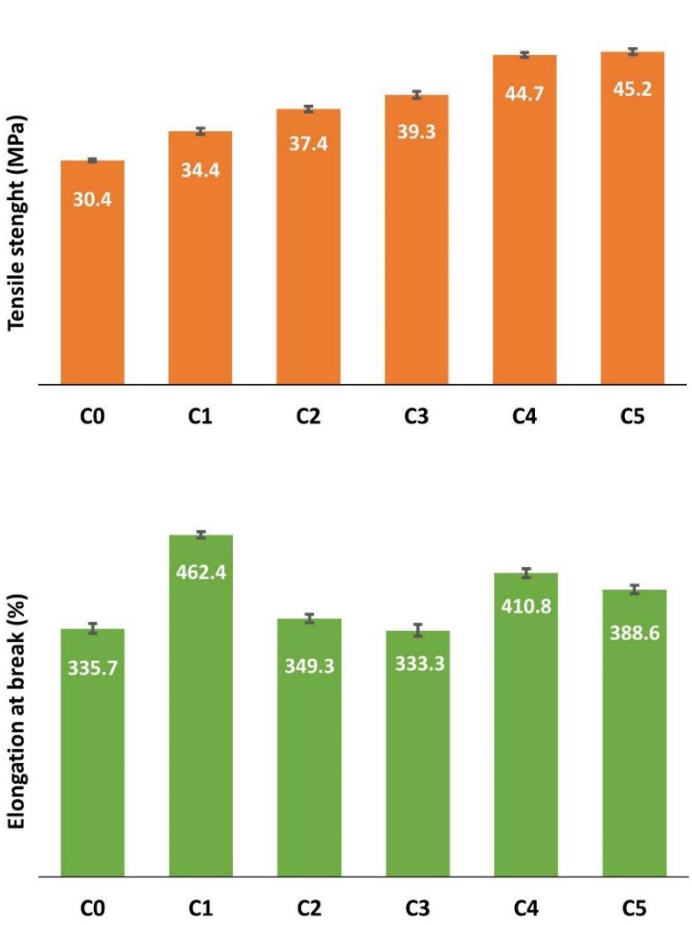

Fig. 84 Tensile strength (a) and elongation at break (b) of bio-composite films: Series C

The favorable effect of chemically modified rice husk fibres (which include alkaline treatment, bleaching step, and acid hydrolysis on the mechanical properties of bio-composite films) compared to the cellulose fibre from fractionation alone reinforced as-prepared composite films were investigated in three series of films.

4.5 Conclusion

Project 2: Rice husk-derived cellulose microfibres/nanofibres for bio-composite film preparation

The development of procedures to produce rice husk-derived cellulose microfibres/nanofibres were successfully extracted through organosolv microwave-assisted pretreatment followed by chemical treatment steps which avoid harsh chemicals

for all processing. The cellulose microfibres/nanofibres were used as a reinforcement filler for enhancing the mechanical properties of bio-composite films. Bio-composite films reinforced by microfibres/nanofibres also possess a good optical, and mechanical properties and also exhibit good thermal stability which can be suitable for film packaging. From these results, three different types of cellulose fibres from rice husk were mixed with the PVA polymer and glycerol for bio-composite films preparation which includes bio-composite films series A prepared from cellulose microfibres after organosolv pretreatment, bio-composite films series B prepared from cellulose micro/nanofibres after bleaching step, and the bio-composite films series C prepared from nanocellulose fibres after acid hydrolysis step. In this part, bio-composite films were successfully prepared by using cellulose micro/nanofibres as reinforcing agent. Whereas the addition of cellulose microfibres could not improve the mechanical properties of bio-composite films (series A). While the addition of the mix phase of cellulose micro/nano fibres and nanofibres as reinforcing agent in film preparation affected the mechanical performance of bio-composite films (Series B and Series C).

The increase of cellulose micro/nano fibres content in the bio-composite films (series B and series C) from 1% to 5% resulted in an increase in tensile strength. The results from TEM images also show that the cellulose nanofibres can be formed the homogenous phase for preparing well dispersed in film preparation (series C), leading to a significant improvement in mechanical performance. The best optical transmittance performance was also obtained from films series C which reveal the relatively high value of light transmittance. C5 bio-composite film shows 95% transmittance at 500 nm for 5% addition of nanofibres in C5 film preparation with also provide the highest tensile strength (45.2 MPa) of all films. This could be suggested that micro/nanocellulose fibres from rice husk could be a promising reinforcing agent for bio-composite films production.

Moreover, the thermal stability of bio-composite films was investigated by DTG analysis reveal that the addition of micro/nano fibres in film preparation can improve the thermal stability of bio-composite films. As evidence of bio-composite films (series C) prepared with the nanocellulose addition illustrated the best optical transmittance and mechanical

property with good thermal stability. It should be noted that the bio-composite film preparation from this work could be useful as an alternative procedure to produce a good quality of bio-composite films which beneficial in the applications that require high strength properties with good thermal stability of biodegradable materials.

4.6 Future work

Project 2: Rice husk-derived cellulose microfibres/nanofibres for bio-composite film preparation

This part has demonstrated the investigation of rice husk-derived cellulose microfibres/nanofibres for using as reinforcing agent in bio-composite film preparation. However, there is further work still needed in the first step of pretreatment by organosolv fractionation under mild conditions.

- It is well represented that after organosolv fractionation of rice husk to produce cellulose fibres, however, the lignin-rich fraction can be separated from this step. Thus, the-as obtained lignin will be further characterised and will be applied for applications such as using as UV-shielding for enhancing UV absorption properties in bio-composite film preparation.

Abbreviations

ATR-IR	Attenuated total reflection infrared spectroscopy
BET	Brunauer-Emmett-Teller
BJH	Barrett Joyner and Halenda
CMF	Cellulose microfibrils
CNC	Cellulose nanocrystal
CrI	Crystallinity Index
CSC	Carbon-silica composite
FTIR	Fourier transform infrared spectroscopy
GC-MS	Gas chromatography-mass spectroscopy
IL	Ionic liquid
IUPAC	International Union of Pure and Applied Chemistry
NMR	Nuclear Magnetic Resonance
MB	Methylene blue
MW	Microwave
ppm	Parts per million
RH	Rice husk
SAXS	Small-Angle X-ray Scattering

SBA-15	Santa Barbara Amorphous-15
SDGs	Sustainable Development Goals
SEM	Scanning Electron Microscopy
STA	Simultaneous Thermal Analysis
TEOS	Tetraethylorthosilicate
TEM	Transmission Electron Microscopy
TGA	Thermogravimetric Analysis
UV-Vis	Ultraviolet–Visible Spectroscopy
XPS	X-ray photoelectron spectroscopy
XRD	X-ray Diffraction
XRF	X-Ray Fluorescence

References

1 K. Aroonrat and S. Wongwises, *Renew Sustain Energy Rev*, 2015, **46**, 70–78.

2 M. Yuttitham, S. H. Gheewala and A. Chidthaisong, *J Clean Prod*, 2011, **19**, 2119–2127.

3 S. Chaijamrus and B. Mouthung, *Songklanakarin J Sci Technol*, 2011, **33**, 163–170.

4 J. K. Saini, R. Saini and L. Tewari, *3 Biotech*, 2015, **5**, 337–353.

5 W. Kajina, P. Rousset, W. H. Chen, T. Sornpitak and J. M. Commandré, *Renew Energy*, 2018, **118**, 113–121.

6 T. Silalertruksa and S. H. Gheewala, *Energy Policy*, 2010, **38**, 7476–7486.

7 T. Silalertruksa, P. Pongpat and S. H. Gheewala, *J Clean Prod*, 2017, **140**, 906–913.

8 J. H. Clark, R. Luque and A. S. Matharu, *Annu Rev Chem Biomol Eng*, 2012, **3**, 183–207.

9 J. H. Clark, *Curr Opin Green Sustain Chem*, 2017, **8**, 10–13.

10 W. Dessie, X. Luo, M. Wang, L. Feng, Y. Liao, Z. Wang, Z. Yong and Z. Qin, *Appl Microbiol Biotechnol*, 2020, **104**, 4757-4770.

11 G. Sharma, M. Kaur, S. Punj and K. Singh, *Biofuel Bioprod Bior*, 2020, **14**, 673-695.

12 Y. Long, L. Xiao and Q. Cao, *Powder Technol*, 2017, **310**, 24–34.

13 J. Kim, Y. Yi, D. H. Peck, S. H. Yoon, D. H. Jung and H. S. Park, *Environ Sci Nano*, 2019, **6**, 916–924.

14 L. Shrestha, M. Thapa, R. Shrestha, S. Maji, R. Pradhananga and K. Ariga, *C-Basel*, 2019, **5**, 10.

15 M. Anshar, D. Tahir, Makhrani, F. N. Ani and A. S. Kader, *Environmental Engineering Research*, 2018, **23**, 250–257.

16 T. Jiang, V. L. Budarin, P. S. Shuttleworth, G. Ellis, C. M. A. Parlett, K. Wilson, J. Macquarrie and A. J. Hunt, *J Mater Chem A*, 2015, **3**, 14148–14156.

17 X. Zhang, K. Rajagopalan, H. Lei, R. Ruan and B. K. Sharma, *Sustain Energy Fuels*, 2017, **1**, 1664–1699.

18 S. Sangon, A. J. Hunt, T. M. Attard, P. Mengchang, Y. Ngernyen and N. Supanchaiyamat, *J Clean Prod*, 2018, **172**, 1128–1139.

19 T. Klamrassamee, N. Laosiripojana, D. Cronin, L. Moghaddam, Z. Zhang and W. O. S. Doherty, *Bioresour Technol*, 2015, **180**, 222–229.

20 Y. Ma, H. Zhang, H. Yang and Y. Zhang, *Cellulose*, 2019, **26**, 8465–8474.

21 S. Yorgun and D. Yildiz, *J Anal Appl Pyrolysis*, 2015, **114**, 68–78.

22 S. F. K. Ahmad, U. F. M. Ali and K. M. Isa, *Environ Eng Res*, 2020, **25**, 18–28.

23 H. M. Liu, B. Feng and R. C. Sun, *J Agric Food Chem*, 2011, **59**, 10524–10531.

24 R. Intasit, B. Cheirsilp, Y. Louhasakul, P. Boonsawang, S. Chaiprapat and J. Yeesang, *Bioresour Technol*, 2020, **298**, 1-9.

25 X. Xiong, I. K. M. Yu, L. Cao, D. C. W. Tsang, S. Zhang and Y. S. Ok, *Bioresour Technol*, 2017, **246**, 254–270.

26 N. Photong and J. Wongthanate, *Waste Management and Research*, 2020, **38**, 69–77.

27 J. Wang, H. Cui, S. Wei, S. Zhuo, L. Wang, Z. Li and W. Yi, *Smart Grid Renew Energ*, 2010, **01**, 98–107.

28 D. Mohan, C. U. Pittman and P. H. Steele, *Energ Fuel*, 2006, **20**, 848–889.

29 C. A. Mullen, G. D. Strahan and A. A. Boateng, *Energ Fuel*, 2009, **23**, 2707–2718.

30 T. Jiang, Y. Yuan, S. Liu, A. J. Hunt and G. Tan, *ACS Omega*, 2020, **5**, 16021–16029.

31 Z. Wu, Q. Lu, W. H. Fu, S. Wang, C. Liu, N. Xu, D. Wang, Y. M. Wang and Z. Chen, *New J Chem*, 2015, **39**, 985–993.

32 K. Sotiriou, N. Supanchaiyamat, T. Jiang, I. Janekarn, A. M. García, V. L. Budarin, D. J. Macquarrie and A. J. Hunt, *RSC Adv*, 2020, **10**, 25228–25238.

33 B. Tsegaye, C. Balomajumder and P. Roy, *Bull Natl Res Cent*, 2019, **43**, 1-10.

34 P. Kumar, D. M. Barrett, M. J. Delwiche and P. Stroeve, *Ind Eng Chem Res*, 2009, **48**, 3713–3729.

35 S. Amin, *Energy Convers Manag*, 2009, **50**, 1834–1840.

36 D. J. Macquarrie, J. H. Clark and E. Fitzpatrick, *Biofuel Bioprod Biorefin*, 2012, **6**, 549–560.

37 S. H. Chang, *Bioenergy Res*, 2020, **13**, 23–42.

38 Z. Ji-lu, *J Anal Appl Pyrolysis*, 2007, **80**, 30–35.

39 N. Hao, H. Ben, C. G. Yoo, S. Adhikari and A. J. Ragauskas, *Energ Fuel*, 2016, **30**, 6863–6880.

40 D. Chiaramonti, A. Oasmaa and Y. Solantausta, *Renew Sustain Energy Rev*, 2007, **11**, 1056–1086.

41 K. Chaiwong, T. Kiatsiriroat, N. Vorayos and C. Thararax, *Maejo Int J Sci Technol*, 2012, **6**, 186–195.

42 Z. Zhu, C. A. Rezende, R. Simister, S. J. McQueen-Mason, D. J. Macquarrie, I. Polikarpov and L. D. Gomez, *Biomass Bioenerg*, 2016, **93**, 269–278.

43 Z. Zhang, D. J. Macquarrie, M. De Bruyn, V. L. Budarin, A. J. Hunt, M. J. Gronnow, J. Fan, P. S. Shuttleworth, J. H. Clark and A. S. Matharu, *Green Chem*, 2015, **17**, 260–270.

44 M. N. Uddin, K. Techato, J. Taweekun, M. M. Rahman, M. G. Rasul, T. M. I. Mahlia and S. M. Ashrafur, *Energies*, 2018, **11**, 1-24.

45 J. Bedia, M. Peñas-Garzón, A. Gómez-Avilés, J. Rodriguez, C. Belver, X. Zhang, K. Rajagopalan, H. Lei, R. Ruan, B. K. Sharma, S. Nizamuddin, H. A. Baloch, M. T. H. Siddiqui, N. M. Mubarak, M. M. Tunio, A. W. Bhutto, A. S. Jatoi, G. J. Griffin and M. P. Srinivasan, *Sustain Energy Fuels*, 2018, **17**, 813–837.

46 P. Khongphakdi, A. Palamanit, N. Phusunti, Y. Tirawanichakul and P. Shrivastava, *Int J Integr Eng*, 2020, **12**, 226–233.

47 D. Liu, W. Zhang, H. Lin, Y. Li, H. Lu and Y. Wang, *RSC Adv*, 2015, **5**, 19294–19300.

48 Y. Zhang, D. Y. Chen, D. Zhang and X. F. Zhu, *J Fuel Chem Technol,* 2012, **40**, 1194–1199.

49 I. K. M. Yu, H. Chen, F. Abeln, H. Auta, J. Fan, V. L. Budarin, J. H. Clark, S. Parsons, C. J. Chuck, S. Zhang, G. Luo and D. C. W. Tsang, *Crit Rev Environ Sci Technol*, 2020, **0**, 1–54.

50 G. Smagulova, A. Imash, A. Baltabay, B. Kaidar and Z. Mansurov, *C-J Carbon res*, 2022, **8**, 1-19.

51 M. M. Alam, M. A. Hossain, M. D. Hossain, M. A. H. Johir, J. Hossen, M. S. Rahman, J. L. Zhou, A. T. M. K. Hasan, A. K. Karmakar and M. B. Ahmed, *Processes*, 2020, **8**, 1-38.

52 D. Singh, R. Kumar, A. Kumar and K. N. Rai, *Ceramica*, 2008, **54**, 203–212.

53 D. Battegazzore, S. Bocchini, J. Alongi and A. Frache, *RSC Adv*, 2014, **4**, 54703–54712.

54 N. Rahmat, F. Hamzah, N. Sahiron, M. Mazlan and M. M. Zahari, *IOP Conf Ser Mater Sci Eng*, 2016, **133**, 1-9.

55 S. H. Chang, *Bioenergy Res*, 2020, **13**, 23–42.

56 X. Wang, H. Chen, K. Luo, J. Shao and H. Yang, *Energ Fuel*, 2008, **22**, 67–74.

57 E. Calcio Gaudino, G. Cravotto, M. Manzoli and S. Tabasso, *Green Chem*, 2019, **21**, 1202–1235.

58 S. Varshney, V. Mulpuru, N. Mishra and M. K. Gupta, *Mater Technol*, 2022, **37**, 2608–2622.

59 T. Thongtem, C. Pilapong, J. Kavinchan, A. Phuruangrat and S. Thongtem, *J Alloys Compd*, 2010, **500**, 195-199.

60 X. Sun, W. Yu, J. Yan, J. Li, G. Jin, J. Feng, Z. Guo and X. Liang, *RSC Adv*, 2018, **8**, 27207–27215.

61 A. de N. de Oliveira, R. da S. Cardoso, I. M. Ferreira, L. S. da Silva, A. A. F. da Costa, L. H. de O. Pires, G. N. da Rocha Filho, R. Luque, R. C. R. Noronha and L. A. S. do Nascimento, *Microporous Mesoporous Mater*, 2023, **354**, 1-50.

62 J. R. Dodson, E. C. Cooper, A. J. Hunt, A. Matharu, J. Cole, A. Minihan, J. H. Clark and D. J. MacQuarrie, *Green Chem*, 2013, **15**, 1203–1210.

63 Y. Shen, *J Agric Food Chem*, 2017, **65**, 995–1004.

64 M. V. Lebedeva, A. B. Ayupov, P. M. Yeletsky and V. N. Parmon, *Int J Electrochem Sci*, 2018, **13**, 3674–3690.

65 J. Sodtipinta, T. Amornsakchai and P. Pakawatpanurut, *Adv Nat Sci: Nanosci Nanotechnol*, 2017, **8**, 1-9.

66 N. Shahi, E. Lee, B. Min and D. J. Kim, *Sensors*, 2021, **21**, 1-16.

67 V. C. Niculescu, *Front Mater*, 2020, **7**, 1-14.

68 T. H. Liou, S. Y. Wang, Y. T. Lin and S. Yang, *Colloids Surf A Physicochem Eng Asp*, 2022, **636**, 1-13.

69 R. Ryoo, C. H. Ko and I. S. Park, *Chem Com*, 1999, **15**, 1413–1414.

70 J. Hu, L. Liu and Z. Xiao, *RSC Adv*, 2015, **5**, 68092–68098.

71 M. S. Abdel Salam, M. A. Betiha, S. A. Shaban, A. M. Elsabagh, R. M. Abd El-Aal and F. Y. El kady, *Egyptian Journal of Petroleum*, 2015, **24**, 49–57.

72 E. B. Celer and M. Jaroniec, *J Am Chem Soc*, 2006, **128**, 14408–14414.

73 Y. Ge, J. Gao and T. Zhao, *Mater Lett*, 2019, **249**, 77–80.

74 V. Chaudhary and S. Sharma, *Journal of Porous Materials*, 2017, **24**, 741–749.

75 Q. Jin, F. Qu, J. Jiang, Y. Dong, W. Guo and H. Lin, *J Solgel Sci Technol*, 2013, **66**, 466–471.

76 Y. H. Chu, Z. M. Wang, M. Yamagishi, H. Kanoh, T. Hirotsu and Y. X. Zhang, *Langmuir*, 2005, **21**, 2545–2551.

77 L. Wang, Z. Schnepp and M. M. Titirici, *J Mater Chem A Mater*, 2013, **1**, 5269–5273.

78 J. P. Thielemann, F. Girgsdies, R. Schlögl and C. Hess, *Beilstein J Nanotechnol*, 2011, **2**, 110–118.

79 Y. Dong, B. Lu, S. Zang, J. Zhao, X. Wang and Q. Cai, *J Chem Technol Biotechnol*, 2011, **86**, 616–619.

80 R. Ryoo, S. H. Joo, M. Kruk and M. Jaroniec, *Adv Mater*, 2001, **13**, 677–681.

81 E. Da'na, *Microporous Mesoporous Mater*, 2017, **247**, 145–157.

82 E. Twumasi, M. Forslund, P. Norberg and C. Sjöström, *J Porous Mater*, 2012, **19**, 333–343.

83 L. Y. Jaramillo, K. Arango-Benítez, W. Henao, E. Vargas, G. Recio-Sánchez and M. Romero-Sáez, *Mater Lett*, 2019, **257**, 126749.

84 V. Zeleňák, J. Magura, A. Zeleňáková and R. Smolková, *Pure Appl Chem*, 2017, **89**, 493–500.

85 B. Bera and N. Das, *Int J Appl Ceram Technol*, 2019, **16**, 294–303.

86 C. T. Cavalcante, C. Molina and T. S. Martins, *J Mater Sci Mater Electron*, 2019, **30**, 16903–16909.

87 A. Banka, T. Komolwanich and S. Wongkasemjit, *Cellulose*, 2015, **22**, 9–29.

88 E. Forgacs, T. Cserháti and G. Oros, *Environ Int*, 2004, **30**, 953–971.

89 V. Nang An, H. T. Chi Nhan, T. D. Tap, T. T. T. Van, P. Van Viet and L. Van Hieu, *J Polym Environ*, 2020, **28**, 1465–1474.

90 R. Muangrat, *Environ Technol Rev*, 2013, **2**, 85–100.

91 S. Jamnongphol, A. Jaturapiree, K. Sukrat, T. Saowapark, E. Chaichana and B. Jongsomjit, *Waste Biomass Valori*, 2020, **11**, 769–779.

92 C. Zhan, P. R. Sharma, H. He, S. K. Sharma, A. McCauley-Pearl, R. Wang and B. S. Hsiao, *Environ Sci (Camb)*, 2020, **6**, 3080–3090.

93 A. E. Karaca, C. Özel, A. C. Özarslan and S. Yücel, *Polym Compos*, 2022, **43**, 6838–6853.

94 N. Johar, I. Ahmad and A. Dufresne, *Ind Crops Prod*, 2012, **37**, 93–99.

95 M. Nogi, S. Iwamoto, A. N. Nakagaito and H. Yano, *Adv Mater*, 2009, **21**, 1595–1598.

96 A. J. Svagan, M. A. S. A. Samir and L. A. Berglund, *Adv Mater*, 2008, **20**, 1263–1269.

97 Y. Gao, X. Guo, Y. Liu, Z. Fang, M. Zhang, R. Zhang, L. You, T. Li and R. H. Liu, *Sci Rep*, 2018, **8**, 1-8.

98 L. Ludueña, D. Fasce, V. A. Alvarez and P. M. Stefani, *Bioresour*, 2011, **6**, 1440-1453.

99 S. Rashid and H. Dutta, *Ind Crops Prod*, 2020, **154**, 1-12.

100 V. B. Carmona, R. M. Oliveira, W. T. L. Silva, L. H. C. Mattoso and J. M. Marconcini, *Ind Crops Prod*, 2013, **43**, 291–296.

101 P. Phanthong, P. Reubroycharoen, X. Hao, G. Xu, A. Abudula and G. Guan, *Carbon Resour Convers*, 2018, **1**, 32–43.

102 K. T. Chaka, *Green Chem Lett Rev*, 2022, **15**, 582–597.

103 A. Bazargan, Z. Wang, J. P. Barford, J. Saleem and G. McKay, *J Clean Prod*, 2020, **260**, 1-12.

104 F. L. Zitzmann, E. Ward, X. Meng and A. S. Matharu, *Molecules*, 2021, **26**, 1-13.

105 Y. Gao, M. Z. Ozel, T. Dugmore, A. Sulaeman and A. S. Matharu, *J Hazard Mater*, 2021, **401**, 1-11.

106 Z. Zhu, D. J. Macquarrie, R. Simister, L. D. Gomez and S. J. McQueen-Mason, *Sustain Chem Process*, 2015, **3**, 1–13.

107 S. Imman, J. Arnthong, V. Burapatana, N. Laosiripojana and V. Champreda, *Appl Biochem Biotechnol*, 2013, **170**, 1982–1995.

108 Q. Wang, S. Kudo, S. Asano and J. I. Hayashi, *ACS Omega*, 2022, **7**, 27638–27648.

109 P. Daorattanachai, N. Viriya-empikul, N. Laosiripojana and K. Faungnawakij, *Bioresour Technol*, 2013, **144**, 504–512.

110 P. Lenihan, A. Orozco, E. O'Neill, M. N. M. Ahmad, D. W. Rooney and G. M. Walker, *Chem Eng J*, 2010, **156**, 395–403.

111 Z. Zhu, Y. Liu, X. Yang, S. J. McQueen-Mason, L. D. Gomez and D. J. Macquarrie, *Biomass Convers Biorefin*, 2021, **11**, 2681-2693.

112 J. S. Kim, Y. Y. Lee and T. H. Kim, *Bioresour Technol*, 2016, **199**, 42–48.

113 G. Bali, X. Meng, J. I. Deneff, Q. Sun and A. J. Ragauskas, *Chem Sus Chem*, 2015, **8**, 275–279.

114 S. Nuchdang, V. Thongtus, M. Khemkhao, S. Kirdponpattara, E. J. Moore, H. D. B. Setiabudi and C. Phalakornkule, *Biomass Convers Biorefin*, 2021, **11**, 2471-2483.

115 M. Raita, N. Denchokepraguy, V. Champreda and N. Laosiripojana, *3 Biotech*, 2017, **7**, 1–10.

116 M. Wang, X. Miao, H. Li and C. Chen, *Polymers*, 2022, **14**, 1-16.

117 S. C. Shi and G. T. Liu, *Cellulose*, 2021, **28**, 6147–6158.

118 T. Wang and Y. Zhao, *Carbohydr Polym*, 2021, **253**, 1-11.

119 M. Mahardika, H. Abral, A. Kasim, S. Arief and M. Asrofi, *Fibers*, 2018, **6**, 1–12.

120 D. Trache, A. F. Tarchoun, M. Derradji, T. S. Hamidon, N. Masruchin, N. Brosse and M. H. Hussin, *fchem*, 2020, **8**, 1-33.

121 A. P. Sulaeman, Y. Gao, T. Dugmore, J. Remón and A. S. Matharu, *Cellulose*, 2021, **28**, 7687–7705.

122 J. Gröndahl, K. Karisalmi and J. Vapaavuori, *Soft Matter*, 2021, **17**, 9842–9858.

123 W. Laumer, L. Andreu, G. Helle, G. H. Schleser, T. Wieloch and H. Wissel, *Rapid Commun Mass Spectrom*, 2009, **23**, 1934–1940.

124 M. Dilamian and B. Noroozi, *Cellulose*, 2019, **26**, 5831–5849.

125 Z. Feng, D. Xu, Z. Shao, P. Zhu, J. Qiu and L. Zhu, *Carbohydr Polym*, 2022, **296**, 1-9.

126 D. W. Indriani, N. Barunawati, S. H. Sumarlan and L. Teresia, *Russ J Agric Socioecon Sci*, 2019, **96**, 195–200.

127 R. Tan, F. Li, Y. Zhang, Z. Yuan, X. Feng, W. Zhang, T. Liang, J. Cao, C. F. De Hoop, X. Peng and X. Huang, *J Nanomater*, 2021, **2021**, 1-9.

128 P. Cazón, G. Velazquez and M. Vázquez, *Food Hydrocoll*, 2019, **89**, 481–491.

129 B. A. de Marco, B. S. Rechelo, E. G. Tótoli, A. C. Kogawa and H. R. N. Salgado, *Saudi Pharm J*, 2019, 27, 1–8.

130 Anastas, P.T. and Warner, J.C. (1998) Green Chemistry: Theory and Practice. Oxford University Press, New York, 29-56.

131 The Sustainable Development Goals Report (2023): Special Edition is the only UN officialreport that monitors global progress on the 2030 Agenda for Sustainable Development.

132 M. Pan, X. Gan, C. Mei and Y. Liang, *J Mol Struct*, 2017, **1127**, 575–582.

133 H. Chen, J. Liu, X. Chang, D. Chen, Y. Xue, P. Liu, H. Lin and S. Han, *Fuel Process Technol*, 2017, **160**, 196–206.

134 A. T. W. M. Hendriks and G. Zeeman, *Bioresour Technol*, 2009, **100**, 10–18.

135 P. A. Larsson, A. V. Riazanova, G. Cinar Ciftci, R. Rojas, H. H. Øvrebø, L. Wågberg and L. A. Berglund, *Cellulose*, 2019, **26**, 1565–1575.

136 D. Trache, M. H. Hussin, C. T. Hui Chuin, S. Sabar, M. R. N. Fazita, O. F. A. Taiwo, T. M. Hassan and M. K. M. Haafiz, *Int J Biol Macromol*, 2016, **93**, 789–804.

137 D. Miyashiro, R. Hamano and K. Umemura, *Nanomaterials*, 2019, **10**, 1-23.

138 A. H. Tayeb, E. Amini, S. Ghasemi and M. Tajvidi, *Molecules*, 2018, **23**, 1-24.

139 C. Zinge and B. Kandasubramanian, *Eur Polym J*, 2020, **133**, 1-20.

140 C. J. Chirayil, J. Joy, L. Mathew, M. Mozetic, J. Koetz and S. Thomas, *Ind Crops Prod*, 2014, **59**, 27–34.

141 I. Niskanen, K. Zhang, M. Karzarjeddi, H. Liimatainen, S. Shibata, N. Hagen, R. Heikkilä, H. Yoda and Y. Otani, *J Polym Res*, 2022, **29**, 1-11.

142 T. Fattahi Meyabadi, F. Dadashian, G. Mir Mohamad Sadeghi and H. Ebrahimi Zanjani Asl, *Powder Technol*, 2014, **261**, 232–240.

143 X. Huang, T. I. Korányi, M. D. Boot and E. J. M. Hensen, *Chem Sus Chem*, 2014, **7**, 2276–2288.

144 V. L. Budarin, J. H. Clark, B. A. Lanigan, P. Shuttleworth and D. J. Macquarrie, *Bioresour Technol*, 2010, **101**, 3776–3779.

145 Y. Gao, H. Xia, A. P. Sulaeman, E. M. De Melo, T. I. J. Dugmore and A. S. Matharu, *ACS Sustain Chem Eng*, 2019, **7**, 11861–11871.

146 H. Mehta and L. Chopra, *AIP Conf Proc*, 2023, **2535**, 40008.

147 Y. Tian, P. Zhu, M. Zhou, Y. Lin and F. Cheng, *J Wuhan Univ Technol Mater Sci Ed*, 2020, **35**, 825–831.

148 N. Aggarwal, P. Pal, N. Sharma and S. Saravanamurugan, *ACS Omega*, 2021, **6**, 27247–27258.

149 Y. Sheng, Z. Ma, X. Wang and Y. Han, *Food Chem*, 2022, **376**, 1-10.

150 J. U. Hernández-Beltrán, I. Hernández-De Lira, M. Cruz-Santos, A. Saucedo-Luevanos, F. Hernández-Terán and N. Balagurusamy, *Appl Sci*, 2019, **9**, 1-29.

151 Office of agriculteral economic, *Agiculteral Statistics of Thailand 2019*, 2019.

152 Department of Alternative Energy Development and Efficiency (DEDE), *Research and Development in the field of Energy Conservation and Renewable Energy in Thailand*, 2012.

153 T. Silalertruksa, S. H. Gheewala and P. Pongpat, *Appl Energy*, 2015, **160**, 603–609.

154 N. Wantaneeyakul, K. Kositkanawuth, S. Q. Turn and J. Fu, *ACS Omega*, 2021, **6**, 28890–28902.

155 W. Roschat, T. Siritanon, B. Yoosuk and V. Promarak, *Energy Convers Manag*, 2016, **119**, 453–462.

156 J. P. de Oliveira, G. P. Bruni, K. O. Lima, S. L. M. El Halal, G. S. da Rosa, A. R. G. Dias and E. da R. Zavareze, *Food Chem*, 2017, **221**, 153–160.

157 V. Gerardi, F. Minelli6 and D. Viggiano, *Biomass Bioenerg*, 1998, **14**, 295-299.

158 S. Steven, E. Restiawaty and Y. Bindar, *Renew Sustain Energy Rev*, 2021, **149**, 1-18.

159 E. Menya, P. W. Olupot, H. Storz, M. Lubwama and Y. Kiros, *Chem Eng Res Des*, 2018, **129**, 271–296.

160 N. Bisht, P. C. Gope and N. Rani, *J Mech Behav Mater*, 2020, **29**, 147–162.

161 B. Sahoo, K. S. P. Devi, S. K. Sahu, S. Nayak, T. K. Maiti, D. Dhara and P. Pramanik, *Biomater Sci*, 2013, **1**, 647–657.

162 W. Wang, J. C. Martin, R. Huang, W. Huang, A. Liu, A. Han and L. Sun, *RSC Adv*, 2012, **2**, 9036–9041.

163 R. A. Bakar, R. Yahya and S. N. Gan, *Procedia Chem*, 2016, **19**, 189–195.

164 F. Adam, J. N. Appaturi and A. Iqbal, *Catal Today*, 2012, **190**, 2–14.

165 Y. V. Larichev, P. M. Yeletsky and V. A. Yakovlev, *J Phys Chem Sol*, 2015, **87**, 58–63.

166 C. Kongmanklang and K. Rangsriwatananon, *J Spectrosc*, 2015, **2015**, 2–7.

167 S. Imman, J. Arnthong, V. Burapatana, V. Champreda and N. Laosiripojana, *Renew Energy*, 2015, **83**, 663–673.

168 D. F. Hincapié Rojas, P. Pineda Gómez and A. Rosales Rivera, *Adv Mater Lett*, 2019, **10**, 67–73.

169 O. Jullaphan, T. Witoon and M. Chareonpanich, *Mater Lett*, 2009, **63**, 1303–1306.

170 L. J. Cárdenas, L. Giraldo and J. C. Moreno-Piraján, *Processes*, 2022, **10**, 1-16.

171 A. A. Sabri, T. M. Albayati and R. A. Alazawi, *Korean J Chem Eng*, 2015, **32**, 1835–1841.

172 J. Wang, L. Fang, F. Cheng, X. Duan and R. Chen, *J Nanomater*, 2013, **2013**, 1–7.

173 M. Chareonpanich, A. Nanta-ngern and J. Limtrakul, *Mater Lett*, 2007, **61**, 5153–5156.

174 S. Singh, R. Kumar, H. D. Setiabudi, S. Nanda and D. V. N. Vo, *Appl Catal A Gen*, 2018, **559**, 57–74.

175 M. R. Oliveira, M. Deon, E. V Benvenutti, V. A. Barros, D. C. De Melo, E. Franceschi, S. M. Egues and J. F. De Conto, *J Solgel Sci Technol*, 2020, **94**, 708–718.

176 S. Xiu and A. Shahbazi, *Renew Sustain Energy Rev*, 2012, **16**, 4406–4414.

177 S. Fukuda, *Int J Green Energy*, 2015, **12**, 215–224.

178 C. Sakdaronnarong, W. Pipathworapoom, T. Vichitsrikamol, T. Sema, P. Posoknistakul, W. Koo-amornpattana and N. Laosiripojana, *Process Safe Environl Prot*, 2018, **116**, 1–13.

179 I. Janekarn, A. J. Hunt, Y. Ngernyen, S. Youngme and N. Supanchaiyamat, *R Soc Open Sci*, 2020, **7**, 1-18.

180 B. Ounphikul, N. Chantarasombat, A. J. Hunt and Y. Ngernyen, *Mater Today: Proc*, 2020, **51**, 1884–1887.

181 H. I. Meléndez-Ortiz, B. Puente-Urbina, J. A. Mercado-Silva and L. García-Uriostegui, *Int J Appl Ceram Technol*, 2019, **16**, 1533–1543.

182 X. G. Chen, S. S. Lv, S. T. Liu, P. P. Zhang, A. B. Zhang, J. Sun and Y. Ye, *Sep Sci Technol*, 2012, **47**, 147–156.

183 M. Rafatullah, O. Sulaiman, R. Hashim and A. Ahmad, *J Hazard Mater*, 2010, **177**, 70–80.

184 H. M. Ng, L. T. Sin, T. T. Tee, S. T. Bee, D. Hui, C. Y. Low and A. R. Rahmat, *Compos B Eng*, 2015, **75**, 176–200.

185 F. Jiang, S. Han and Y. Lo Hsieh, *RSC Adv*, 2013, **3**, 12366–12375.

186 K. Pacaphol and D. Aht-Ong, *J Clean Prod*, 2017, **142**, 1283–1295.

187 X. Yu, Y. Jiang, Q. Wu, Z. Wei, X. Lin and Y. Chen, Front Energy Res, 2021, **9**, 1-10.

188 K. Choi, J. Do Nam, S. H. Kwon, H. J. Choi, M. S. Islam and N. Kao, *Polym*, 2019, **11**, 1-11.

189 P. Pantamanatsopa, W. Ariyawiriyanan and S. Ekgasit, *J Nat Fibers*, 2023, **20**, 1-14.

190 G. K. Gupta and P. Shukla, *Front Chem*, 2020, **8**, 601256.

191 J. K. Singh, B. Chaurasia, A. Dubey, A. M. F. Noguera, A. Gupta, R. Kothari, C. P. Upadhyaya, A. Kumar, A. Hashem, A. A. Alqarawi and E. F. A. Allah, *Sustain*, 2021, **13**, 1–16.

192 T. Klamrassamee, T. Tana, N. Laosiripojana, L. Moghaddam, Z. Zhang, J. Rencoret, A. Gutierrez, J. C. Del Rio and W. O. S. Doherty, *RSC Adv*, 2016, **6**, 92638–92647.

193 P. Asawaworarit, P. Daorattanachai, W. Laosiripojana, C. Sakdaronnarong, A. Shotipruk and N. Laosiripojana, *Chem Eng J*, 2019, **356**, 461–471.

194 C. Inkrod, M. Raita, V. Champreda and N. Laosiripojana, *Bioenergy Res*, 2018, **11**, 277–290.

195 T. Li, J. Remón, Z. Jiang, V. L. Budarin and J. H. Clark, *Energy Convers Manag*, 2018, **155**, 147–160.

196 E. Lam and U. D. Hemraz, *Nanomaterials*, 2010, **11**, 1-32.

197 H. P. S. Abdul Khalil, A. H. Bhat and A. F. Ireana Yusra, *Carbohydr Polym*, 2012, **87**, 963–979.

198 I. Siró and D. Plackett, *Cellulose*, 2010, **17**, 459–494.

199 D. Tian, J. Hu, J. Bao, R. P. Chandra, J. N. Saddler and C. Lu, *Biotechnol Biofuel*, 2017, **10**, 1-11.

200 J. A. Sirviö, M. Visanko, J. P. Heiskanen and H. Liimatainen, *J Mater Chem A Mater*, 2016, **4**, 6368–6375.

201 N. El Miri, K. Abdelouahdi, M. Zahouily, A. Fihri, A. Barakat, A. Solhy and M. El Achaby, *J Appl Polym Sci*, 2015, **42004**, 1-13.

202 H. C. Oyeoka, C. M. Ewulonu, I. C. Nwuzor, C. M. Obele and J. T. Nwabanne, *J Bioresour Bioprod*, 2021, **6**, 168–185.

203 A. Mandal and D. Chakrabarty, *J Ind Eng Chem*, 2014, **20**, 462–473.

204 A. A. Ebnalwaled, A. H. Sadek, S. H. Ismail and G. G. Mohamed, *Opt Quantum Electron*, 2022, **54**, 1-31.

205 X. Kang, S. Kuga, C. Wang, Y. Zhao, M. Wu and Y. Huang, *ACS Sustain Chem Eng*, 2018, **6**, 2954–2960.

206 A. Sharma, M. Thakur, M. Bhattacharya, T. Mandal and S. Goswami, *Biotechnol Rep*, 2019, **21**, 1-15.

207 S. Virtanen, S. Vuoti, H. Heikkinen and P. Lahtinen, *Cellulose*, 2014, **21**, 3561–3571.

208 G. de J. C. Fernandes, P. H. Campelo, J. de Abreu Figueiredo, H. J. Barbosa de Souza, M. R. S. Peixoto Joele, M. I. Yoshida and L. de F. Henriques Lourenço, *Sci Rep*, 2022, **12**, 1-12.

209 K. J. Nagarajan, M. R. Sanjay, K. Sathick Basha, G. R. Raghav, R. Ashok Kumar, S. Siengchin, B. Surya Rajan, P. Sabari Nath and A. Khan, *Polym Compos*, 2022, **43**, 4942–4958.

210 A. S. Patil, R. D. Waghmare, S. P. Pawar, S. T. Salunkhe, G. B. Kolekar, D. Sohn and A. H. Gore, *J Photochem Photobiol A Chem*, 2020, **400**, 1-9.

211 S. Virtanen, J. Vartianen, H. Setälä, T. Tammelin and S. Vuoti, *RSC Adv*, 2014, **4**, 11343–11350.

212 A. Briddick, P. Li, A. Hughes, F. Courchay, A. Martinez and R. L. Thompson, *Langmuir*, 2016, **32**, 864–872.

213 S. Suganthi, S. Vignesh, J. Kalyana Sundar and V. Raj, *Appl Water Sci*, 2020, **10**, 1-11.

214 D. Rahmadiawan, H. Abral, R. M. Railis, I. C. Iby, M. Mahardika, D. Handayani, K. D. Natrana, D. Juliadmi and F. Akbar, *J Compos Sci*, 2022, **6**, 1-15.

215 P. Cazón, M. Vázquez and G. Velazquez, *Biomacromolecules*, 2019, **20**, 2084–2095.

216 Z. Wang, X. Qiao and K. Sun, *Carbohydr Polym*, 2018, **197**, 442–450.

217 J. Wongwatanapaiboon, K. Kangvansaichol, V. Burapatana, R. Inochanon, P. Winayanuwattikun, T. Yongvanich and W. Chulalaksananukul, *J Biomed Biotechnol*, 2012, **2012**, 1-10.

218 C. Sorapipatana and S. Yoosin, *Renew Sustain Energy Rev*, 2011, **15**, 1343–1349.

219 C. Sakdaronnarong, A. Saengsawang, A. Siriyutta, W. Jonglertjunya, N. Nasongkla and N. Laosiripojana, *Chem Eng J*, 2016, **285**, 144–156.

220 A. Saning, S. Herou, D. Dechtrirat, C. Ieosakulrat, P. Pakawatpanurut, S. Kaowphong, C. Thanachayanont, M. M. Titirici and L. Chuenchom, *RSC Adv*, 2019, **9**, 24248–24258.

221 C. Santasnachok, W. Kurniawan and H. Hinode, *J Environ Chem Eng*, 2015, **3**, 2115–2126.

222 M. N. Sahmoune, *Environ Chem Lett*, 2019, **17**, 697–704.

223 P. Buapeth, W. Watcharin, D. Dechtrirat and L. Chuenchom, *IOP Conf Ser Mater Sci Eng*, 2019, **515**, 1-7.

224 K. Özdenkçi, C. De Blasio, H. R. Muddassar, K. Melin, P. Oinas, J. Koskinen, G. Sarwar and M. Järvinen, *Energy Convers Manag*, 2017, **149**, 974–987.

225 P. P. Thoresen, L. Matsakas, U. Rova and P. Christakopoulos, *Bioresour Technol*, 2020, **306**, 1-10.

226 N. Suriyachai, V. Champreda, C. Sakdaronnarong, A. Shotipruk and N. Laosiripojana, *Renew Energy*, 2017, **113**, 1141–1148.

227 S. Suwannarangsee, B. Bunterngsook, J. Arnthong, A. Paemanee, A. Thamchaipenet, L. Eurwilaichitr, N. Laosiripojana and V. Champreda, *Bioresour Technol*, 2012, **119**, 252–261.

228 J. Manaso, A. Luengnaruemitchai and S. Wongkasemjit, *Int J Chem Molecular Nuclear Mater Metall Eng*, 2013, **7**, 192–196.

229 P. Tatijarern, S. Prasertwasu, T. Komalwanich, T. Chaisuwan, A. Luengnaruemitchai and S. Wongkasemjit, *Bioresour Technol*, 2013, **143**, 423–430.

230 T. Komolwanich, S. Prasertwasu, D. Khumsupan, P. Tatijarern, T. Chaisuwan, A. Luengnaruemitchai and S. Wongkasemjit, *Mater Res Innov*, 2016, **20**, 259–267.

231 A. Kruse and E. Dinjus, *J Supercrit Fluids*, 2007, **39**, 362–380.

232 S. Imman, J. Arnthong, V. Burapatana, V. Champreda and N. Laosiripojana, *Bioresour Technol*, 2014, **171**, 29–36.

233 K. Weerasai, V. Champreda, C. Sakdaronnarong, A. Shotipruk and N. Laosiripojana, *Food Bioprod Process*, 2018, **110**, 136–144.

234 M. R. Zakaria, S. Hirata, S. Fujimoto and M. A. Hassan, *Bioresour Technol*, 2015, **193**, 128–134.

235 C. Sakdaronnarong, K. Jiratanakittiwat, T. Tangkitthanasakul and N. Laosiripojana, *Food Bioprod Process*, 2017, **105**, 104–116.

236 Z. Zhang, M. D. Harrison, D. W. Rackemann, W. O. S. Doherty and I. M. O'Hara, *Green Chem*, 2016, **18**, 360–381.

237 C. Chotirotsukon, M. Raita, V. Champreda and N. Laosiripojana, *Ind Crops Prod*, 2019, **141**, 1-9.

238 J. J. Bozell, S. K. Black, M. Myers, D. Cahill, W. P. Miller and S. Park, *Biomass Bioenerg*, 2011, **35**, 4197–4208.

239 M. F. Li, S. N. Sun, F. Xu and R. C. Sun, *Chem Eng J*, 2012, **179**, 80–89.

240 C. Santasnachok, W. Kurniawan and H. Hinode, *J Life Sci*, 2015, **10**, 127–130.

241 T. Sonobe, N. Worasuwannarak and S. Pipatmanomai, *Fuel Process Technol*, 2008, **89**, 1371–1378.

242 T. Wongsiriamnuay and N. Tippayawong, *Bioresour Technol*, 2010, **101**, 5638–5644.

243 A. Boonpoke, S. Chiarakorn, N. Laosiripojana, S. Towprayoon and A. Chidthaisong, *Korean J Chem Eng*, 2012, **29**, 89–94.

244 S. Sirijanusorn, K. Sriprateep and A. Pattiya, *Bioresour Technol*, 2013, **139**, 343–348.

245 W. Charusiri, *Energy Procedia*, 2015, **74**, 933–941.

246 A. Palamanit, P. Khongphakdi, Y. Tirawanichakul and N. Phusunti, *Biofuel Res J*, 2019, **6**, 1065–1079.

247 R. Kempegowda, S. Assabumrungrat and N. Laosiripojana, *Int J Chem React Eng*, 2010, **8**, 1-27.

248 C. Phuhiran, T. Takarada and S. Chaiklangmuang, *Int J Hydrogen Energy*, 2014, **39**, 3649–3656.

249 J. Chumpoo and P. Prasassarakich, *Energ Fuel*, 2010, **24**, 2071–2077.

250 K. Khampuang, N. Boreriboon and P. Prasassarakich, *Biomass Bioenerg*, 2015, **83**, 460–466.

251 C. A. Mullen and A. A. Boateng, *Fuel Process Technol*, 2010, **91**, 1446–1458.

252 P. Prasertpong and N. Tippayawong, *Energ Sources Part A J*, 2020, **2020**, 1-12.

253 P. Payakkawan, S. Areejit and P. Sooraksa, *Renew Energ*, 2014, **66**, 49–55.

254 S. Nizamuddin, H. A. Baloch, M. T. H. Siddiqui, N. M. Mubarak, M. M. Tunio, A. W. Bhutto, A. S. Jatoi, G. J. Griffin and M. P. Srinivasan, *Rev Environ Sci Biotechnol*, 2018, **17**, 813–837.

255 M. R. Oliveira, J. A. Cecilia, J. F. De Conto, S. M. Egues and E. Rodríguez-Castellón, *J Solgel Sci Technol*, 2023, **105**, 370–387.

256 J. Chun, Y. Mo Gu, J. Hwang, K. K. Oh and J. H. Lee, *J Ind Eng Chem*, 2020, **81**, 135–143.

257 A. Mandal and D. Chakrabarty, *Carbohydr Polym*, 2011, **86**, 1291–1299.

258 T. J. Bondancia, J. De Aguiar, G. Batista, A. J. G. Cruz, J. M. Marconcini, L. H. C. Mattoso and C. S. Farinas, *Ind Eng Chem Res*, 2020, **59**, 11505–11516.

259 T. S. Ng, Y. C. Ching, N. Awanis, N. Ishenny and M. R. Rahman, *Mater Res Innov*, 2014, **18**, 400-404.

260 N. Quiévy, N. Jacquet, M. Sclavons, C. Deroanne, M. Paquot and J. Devaux, *Polym Degrad Stab*, 2010, **95**, 306–314.

261 S. Azat, A. V. Korobeinyk, K. Moustakas and V. J. Inglezakis, *J Clean Prod*, 2019, **217**, 352–359.

262 Y. Shen, P. Zhao and Q. Shao, *Microporous Mesoporous Mater*, 2014, **188**, 46–76.

263 X. Yang, P. Roonasi and A. Holmgren, *J Colloid Interface Sci*, 2008, **328**, 41–47.

264 J. Yang, T. Zhang, L. Guo, S. Zhi and J. Han, *Metals-Basel*, 2023, **13**, 1-14.

265 A. Zeleňáková, P. Hrubovčák, O. Kapusta, N. Kučerka, A. Kuklin, O. Ivankov and V. Zeleňák, *Sci Rep*, 2019, **9**, 1-9.

266 T. H. Liou, G. W. Chen and S. Yang, *Nanomater*, 2022, **12**, 1-18.

267 Y. Xu, C. Wang, G. Zhou, Y. Wu and J. Chen, *Appl Surf Sci*, 2012, **258**, 6366–6372.

268 A. M. Basso, B. P. Nicola, K. Bernardo-Gusmão and S. B. C. Pergher, *Appl Sci*, 2020, **10**, 1-16.

269 B. L. Newalkar, J. Olanrewaju and S. Komarneni, *J Phys Chem B*, 2001, **105**, 8356–8360.

270 N. Juárez-Serrano, D. Berenguer, I. Martínez-Castellanos, I. Blasco, M. Beltrán and A. Marcilla, *Catalysts*, 2021, **11**, 1-21.

271 K. Bai, J. Hao, Y. Yang and A. Qian, *Heliyon*, 2020, **6**, 1-5.

272 P. F. Fulvio, S. Pikus and M. Jaroniec, *J Mater Chem*, 2005, **15**, 5049–5053.

273 P. Verma, Y. Kuwahara, K. Mori, R. Raja and H. Yamashita, *Nanoscale*, 2020, 12, 11333–11363.

274 S. Shen, F. Chen, P. S. Chow, P. Phanapavudhikul, K. Zhu and R. B. H. Tan, *Microporous Mesoporous Mater*, 2006, **92**, 300–308.

275 J. Alvarez, G. Lopez, M. Amutio, J. Bilbao and M. Olazar, *Fuel*, 2014, **128**, 162–169.

276 Z. Yi, C. Deng-yu, Z. Dong and Z. H. U. Xi-feng, *J Fuel Chem Technol*, 2012, **40**, 1194–1199.

277 A. K. Varma and P. Mondal, *Ind Crops Prod*, 2017, **95**, 704–717.

278 F. Xu, Y. Xu, R. Lu, G. Sheng and H. Yu, *J Agric Food Chem*, 2011, **59**, 9243–9249.

279 Q. H. Song, J. Q. Nie, M. G. Ren and Q. X. Guo, Energ Fuel, 2009, 23, 3307–3312.

280 J. Chen and S. Li, *RSC Adv*, 2020, **10**, 2160–2169.

281 X. Chen, X. Wang and D. Fang, *Fuller Nanotub Car N*, 2020, **28**, 1048–1058.

282 J. C. C. Freitas, D. F. Cipriano, C. G. Zucolotto, A. G. Cunha and F. G. Emmerich, *J Spectrosc*, 2016, **2016**, 1–7.

283 M. Y. Nassar, I. S. Ahmed and M. A. Raya, *J Mol Liq*, 2019, **282**, 251–263.

284 X. L. Wu, Y. Shi, S. Zhong, H. Lin and J. R. Chen, *Appl Surf Sci*, 2016, **378**, 80–86.

285 M. Wiśniewska, M. Wawrzkiewicz, M. Onyszko, M. Medykowska, A. Nosal-wiercińska and V. Bogatyrov, *Materials*, 2021, **14**, 1-17.

286 M. Abboud, T. Sahlabji, M. A. Haija, A. A. El-Zahhar, S. Bondock, I. Ismail and S. M. A. S. Keshk, *New Journal of Chemistry*, 2020, **44**, 2291–2302.

287 M. Zirak, A. Abdollahiyan, B. Eftekhari-Sis and M. Saraei, *Cellulose*, 2018, **25**, 503–515.

288 G. R. Bardajee, Z. Hooshyar and F. E. Shahidi, *Int J Environ Sci Technol*, 2015, **12**, 1737–1748.

289 T. Qiang, Y. Song, J. Zhao and J. Li, *J Alloys Compd*, 2019, **770**, 792–802.

290 T. H. Kim, H. Kwak, T. H. Kim and K. K. Oh, *Energies (Basel)*, 2021, **14**, 1-14.

291 J. Dai, A. F. Patti and K. Saito, *Tetrahedron Lett*, 2016, **57**, 4945–4951.

292 M. A. Usmani, I. Khan, A. Haque, A. H. Bhat, D. Mondal and U. Gazal*, Compos Sci Eng,* 2017, **2017**, 45-76.

293 M. Parchami, S. Agnihotri and M. J. Taherzadeh, *Bioresour Technol*, 2022, 362, 1-13.

294 T. A. Pham, D. S. Ngo and K. A. To, *Sugar Tech*, 2022, **24**, 779–787.

295 C. Sakdaronnarong, N. Srimarut and N. Laosiripojana, *Key Eng Mater*, 2015, **659**, 527–532.

296 N. Shahi, B. Min, B. Sapkota and V. K. Rangari, *Sustain*, 2020, **12**, 1-15.

297 O. Somseemee, P. Sae-Oui and C. Siriwong, *Ind Crops Prod*, 2021, **171**, 1-11.

298 R. Santi, A. Cigada, B. Del Curto and S. Farè, *J Appl Biomater Funct Mater*, 2019, **17**, 1-7.

299 W. Yang, H. Ding, G. Qi, C. Li, P. Xu, T. Zheng, X. Zhu, J. M. Kenny, D. Puglia and P. Ma, *React Funct Polym*, 2021, **162**, 1-10.

300 N. Samsalee, J. Meerasri and R. Sothornvit, *Carbohydr. Polym.*, 2023, **6**, 1-10.

301 S. Ren, X. Sun, T. Lei and Q. Wu, *J Nanomater*, 2014, **2014**, 1-11.

302 P. P. Nayak, S. Nandi and A. K. Datta, *Eng Rep*, 2019, **1**, 1-13.

303 N. I. Abdo, Y. M. Tufik and S. M. Abobakr, *Curr Res Green Sustain Chem*, 2023, **6**, 1-7.

304 S. M. L. Rosa, N. Rehman, M. I. G. De Miranda, S. M. B. Nachtigall and C. I. D. Bica, *Carbohydr Polym*, 2012, **87**, 1131–1138.

305 I. Made Joni, Rukiah and C. Panatarani, *AIP Conf Proc*, 2020, **2219**, 80018.

306 X. Sun, Q. Wu, X. Zhang, S. Ren, T. Lei, W. Li, G. Xu and Q. Zhang, *Cellulose*, 2018, **25**, 1103–1115.

307 A. R. Kakroodi, S. Cheng, M. Sain and A. Asiri, *J Nanomater*, 2014, **2014**, 1-7.

308 J. Tarique, S. M. Sapuan and A. Khalina, *Sci Rep*, 2021, **11**, 1-17.

309 X. He, F. Luzi, X. Hao, W. Yang, L. Torre, Z. Xiao, Y. Xie and D. Puglia, *Int J Biol Macromol*, 2019, **127**, 665–676.

310 K. K. Packiam, B. Murugesan, P. M. Kaliyannan Sundaramoorthy, H. Srinivasan and K. Dhanasekaran, *J Nat Fibers*, 2022, **19**, 7424–7435.

311 S. Lal, V. Kumar and S. Arora, *Polym Polym Compos*, 2021, **29**, 1505–1514.

312 W. Yang, X. He, F. Luzi, W. Dong, T. Zheng, J. M. Kenny, D. Puglia and P. Ma, *Int J Biol Macromol*, 2020, **161**, 617–626.

313 R. J. Fong, A. Robertson, P. E. Mallon and R. L. Thompson, *Polymers*, 2018, **10**, 1-15.

314 A. Bahrami and R. Fattahi, *Food Sci Nutr*, 2021, **9**, 4974–4985.

315 P. A. Sreekumar, M. A. Al-Harthi and S. K. De, *J Appl Polym Sci*, 2012, **123**, 135–142.

316 T. V. Panova, A. A. Efimova, A. K. Berkovich and A. V. Efimov, *RSC Adv*, 2020, **10**, 24027–24036.

317 M. Mohsin, A. Hossin and Y. Haik, *J Appl Polym Sci*, 2011, **122**, 3102–3109.

318 W. Yang, G. Qi, J. M. Kenny, D. Puglia and P. Ma, *Polymers*, 2020, **1364**, 1-15.

319 C. T. Chou, S. C. Shi, T. H. Chen and C. K. Chen, *Sci Prog*, 2023, **106**, 1-15.

320 W. Li, Q. Wu, X. Zhao, Z. Huang, J. Cao, J. Li and S. Liu, *Carbohydr Polym*, 2014, **113**, 403–410.

321 Y. Wu, Q. Tang, F. Yang, L. Xu, X. Wang and J. Zhang, *Cellulose*, 2019, **26**, 3193–3204.

322 Z. Wang, Y. Ding and J. Wang, *Nanomaterials*, 2019, **9**, 1-17.

323 W. Zhang, X. He, C. Li, X. Zhang, C. Lu, X. Zhang and Y. Deng, *Cellulose*, 2014, **21**, 485–494.

324 S. Cheng, Y. Zhang, R. Cha, J. Yang and X. Jiang, *Nanoscale*, 2016, **8**, 973–978.

325 Z. Yan, L. Meng, X. Huang, Q. Wei, J. Liu, Z. Sun and S. Ding, *J Text Inst*, 2023, **114**, 1881-1886.